Final Report of NASA Innovative Advanced Concepts (NIAC) Phase 1 Task 12-NIAC12B-0038

ORBITING RAINBOWS: OPTICAL MANIPULATION OF AEROSOLS AND THE BEGINNINGS OF FUTURE SPACE CONSTRUCTION *

Dr. Marco B. Quadrelli, P.I.† Dr. Scott Basinger ‡
Prof. Grover Swartzlander, Jr. §

June 18, 2013

†Research Technologist, Mobility and Robotic Systems Section, Autonomous Systems Division, Mail Stop 198-219, Jet Propulsion Laboratory, California Institute of Technology, 4800 Oak Grove Drive, Pasadena, CA 91109-8099, phone: (818) 354-7548, marco.b.quadrelli@jpl.nasa.gov

‡Jet Propulsion Laboratory/California Institute of Technology Mail Stop 306-451, 4800 Oak Grove Drive, Pasadena, CA, 91109-8099 Phone: (818) 354-3065, Fax: (818) 393-6869, Email: scott.a.basinger@jpl.nasa.gov

§Center for Imaging Science and Physics Dept., Rochester Institute of Technology 54 Lomb Memorial Drive, Rochester, NY 14623 (585) 475-4247 (Office), Room 3116 Bldg 76 (Chester F. Carlson) (585) 475-5988 (Fax), email: grovers@mail.rit.edu

Contents

List of Figures

1 Executive Summary

Our objective is to investigate the conditions to manipulate and maintain the shape of an orbiting cloud of dust-like matter so that it can function as an ultra-lightweight surface with useful and adaptable electromagnetic characteristics, for instance, in the optical, RF, or microwave bands. Inspired by the light scattering and focusing properties of distributed optical assemblies in Nature, such as rainbows and aerosols, and by recent laboratory successes in optical trapping and manipulation, we propose a unique combination of space optics and autonomous robotic system technology, to enable a new vision of space system architecture with applications to ultra-lightweight space optics and, ultimately, in-situ space system fabrication. Typically, the cost of an optical system is driven by the size and mass of the primary aperture. The ideal system is a cloud of spatially disordered dust-like objects that can be optically manipulated: it is highly reconfigurable, fault-tolerant, and allows very large aperture sizes at low cost. See Figure 1 for a scenario of application of this concept. The solution that we propose is to construct an optical system in space in which the nonlinear optical properties of a cloud of micron-sized particles are shaped into a specific surface by light pressure, allowing it to form a very large and lightweight aperture of an optical system, hence reducing overall mass and cost. Other potential advantages offered by the cloud properties as optical system involve possible combination of properties (combined transmit/receive), variable focal length, combined refractive and reflective lens designs, and hyper-spectral imaging. A cloud of highly reflective particles of micron size acting coherently in a specific electromagnetic band, just like an aerosol in suspension in the atmosphere, would reflect the Suns light much like a rainbow. The only difference with an atmospheric or industrial aerosol is the absence of the supporting fluid medium. This new concept is based on recent understandings in the physics of optical manipulation of small particles in the laboratory and the engineering of distributed ensembles of spacecraft clouds to shape an orbiting cloud of micron-sized objects. In the same way that optical tweezers have revolutionized micro- and nano-manipulation of objects, our breakthrough concept will enable new large scale NASA mission applications and develop new technology in the areas of Astrophysical Imaging Systems and Remote Sensing because the cloud can operate as an adaptive optical imaging sensor. While achieving the feasibility of constructing one single aperture out of the cloud is the main topic of this work, it is clear that multiple orbiting aerosol lenses

could also combine their power to synthesize a much larger aperture in space to enable challenging goals such as exo-planet detection. Furthermore, this effort could establish feasibility of key issues related to material properties, remote manipulation, and autonomy characteristics of cloud in orbit. There are several types of endeavors (science missions) that could be enabled by this type of approach, i.e. it can enable new astrophysical imaging systems, exo-planet search, large apertures allow for unprecedented high resolution to discern continents and important features of other planets, hyperspectral imaging, adaptive systems, spectroscopy imaging through limb, and stable optical systems from Lagrange-points. Future micro-miniaturization might hold promise of a further extension of our dust aperture concept to other more exciting smart dust concepts with other associated capabilities.

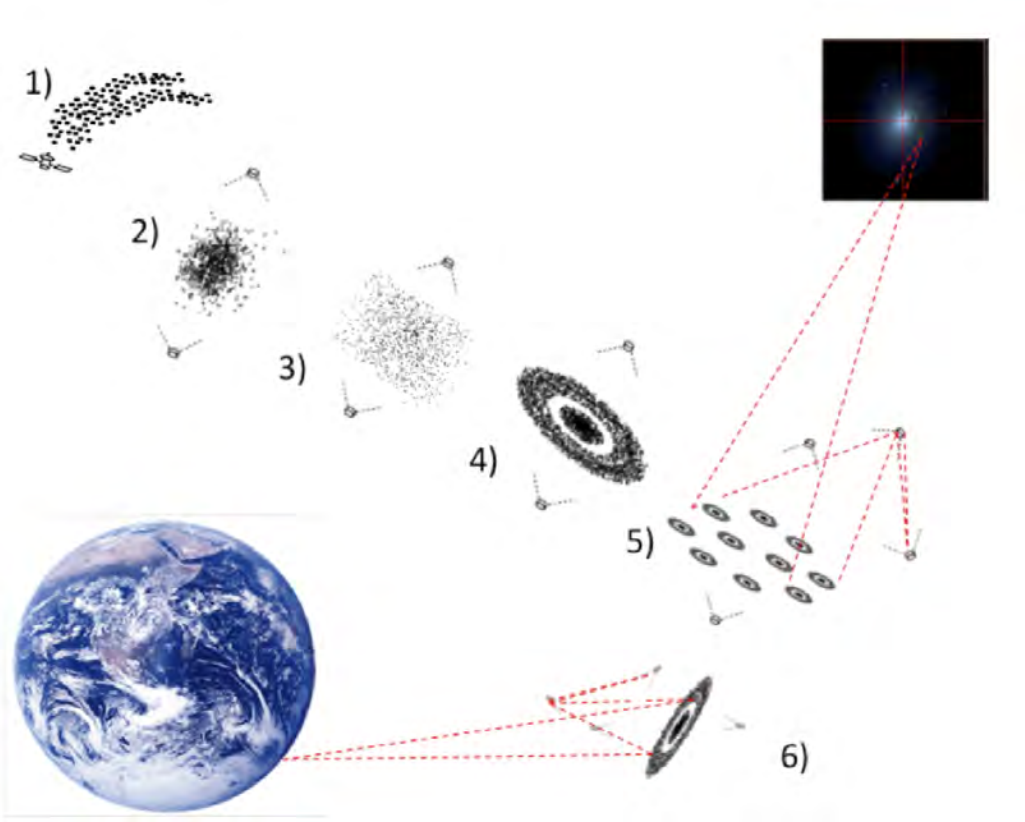

Figure 1: 1) the cloud is first released; 2) it is contained by laser pressure to avoid dissipation and disruption by gravitational tidal forces, 3) it is shaped by optical manipulation into a two-dimensional object (coarse control), and 4) ultimately into a surface with imaging characteristics (fine control). The cloud shape has to be maintained against orbital disturbances by continuous figure control, also achieved optically. Applying differential light pressure retargets the entire cloud, so that a change of the optical axis can be induced. Selected parts of the cloud are reshaped when required for wavefront control, thus enabling higher quality optics. The entire imaging system is now in full operation, as 5) a multilens system searching for exo-planets, or 6) as a radio receiver engaged in remote sensing investigations.

2 What is an orbiting rainbow?

The objective of Phase I was to investigate the conditions to manipulate and maintain the shape of an orbiting cloud of dust-like matter so that it can function as an ultra-lightweight surface with useful and adaptable electromagnetic characteristics.

Recent successes in optical trapping and manipulation, and the observation that distributed assemblies in Nature, such as rainbows and aerosols, have interesting light scattering and focusing properties, led us to the following question: *...can we use optical manipulation technology to create an artificial rainbow or aerosol with useful optical or electromagnetic properties?...* A cloud of highly reflective particles of micron size acting coherently in a specific electromagnetic band, just like an aerosol in suspension in the atmosphere, would reflect the Suns light much like a rainbow. The only difference with an atmospheric or industrial aerosol is the absence of the supporting fluid medium.[1] Figure 2 shows two types of manifestations in Nature that have been an inspiration for this work.

The potential advantages of our concept are that: a) it can result in an ultra-lightweight system, made of very simple, very low cost, units; b) it can be very big: the cloud can distribute itself to kilometer scales, without the need to fill the aperture; c) the cloud is easy to package, transport and deploy; d) it is reconfigurable, and can be retargeted and repointed with non-mechanical means; e) the cloud is a highly fault-tolerant system with very low vulnerability to impacts. Other potential advantages offered by the cloud properties as optical system involve possible combination of properties (combined transmit/receive), variable focal length, combined refractive and reflective lens designs, and hyper-spectral imaging. The study identified technology gaps and candidate system architectures for the space-borne cloud as an aperture. We looked at the feasibility of a crosscutting concept that contributes new technological approaches for space optics, autonomous systems, and space applications of optical manipulation. The novel concept hereby proposed addresses the following NASAs Space Technology Grand Challenges:

- TA04, Robotics and Autonomous Systems, as it may open the door to

[1] In this report, we equivalently use the term aerosol, "cloud", rainbow", "granular spacecraft" or, simply, "swarm", for the cloud of dusty material that we want to manipulate, and we use the term grain to refer to the single elements of the cloud.

innovative applications of formation flying and autonomy technology for large optical systems in space.

- TA08, Science Instruments, Observatories, and Sensor Systems, as it develops a system that may provide advancements in High Contrast Imaging, Optical Systems, and Detector and Focal Planes.
- TA12, Materials, Structures, Mechanical Systems and Manufacturing, as it addresses innovative types of lightweight and multifunctional structures.

Finding a way to manipulate such distribution of matter in space would lead to a potentially affordable new way of generating very large and potentially re-shapeable optics in space, and open the way to revolutionizing large-scale optics, and indirectly open the way to future technologies for space construction by means of light.

(a) (b)

Figure 2: (a) Sun on clouds and (b) full Rainbow.

3 Benefits to NASA Programs/Projects

The evolution of space telescopes (see Figure 3), from Hubble, James Webb, inflatable concepts, formation flying, up to hyper-telescopes, where distributed apertures form the primary, naturally leads to the concept investigated in this study. This concept would increase the aperture several times compared to ATLAS, allowing for a true Terrestrial Planet Imager that would be able to resolve exo-planet details and do meaningful spectroscopy on distant worlds. The aperture does not need to be continuous. Used interferometrically, for example, as in a Golay array,[15] imagery can be synthesized over an enormous scale. We leveraged our experience working with large optical systems to consider refractive, reflective and holographic systems. Finding a way to manipulate such distribution of matter in space would lead to a potentially affordable new way of generating very large and potentially re-shapeable optics in space, and indirectly open the way to future technologies for space construction by means of light. It will also enable new astrophysical imaging systems, exo-planet search, hyperspectral imaging, adaptive systems, spectroscopy imaging through limb, and stable optical systems from Lagrange-points.

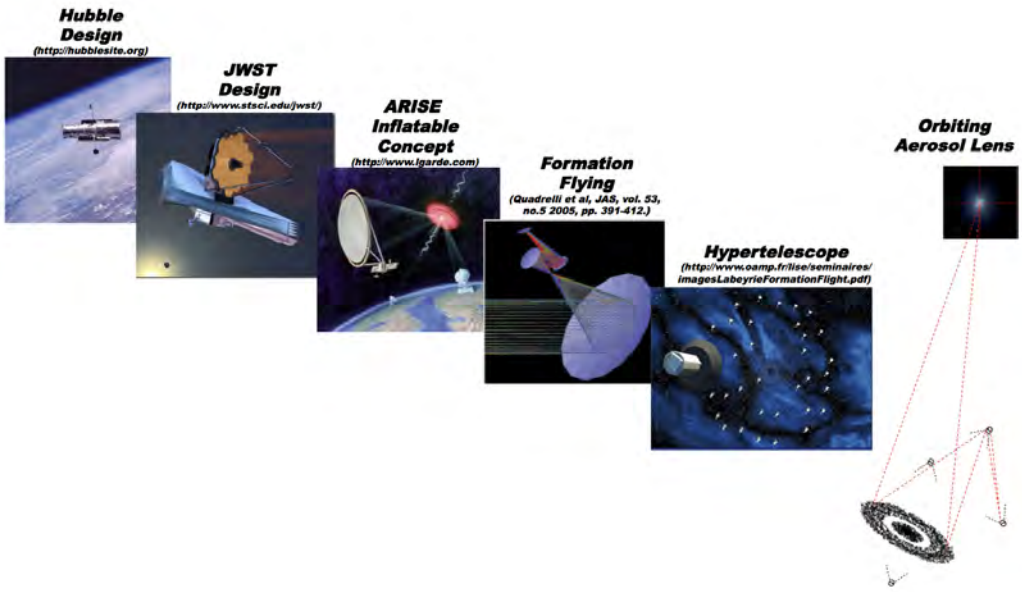

Figure 3: Evolution of large space telescopes.

4 The team contributions

Dr. Marco B. Quadrelli (P.I.) investigated the physical behavior of the orbiting cloud and proposed autonomous system options. Dr. S. Basinger (JPL) assessed adaptive electromagnetic system requirements and solutions for utilization of the cloud as element of an imaging system. Prof. G. Swarzlander (Rochester Inst. of Technology) proposed solutions to extrapolate optical lift manipulation and optical trapping technology to this application. We have also engaged experts in the relevant areas and developed partnerships that may lead to future funding avenues. These experts included:

- Dr. Adrian Stoica (JPL), an expert of micro-miniaturization and evolvable software and hardware,
- Dr. Bob Balaram (JPL), an expert of autonomy of space robotic systems,
- Prof. Liz McCormack (Bryn Mawr College), P.I. of the past NIAC task on laser-trapped mirrors,
- Dr. Tomasz M. Grzegorczyk (Delpsi LLC.), expert in optical binding simulation, also involved in McCormacks NIAC,
- Prof. Jean-Marc Fournier (Swiss Federal Institute of Technology), expert in optical binding experiments, also involved in McCormacks NIAC,
- Prof. David Brady (Duke Univ.), expert in coded aperture and computational optics technology,
- Prof. James Fienup (University of Rochester), expert in speckle interferometry and also in computational optics.

5 Background

A major challenge in space missions involving astrophysics or remote sensing is related to the size, mass, and cost of the imaging aperture. In the same way that optical tweezers have revolutionized micro- and nano-manipulation of objects, our breakthrough concept will enable new large scale NASA mission applications and develop new technology in the areas of Astrophysical

Imaging Systems and Remote Sensing because the cloud can operate as an adaptive optical imaging sensor. While achieving the feasibility of constructing one single aperture out of the cloud is the main topic of this work, it is clear that multiple orbiting aerosol lens could also combine their power to synthesize a much larger aperture in space to enable challenging goals such as exo-planet detection. Furthermore, this effort could establish feasibility of key issues related to material properties, remote manipulation, and autonomy characteristics of cloud in orbit. The focusing electromagnetic properties of randomly distributed orbiting arrays have never been investigated. The imaging through retargeting, and realization of boresight and wavefront control of an orbiting cloud represent a rich area of investigation, independently of the application, because of the multiple spatial and temporal scales involved to enable a integrated mission design. There are several types of endeavors (science missions) that could be enabled by this type of approach, i.e. it can enable new astrophysical imaging systems, exo-planet search, large apertures allow for unprecedented high resolution to discern continents and important features of other planets, hyperspectral imaging, adaptive systems, spectroscopy imaging through limb, and stable optical systems from Lagrange-points. Furthermore, future micro-miniaturization might hold promise of a further extension of our dust aperture concept to other more exciting smart dust concepts with other associated capabilities. Given that the size and mass of the imaging aperture is the major cost driver, the knowledge and technology being developed in this NIAC project will allow space technologists to include highly distributed systems in their plans of future imaging systems in space, with the consequent savings in cost.

6 Past Relevant Work

This section reviews past relevant work in this new area.

6.1 Prior Related NIAC studies

Several NIAC tasks have dealt with systems composed of very large number of elements in space, and techniques to deploying and controlling them. We found the following ones as relevant to the study at hand:

- Phase I, Practicality of a Solar Shield in Space to Counter GLobal Warming, (`www.niac.usra.edu/studies/1298Angel.html`)

- Phase II, A Contamination-Free Ultrahigh Precision Formation Flight Method Based on Intracavity Photon Thrusters and Tethers: Photon Tether Formation Flight, (www.niac.usra.edu/studies/1374Bae.html)
- Phase I, Extremely Large Swarm Array of Picosats for Microwave/RF Earth Sensing, Radiometry, and Mapping, (www.niac.usra.edu/studies/942Bekey.html)
- Phase I, Assessment of the Feasibility of Extremely Large, Structureless Optical Telescopes and Arrays, (www.niac.usra.edu/studies58Bekey.html)
- Phase I, Ultralight Solar Sails for Interstellar Travel, (www.niac.usra.edu/studies/333Christensen.html)
- Phase I, Propellantless Control of Spacecraft Swarms using Coulomb Forces, (www.niac.usra.edu/studies/601King.html)
- Phase I, Advanced Solar and Laser Pushed Lightsail Concepts, (www.niac.usra.edu/studies/4Landis.html)
- Phase II, Investigation of the Feasibility of Laser Trapped Mirrors in Space, (www.niac.usra.edu/studies/1202McCormack.html)
- Phase I, Electromagnetic Formation Flight, (www.niac.usra.edu/studies/793Miller.html)
- Phase I, Large Telescope Using Holographically Corrected Membranes, (www.niac.usra.edu/studies/416Palisoc.html)
- Phase I, Large Ultra-Lightweight Photonic Muscle Telescope, (www.niac.usra.edu/studies/1350Ritter.html)
- Phase II, Electromagnetic Formation Flight, (www.niac.usra.edu/studies/838Sedwick.html)
- Phase I, High Resolution Structureless Telescope, (www.niac.usra.edu/studies/868Wertz.html)
- Phase II, Very Large Optics for the Study of Extrasolar Terrestrial Planets, (www.niac.usra.edu/studies/374Woolf.html)

In this section, we briefly discuss how our concept is different that the one on laser-trapped mirrors, and the one on picosats.

6.2 Westford Needles Experiment

At the height of the Cold War in the late 1950s, all international communications were either sent through undersea cables or bounced off of the natural ionosphere. The solution of the US Military with the Project West Ford[71] was to create an artificial ionosphere. In May 1963, the US Air Force launched 480 million tiny copper needles that briefly created a ring encircling the entire globe. Figure 4 shows a detailed view of the West-Ford needles. The engineers behind the project hoped that it would serve as a prototype for two more permanent rings that would forever guarantee their ability to communicate across the globe. Inside the West Ford spacecraft, the needles were packed densely together in blocks made of a napthalene gel that would rapidly evaporate in space. This entire package of needles weighed only 20 kg. After being released, the hundreds of millions of copper needles gradually spread throughout their entire orbit over a period of two months. The final donut-shaped cloud was 15 km wide and 30 km thick and encircled the globe at an altitude of 3700 km. The West Ford copper needles were each 1.8 cm long and 0.0018 cm in diameter and weighed only 40 micrograms. They were designed to be exactly half of the wavelength of 8000 MHz microwaves. This length created strong reflections when the microwaves struck the copper needles, in effect making them tiny dipole antennae each repeating in all directions the exact same signal they received. While it was a passive reflector, this experiment demonstrated the large-scale electromagnetic utilization of a cloud of incoherent matter.

6.3 Labeyrie pellicle telescope

The Laser Trapped Mirror (LTM) was first proposed by Antoine Labeyrie,,[43],[4445] as an innovative way of producing large lightweight optics in space. Labeyrie suggested using laser light to structure standing wave fringe surfaces in the space between counter-propagating laser beams. This concept is shown in Figure 5. With appropriate optics, these fringe surfaces might have the shape of a family of parabolic sheets and the same principles that underlie optical traps (optical tweezers, for example), could, in principle, permit trapping of atoms, molecules or larger particles along the standing-wave (fringe) maxima. The result of this process is a reflective parabolic surface, of almost arbitrary size, which could serve as a large telescope. A 100-nm thick, 35-meter diameter mirror would require less than 100 grams of material.

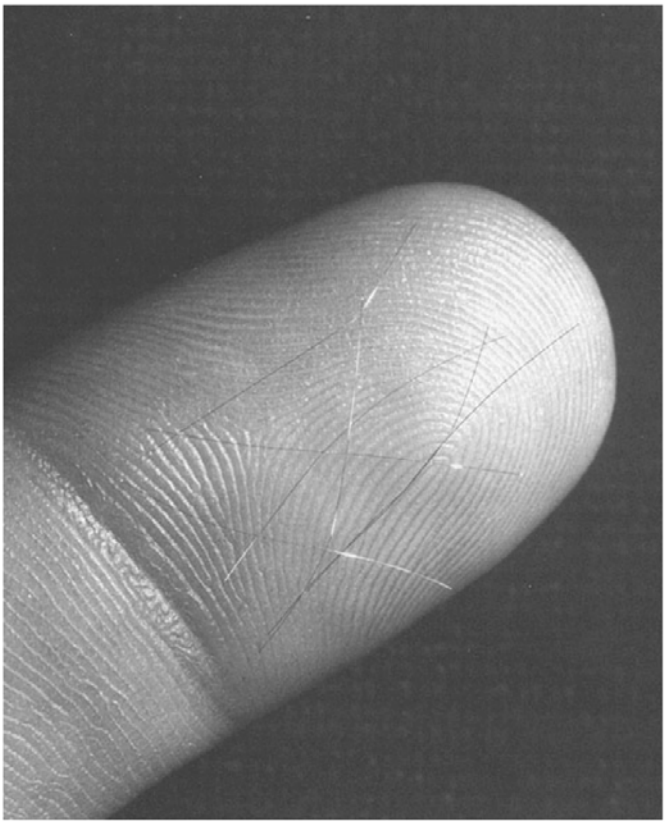

Figure 4: Picture of West-ford needles.

6.4 Holographic aerosol optics

The first idea on using the nonlinear optical properties of aerosols as a lens was proposed by A.J. Palmer,[60],[61],[62] in which an aerosol of dielectric particles is identified as a broadband, low-power third-order nonlinear optics medium, intended for use as a holographic lens, as shown in Figure 6. The nonlinear interaction mechanism under consideration is the electrostrictive modulation of the density of the particles. More recently, the optical trapping of aerosols at the micro-scale has been demonstrated in the laboratory.[74]

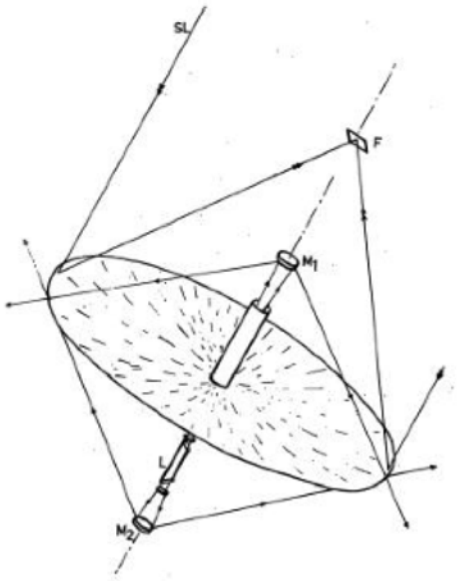

Figure 5: Labeyries pellicle mirror

6.5 Bekeys pico-sats

Another prior NIAC study[11] investigated the possibility of deploying large numbers of pico-sats (with a mass of the order of 1-10 kg) to synthesize very large sparse apertures for remote sensing applications. Out concept is different in that the pico-sats can now be orders of magnitude smaller in size and mass, and use the optical-lift effect to position themselves in a stable configuration.

6.6 JPLs prior work on super-precision formation flying

In previous work,[55] we had investigated the dynamics, control, and estimation feasibility for a formation flying space telescope composed of separate optics: Primary Mirror Membrane, Free Flying Mirror, Focal Plane Assembly, Primary Figure Sensor, Scanning Electron Beam, and the Orbiting Sunshade. This configuration is shown in Figure 8. Applications of such concepts were envisioned in the areas of astrophysical imaging in optical wavelengths, as

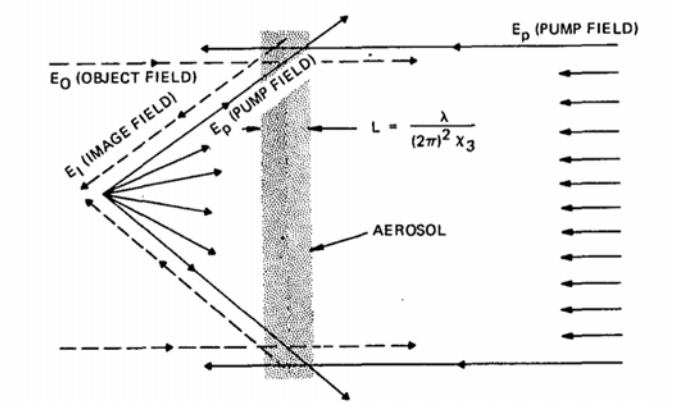

Figure 6: Palmers holographic plasmon lens.

well as precision Earth observation. The analysis included dynamics modeling in the GEO environment, formation flying estimation, and control design with metrology and actuator models. In [JAS report], a hybrid centralized/decentralized control system for a GEOTEL type formation flying of spacecraft with one free flying optical module and four primary mirror membrane spacecraft was presented. Using a leader-follower approach, the optimal control system relied on a virtual optical truss that was maintained with the desired level of precision for the interferometry applications. We have ascertained the formation control feasibility of the desired performance of the system in station-keeping and during a retargeting maneuver that was demonstrated by numerical simulation. The Formation Metrology and Control System overall performance objectives were several. First, to initialize the image formation process using Open loop Predictive Control to place the target image within the entrance aperture of the focal Assembly with an accuracy that enables an image sensed vernier centering and stabilization stage to function. Second, to respond in a closed loop mode to focal plane image tracking offset correction signals that may be generated by the vernier stage on the Focal Assembly. Third, to reorient the separated formation ensemble as a unit to slowly repoint the telescope field of view for new imaging operations. Fourth, to control the Free-Flying (relay) Mirror positioning and attitude for agile targeting.

Overall formation station-keeping and target image placement precision, using proportional FEEP micro-thrusters and combined RF and optical vec-

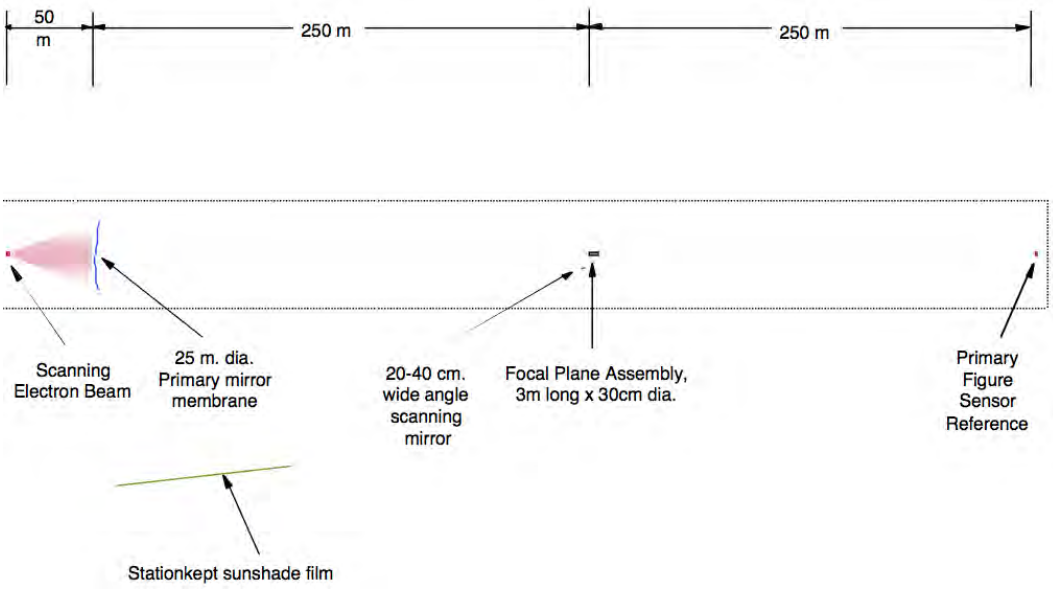

Figure 7: Adaptive structureless telescope proposed by I. Bekey .

tor metrology, was expected to be 200 to 300 microns, and several microradians orientation. This precision both centers the target image in the FPA and is within the desired 500 microns dynamic range of the wavefront corrector in the FPA. Advanced formation flying metrology, estimation, and control technology is enabling for all virtual structure gossamer space telescope concepts. The general feasibility of formation flying the telescopes separated optical elements was based on new metrology and control architectures, implementation innovations, and our near-term performance projections for these technologies. The formation system definition and analysis scope of the study included:

- Centralized relative optical/laser metrology
- Decentralized relative RF metrology and absolute celestial-inertial referencing
- Centralized formation state estimation, and onboard telescope model-based optics module location prediction and positioning reference

- Telescope Commanding and Control methodology from acquisition to precision targeting
- Primary mirror shape sensing and formation vector metrology
- Telescope element(s) positioning error allocations, and analysis of metrology error sensitivities

The optical metrology proposed in[55] was a novel system that enabled determination of range, bearing, and orientation of all formation system elements along with the figure of the Primary Mirror. This underlying vector metrology is based on the following concepts:

- Array Heterodyne Interferometer (AHI). The Array Heterodyne Interferometer (AHI) is a heterodyne interferometer that simultaneously measures relative range of multiple targets on a surface and enables multi-target high precision linear and angular metrology. The target surface is illuminated with a beam of light which is reflected and then interfered with a reference wavefront. The resulting interference pattern is detected with an array of detectors, for example a CCD or an APS (Active Pixel Sensor).
- Modulation Sideband Technology for Absolute Ranging (MSTAR). The MSTAR enables unambiguous range determination for moving targets. The MSTAR sensor is an upgrade to a heterodyne interferometer that turns it into a range sensor with a long ambiguity range, while retaining high precision of a heterodyne interferometer. MSTAR technology provides a breakthrough for future separated spacecraft applications. It is a two-color interferometer implemented with a single frequency stable laser, a key consideration for long-range metrology. Use of a single stable frequency greatly mitigates frequency stability issues.
- Boresight Pointing Sensor (BPS). The BPS allows enables high-precision angular metrology without high-precision pointing optics. The addition of MSTAR and BPS to the AHI turns the AHI from a static figure sensor into a dynamic formation metrology sensor.
- RF Metrology (AFF) Model. The Autonomous Formation Flying RF metrology (AFF) on each optics element receives range and phase data,

at each of 3 antennae, from Ka-band signals transmitted by each element. There are 6 one-way links for each element pair. The 6 links provide an RF truss to determine the relative position and attitude of the two elements.

The above innovations enabled us to combine primary figure sensing and formation vector metrology into a single package located on the primary figure sensor. Because only retro-reflective patches need to be mounted on other elements, this results in significant savings in terms of cost, weight and hardware complexity. A practical (realistic funding profile and prototype developments) time horizon of technology readiness for spaceflight demonstration of the identified methods and implementations described in[55] was within ten years from the current art. This is a conservative forecast and is grounded in the foundation of precursor research and development now taking place in many government and industry laboratories in the U.S. and Europe. The impact of formation flying large aperture lightweight telescopes on Earth remote sensing and astrophysics will be revolutionary, and make possible first-order observability breakthroughs at an affordable investment of national resources.

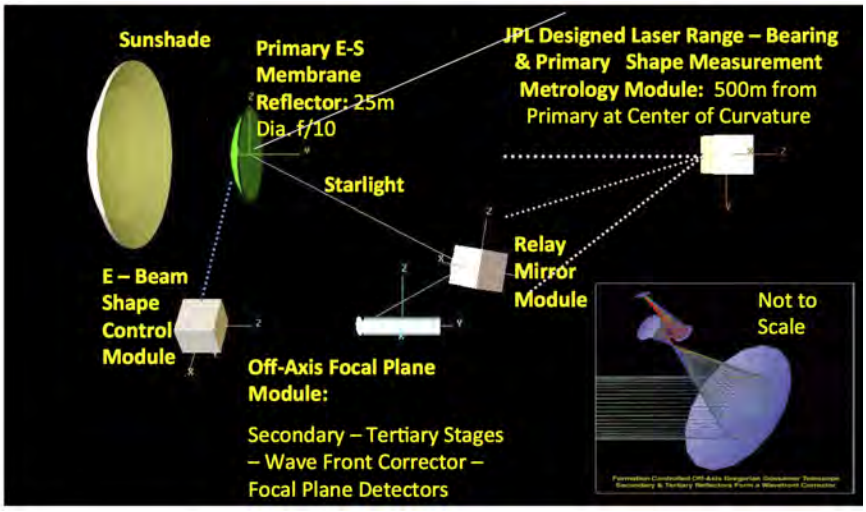

Figure 8: JPLs super-precision control of large telescopes in formation.

6.7 Laser trapped mirror

Prior NIAC work on laser-trapped mirrors[50] found that a 100-nm thick, 35-meter diameter mirror would require less than 100 grams of material, but would tend to disperse very quickly. A depiction of their concept is shown in Figure 9. They found that the laser trapped mirror could have the following advantages: lead to very large apertures, exceptionally low areal mass, self-healing properties, in-space deployment, and high packaging efficiency. They also identified the following difficulties associated with this concept: hard to deal with the lack of natural damping existing in free space, issues of laser power and coherence, their optical binding approach led to difficulties related to single fringe trapping and resistance to free space environment, and difficulties related to charging of the grains. Our multi-stage trapping and shaping approach based on optical manipulation (stable optical lift) exploits the orbital environment and system autonomy at the grain level to increase the stability and maneuverability so the cloud does not evaporate over time.

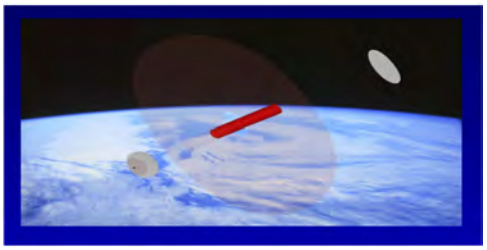

Figure 9: Liz McCormack prior NIAC laser trapped mirror.

6.8 Optics of disordered media and turbid lenses

Recently, promising developments in the optics of disordered media have been carried out. In,[79] scattering in a medium behind a lens was used to improve the focusing resolution to beyond the diffraction limit of that lens. The authors found that, surprisingly, the shape of the focus is not affected by experimental limitations of the wavefront modulator: the focus is always exactly as sharp as is theoretically possible. In Figure 10, light coming from a phase modulator is imaged on the center plane of a lens, L1 (modulator and imaging telescope not shown). The numerical aperture of the lens is

controlled by a pinhole. A CCD camera is positioned in the focal plane of the lens. (a), Clean system without disorder. Light is focused to a spot that is, at best, equal to the diffraction limit of the lens. (b), System with disorder. A disordered sample randomly changes the direction of the incident light. The scattering object can be moved to change the distance to the camera. When the incident wavefront is shaped to create a focus through the sample, the resulting focus is sharper the best focus the lens can create without disorder. Disordered scattering has been applied to improve resolution and bandwidth in imaging and communication with ultrasound, radio waves and microwaves[5, 16, 17], and significant sub-wavelength effects have been demonstrated [18]. The results in[79] were the first demonstration that similar resolution improvements can be obtained in photonics. Calculations[21] indicate that useful optical superresolution can also be achieved using disordered plasmonic nanostructures.

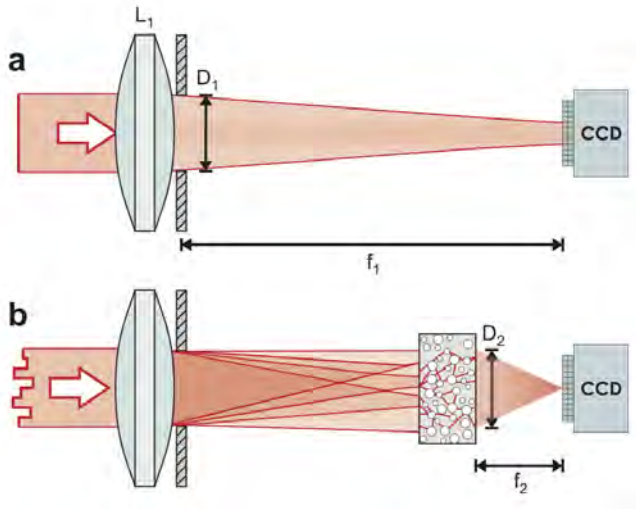

Figure 10: Disordered lenses: scattering in a medium behind a lens can be used to improve the focusing resolution to beyond the diffraction limit of that lens.

In,[18] the authors demonstrated that turbidity both improves the spatial resolution of an objective lens beyond its diffraction limit and extends its field of view. This is called Turbid Lens Imaging (TLI). These two improvements result from the angular and spatial spread of light by multiple scatterings

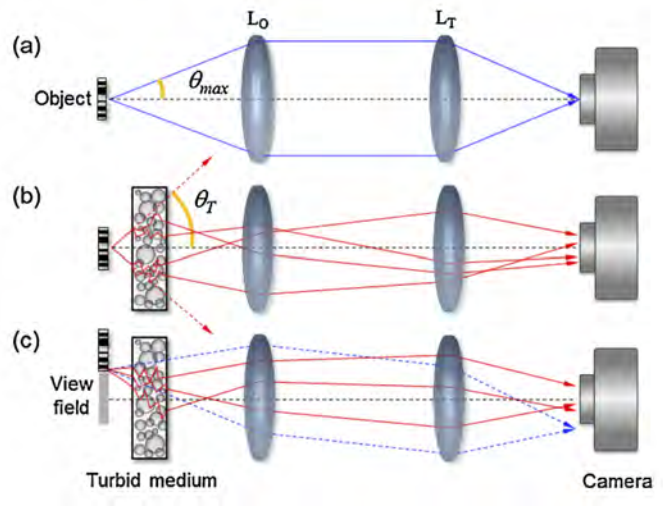

Figure 11: Turbid Lens Imaging: the turbid lens can perform wide-area imaging, rather than focusing a beam, with dramatically improved spatial resolution and an enlarged field of view.

in a disordered medium. Figure 11 shows (a) conventional imaging with an objective (LO) and a tube (LT) lenses. θ_{max} is the maximum angle that the object lens can accept. (b) Scattered wave whose angle θ_T exceeding θ_{max} can be captured after inserting a disordered medium. (c) The scattered waves reach the camera sensor through multiple scattering process (solid red lines), although the object is shifted away from the conventional field of view (gray area). The development of TLI to exploit multiple scattering allows a turbid medium to become a unique lens with counterintui- tive imaging properties. This work is an important step beyond previous studies that used a turbid medium to achieve subdiffraction focusing in ultrasound and optics and near-field focusing with microwaves.[19] Our work uses turbid media to achieve subdiffraction imaging, not focusing. We open a way to convert a random medium into a superlens with no need of any metamaterial by using the fact that disordered media with structures finer than a wavelength can capture evanescent waves.

7 Limitations of Related Current Approaches

In this section, we identify the limitations of past work, and how we addressed those issues in our study.

7.1 Limitations related to cooling

In the past NIAC on the Laser trapped mirror, the main challenge the investigators found was related to the cloud cooling. Since most of the optical manipulation experiments are done on Earth either in air or water, there is a natural medium that can realize the cooling due to the intrinsic dissipation of the medium. In space, there is no intervening medium (except for the tenuous space plasma, which does induce cooling, but much less than air or water), hence cooling in optical binding experiments, such as those carried out in the past NIAC study, cannot be achieved. In our study, we addressed cooling via active control induced by rotating the polarization of the electromagnetic signal, so that the initially randomly rotating grains can be synchronized to the polarization rate, which is then gradually reduced to zero.

7.2 Limitations related to mass and cost of imaging system

The desired characteristics of space optical systems compared to proposed concept are summarized in Figure 12.Typically, the cost of an optical system is driven by the size and mass of the primary aperture. The solution that we propose uses a method to construct an optical system in space in which the nonlinear optical properties of a cloud of micron-sized particles, shaped into a specific surface by light pressure, allow to form a very large and lightweight aperture of an optical system, hence reducing overall mass and cost. The uniqueness and innovation of our concept lies in that: a) it would be a very lightweight system, leading to areal densities of 0.1 kg/m^2 or less, compared to 10 kg/m2 of an inflatable antenna; b) one cloud could combine with other clouds to form much larger apertures than the 6.5 meter size of the James Webb Telescope; c) would be easy to transport and deploy, not requiring structural elements; d) line-of-sight retargeting and figure control would be realized optically. These properties enable new mission architectures, and

are in contrast to current state-of-the-art systems which are limited to much smaller sizes and are quite massive.

	Desired	Proposed concept
Structure	Lightweight and no back-up structure	Structure-less
Area density	< 1 kg.m2	0.1 kg/m2 or less
Aperture size	> 10 m	Can combine multiple clouds to synthesize very large apertures
EM properties	Fixed by design	Adaptive
Stability in orbit	Gravity gradient	Optical trapping
retargeting	Minimal fuel	Optically
deployment	Mechanical,simple	Very compact
packaging	Efficient Folding for compact stowing	No mechanization

Figure 12: Desired characteristics of space optical systems compared to proposed concept.

8 Key Unknowns that we address in this Study

The plan in Phase I was to set aside top-level showstoppers, to further study the concept and determine if significant investment is warranted in Phase II. At the time of writing of this report the perceived technological risk is in the following areas:

- high levels of light scattering may be deleterious for image formation, unless a sunshade element can be used;
- it may be very challenging to provide the needed phase coherence between elements of the cloud to be able to be of any use in visible band, but may be possible in the radio or other bands;
- optical manipulation at large scales may require very large laser power, or too many lasers, hence excessive cost to implement;

- many dust clouds might create unwanted orbital debris due to leakage, hence a mitigation plan based on back-up trapping systems will be necessary;
- electrostatic charging might cause undesired aggregation and clustering that might affect the surface accuracy of the aperture.

The more detailed feasibility analysis to be conducted in Phase II will address these risks.

9 Our Innovative Approach

Our approach is a top down approach. The large scale imaging system is held in shape by means of formation flying technology. The aerosol cloud forming the primary aperture can then be thought of behaving as an equivalent rigid object. Wavefront sensing and control techniques of adaptive optics are then used to stabilize the image assuming the aerosol cloud is a monolithic aperture. Through optical manipulation technology, we control the shape and alignment of the aerosol within the envelope forming the equivalent rigid aperture Therefore, the top-down formation flying and adaptive optics approach merges with the bottom-up optical manipulation approach to achieve our goal.

Granular matter is considered to be the 5th state of matter (after solid, liquid, gaseous, and plasma) by virtue of its peculiar response characteristics (cohesiveness, fluid behavior, compactification, phase transformation capability, and others,[78],[24],[25] and[41]). However, it is a fact that the dynamics, controllable properties, and consequent benefits of engineering and manipulating granular matter such as dust grains, powders, and aerosols is poorly known to the space exploration community. Inspired by the light scattering and focusing properties of distributed optical assemblies in Nature, such as rainbows and aerosols,[41] and by recent laboratory successes in optical trapping and manipulation, we propose a unique combination of space optics and autonomous robotic system technology, to enable a new vision of space system architecture with applications to ultra-lightweight space optics and, ultimately, in-situ space system fabrication. This research will leverage the expertise developed in autonomous space systems technology at NASA/JPL (specifically, formation flying for astrophysical imaging[55]), adaptive optics of astrophysical space borne observatories such as Spitzer Space Telescope, SIM

Planetquest, Terrestrial Planetfinder, and the James Webb Space Telescope,[1] and recent achievements in optical manipulation at Rochester Institute of Technology on optical trapping,[75] to investigate the possibility of deploying, focusing, retargeting the cloud in space, and adding autonomy to the cloud of particles in order to produce an adaptive optics light collector. Typically, the cost of an optical system is driven by the size and mass of the primary aperture. The solution that we propose is to construct an optical system in space in which the nonlinear optical properties of a cloud of micron-sized particles are shaped into a specific surface by light pressure, allowing it to form a very large and lightweight aperture of an optical system, hence reducing overall mass and cost.

10 Summary of Research

In this section, we summarize our progress in the areas of cloud physics and cloud engineering.

10.1 Cloud Physics

10.1.1 Granular spacecraft

We present some ideas regarding the engineering and control aspects of granular spacecraft. *Granular spacecraft* are complex multibody systems composed of a spatially disordered distribution of a large number of elements, for instance a cloud of N grains in orbit, with $N > 10^3$. We address the modeling and autonomous operation of a distributed assembly (the cloud) of large numbers of highly miniaturized space-borne elements (the grains). A granular spacecraft can be defined as a collection of a large number of space-borne elements (in the 1000s) designed and controlled such that a desirable collective behavior emerges, either from the interactions among neighboring grains, and/or between the grains and the environment. The ultimate objective would be to study the behavior of the single grains and of large ensembles of grains in orbit and to identify ways to guide and control the shape of a cloud composed of these grains so that it can perform a useful function in space, for instance, as an element of an optical imaging system for astrophysical applications. This concept, in which the aperture does not need to be continuous and monolithic, would increase the aperture size several times compared to large NASA space-borne observatories currently en-

visioned such as ATLAST, allowing for a true Terrestrial Planet Imager that would be able to resolve exo-planet details and do meaningful spectroscopy on distant worlds. To accomplish this goal, we need to investigate the conditions to manipulate and maintain the shape of an orbiting cloud of dust-like matter so that it can function as an ultra-lightweight surface with useful and adaptable electromagnetic characteristics. Consider the following scenario, shown in Figure 1: 1) the cloud is first released; 2) it is contained by laser pressure to avoid dissipation and disruption by gravitational tidal forces, 3) it is shaped by optical manipulation into a two-dimensional object (coarse control), and 4) ultimately into a surface with imaging characteristics (fine control). The cloud shape has to be maintained against orbital disturbances by continuous figure control, also achieved optically. Applying differential light pressure retargets the entire cloud, so that a change of the optical axis can be induced. Selected parts of the cloud are reshaped when required for wavefront control, thus enabling higher quality optics. The entire imaging system is now in full operation, as 5) a multilens system searching for exo-planets, or 6) as a radio receiver engaged in remote sensing investigations. The potential advantages of the granular spacecraft concept are that: a) it can result in an ultra-lightweight system, made of very simple, very low cost, units; b) it can be very big: the cloud can distribute itself to kilometer scales, without the need to fill the aperture; c) the cloud is easy to package, transport and deploy; d) it is reconfigurable, and can be retargeted and repointed with non-mechanical means; e) the cloud is a highly fault-tolerant system with very low vulnerability to impacts. Other potential advantages offered by the cloud properties as optical system involve possible combination of properties (combined transmit/receive), variable focal length, combined refractive and reflective lens designs, and hyper-spectral imaging.

The study of clouds of assets as *granular spacecraft* involves different disciplines, some of which are outlined in Figure 13: gravito-electrodynamics, optics, laser-matter interaction, disordered and distributed systems, multi-scale simulation, formation-flying, granular media, and plasma physics, among others. Some of these disciplines are discussed in this section.

The physical behavior of granular spacecraft is more challenging than modeling of conventional space-borne vehicles because we are faced with a probabilistic vehicle composed of a large number of physically disconnected vehicles.

Three spatial and temporal domains can be identified:

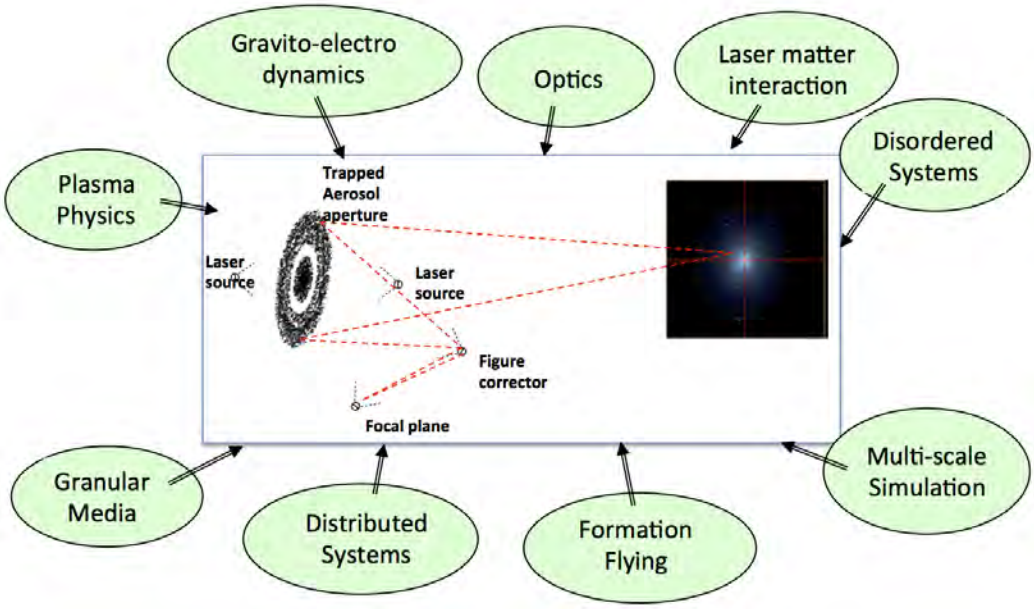

Figure 13: Multi-disciplinary elements of problem.

- micro-, at the scale of the individual vehicle;
- meso-, at an intermediate scale within the cloud; and
- macro-, at the scale of a very large number of grains.

First, different scales of motion occur simultaneously in a cloud: translations and rotations of the cloud as a whole (macro-dynamics), relative rotation and translation of one cloud member with respect to another (meso-dynamics), and individual cloud member dynamics (micro-dynamics). There exist at least two time scales, as well as at least two space scales, in the description of the dynamics of a cloud. The dynamics of an individual vehicle begin to emerge when the time scale of a stimulus (internal or external to the cloud) is smaller than the time scale representative of the cloud dynamics itself. Similarly, in the opposite case the cloud behavior as an integrated unit is predominant. This behavior affects the stability of the system as cloud cohesiveness depends on the internal space and time scales. Furthermore, these effects become more complicated and nonlinear when the cloud undergoes large reconfigurations, both in relative translation and in attitude with

respect to a reference configuration. These systems also display both a local and a non-local aspect. The local aspect pertains to the near-collocation represented by a sensor and an actuator located on the cloud. The non-local aspect appears when a sensor located on one end of the cloud feels the effect of an actuator mounted on another one at a different location. Second, the control design needs to be tolerant of the system complexity, of the system architecture (centralized vs. decentralized large scale system control) as well as robust to un-modelled dynamics and noise sources. Optimized sensor locations and robust dynamics estimation schemes are required to achieve full knowledge of the states of the system within a significant cluster of individual grains. Additionally, information processing on a granular spacecraft is inherently distributed by nature. Modeling of a cloud cannot dispense with the need to appropriately model the latencies and bandwidth limitations associated with inter-cloud communications. Single vehicle applications are immune to such considerations. Simulation of a cloud must also address a large range of spatial and temporal scales, which intrinsically make the problem numerically stiff in nature. It is in effect a multiple-scale problem, a solution to which will require a new class of numerical algorithms with special demands on accuracy, stability, and provision for coexisting multiple time scales. Table 1 shows a comparison of various requirements for simulation of single spacecraft vs. granular spacecraft, indicating the high degree of complexity that needs to be taken into consideration.

Figure 14 shows the different spatial and temporal scales involved in the system. While the micro-, meso-, macro-scales affect the spatial frequency distribution, depending on the disturbance frequency various parts of the system are excited differently. Furthermore, to be useful as an engineering system, the various control bandwidths of interest must be considered at the orbital level, grain level, and cloud level.

Figure 15 depicts some of the modes of motion of these types of systems. Macro-translations, macro-rotations, macro-deformations, micro-rotations, and micro-deformations all contribute to the dynamics.

Figure 16 shows a comparison of requirements for simulation of single spacecraft vs. granular spacecraft.

Figure 17 shows two possibilities of boresight retargeting and adaptive wavefront control of the cloud, which involve macro- and micro- motions, respectively.

From the point of view of modeling the system, two main problems are identified. First, the Direct Problem, in which given the individual cloud el-

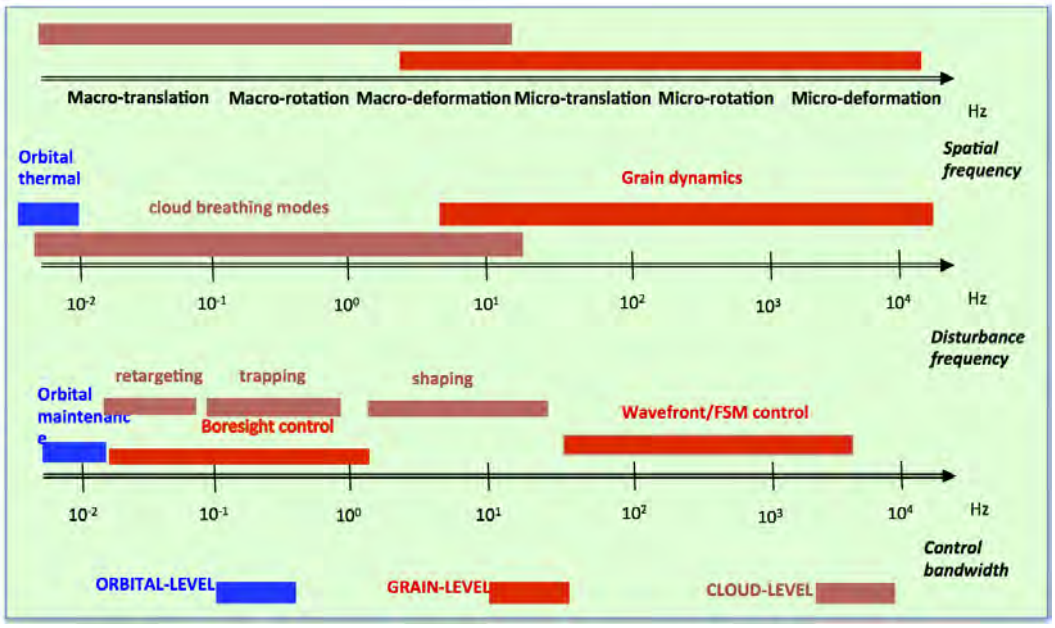

Figure 14: Spatial, temporal, and control scales involved in the granular spacecraft problem.

ements, interconnectivity dictated by communication constraints, and local potential functions describing the interaction (or collision avoidance constraint) between adjacent elements, predict the global motion of the cloud and control it according to an optimality criterion. Second, the Inverse Problem: given a desired trajectory for the cloud, determine the interconnectivity and local potential functions between adjacent elements of the cloud that result in the desired motion. In this report we deal only with the Direct problem.

By means of micro-continuum field theory,[7],[22] we can unify the deformation and dynamics modalities of a cloud. We use continuum mechanic constructs for this analysis. Each individual grain is endowed with a position vector, a rotation tensor, and a deformation gradient tensor, in the spirit of micromorphic kinematics. This means that each individual grain is capable of changing its configuration in response to stimuli originated either from the exterior of the cloud or within the cloud itself. The cloud is therefore treated as a continuum at the macroscopic level, with added extra

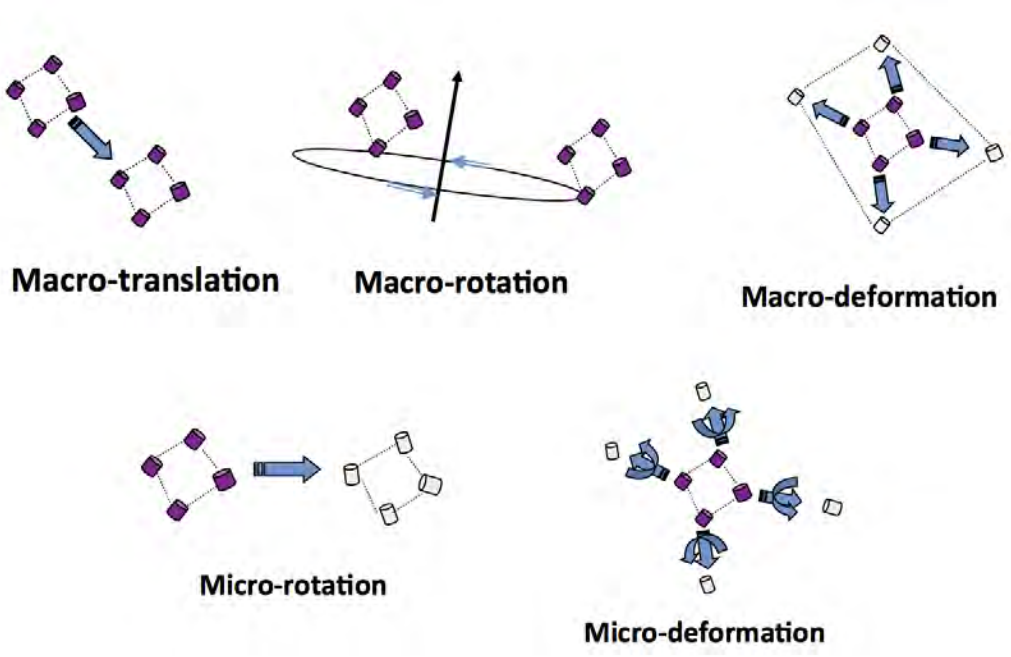

Figure 15: Modes of motion of granular spacecraft.

structure at the micro-continuum, or particle, level. A set of balance laws for the cloud can then be derived, assuming invariance of the cloud energy functional to translations and rigid rotations. These balance laws include the conservation of the cloud mass, the balance of cloud linear momentum, the balance of macroscopic cloud angular momentum and of particle angular momentum, the cloud entropy inequality, and the boundary conditions at the boundary of the cloud. The description of the internal constitution of the cloud, i.e. the constitutive relation between internal reconfiguration kinematic variables (strains) and internal reconfiguration momenta, completes the mechanical description of the cloud. The internal reconfiguration momenta represent the generalized inertia and the generalized stresses that the individual grain experiences when a reconfiguration is taking place. The constitutive functional includes memory dependent terms and nonlocality in the cloud response,[?].[38] That this must be included stems from the fact that the behavior of the cloud can be influenced both at the system level and at the individual grain level. Therefore, two time scales enter the picture, as

	Single SC	cloud
Propagation model	Serial	Distributed/parallel
Workspace volume	Small	Very large
Input data structure	Small	Very large
Output data structure	Small	Very large
Significant digits	Many	few
Spatial scales of motion	Orbital/attitude/flex	Orbital/micro/meso/macro
Temporal scales of motion	Orbital/attitude/flex	Orbital/micro/meso/macro
Disturbance frequency	Orbital period	Orbital/micro/macro
Controller bandwidth	ACS+DV	ACS+DV+reconfiguration +containment
Computation on GPU	Not needed	Recommended

Figure 16: Comparison of requirements for simulation of single spacecraft vs. granular spacecraft.

well as two space scales. The individual grain dynamics begins to emerge when $(\lambda/L)1$, where λ is the time (or space) scale of the stimuli internal or external to the cloud, whereas L is a time (or space) scale representative of the cloud itself. When $(\lambda/L) << 1$, the individual grain behavior is predominant, and when $(\lambda/L) >> 1$, the cloud behavior as a unit is predominant. The spatial nonlocality occurs since one grain may respond to stimuli from another grain located far away from it in the cloud, and it occurs also at a global level, since each grain may respond to stimuli of the cloud as a unit. This multilevel behavior is reflected in the nonlocal constitutive functional. Memory dependence, also known as time nonlocality, enters the constitutive functional through time dependence of the current instant from previous instants. Since both the target location knowledge and the physical grain (and sensor) locations are stochastic in nature, we use the concept of random fields to set up an equivalent boundary value problem in the time domain where the coefficients of the differential operator are random processes. A description of the cloud dynamics within the spatial domain can then be cast as a boundary value problem as.[28]

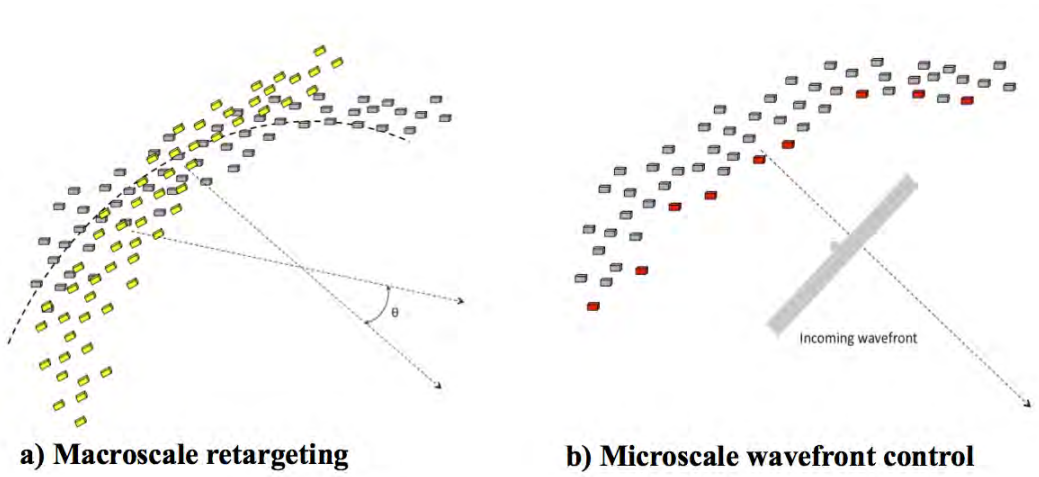

Figure 17: Possibilities of boresight retargeting and adaptive wavefront control.

$$[B(x,t) + G(x,t;\omega)]u(x,t;\omega) = f(x,t;\omega) \tag{1}$$

together with the appropriate boundary conditions at the boundary of , where x is the spatial scale, t is the temporal scale, ω is a random fluctuation, B is the deterministic operator describing the dynamics, G is the stochastic part whose coefficients are zero-mean random processes, and f is the vector of exogenous and control inputs. It is clear that, depending on the connectivity between the elements of the cloud, the B and G operators may be local or nonlocal operators derived from variational principles expressed in their weak form. This approach ensures a robust mathematical formulation since the stochastic nature of the states is reflected in the stochastic nature of the differential operators.

10.1.2 Forces acting on cloud

To address the engineering applications, we need to have insight on physics of disorder systems and the dominant forces that perturb the cloud. Related background can be found in refs,[41],[60].[78] Cloud gravito-electrodynamics leads to self-organization: for a cloud of particles released from an orbiting vehicle,

the diffusion characteristics are important, as well as the tendency to form natural ring-like structures governed by the local gravity gradients, solar pressure, and radiation properties of each individual grain. The electrodynamic Lorentz coupling in LEO-GEO provides high degree of structural coherence which can be exploited in applications. Once illuminated, the diffraction pattern from a disordered assembly leads to a strong focusing potential: the intensity of the signal is more collimated when the distribution of apertures is randomized, the separation between apertures increases, and the number of apertures increases. Focusing is achieved by modulating the phase of the distributed radiators so as to obtain a conic phase surface, and this leads naturally to the shaping a cloud in the form of a lens. In summary, in space the cloud behavior depends on the dynamic balance of different force fields:

- Laser light pressure, as light can induce motion;
- Solar illumination radiation pressure, which carries momentum;
- Gravitational forces and gradients, resulting in orbital and tidal effects;
- Electrostatic Coulomb or dielectrophoretic forces, since the grains are charged;
- Electromagnetic Lorentz forces resulting from the interaction with local magnetic field;
- Cloud self-gravity caused by the cloud being an extended body;
- Poynting-Robertson drag, in which grains tends to spiral down towards the Sun; and
- Yarkovstky (YORP) effect, caused by the anisotropic emission of thermal photons, which carry momentum.

Figure 18 describes some of the forces that are involved in this problem, and their relevance either as a disturbance or as a control mechanism.

In the next sections, we describe the gravito-electrodynamics coupling, and the opto-mechanical interaction.

Force	Expression	Relevance
Gravity	$m_d g = (4\pi/3)a^3 \rho g$	Can be used to align cloud.
Electromagnetic	$Q_d E$	Can be used to levitate dust.
Neutral drag	$u_d >> v_T$ $F_{nd} = \pi a^2 \rho_g m_n u_d^2$ $u_d << v_T$ $F_{nd} = m_d u_d \left(\delta \frac{8\sqrt{\pi}}{3} a^2 \rho_g \frac{m_g}{m_d} v_T \right)$	Dissipative.
Thermophoretic	$F_{th} = \frac{4\sqrt{2\pi}}{15} \frac{a^2}{v_T} \kappa \nabla T$	*Arises if there is a temperature gradient in the neutral gas. It is due to the asymmetry in the momentum transfer to dust from neutrals and is directed toward lower gas temperatures. This force can be used to levitate particles against gravity.*
Ion drag	$F_{id} = n_i m_i u_i u_s \pi \left(b_c^2 + 4\Lambda b_{\pi/2}^2 \right)$	*Arises from the momentum transfer from flowing ions to charged microparticles in a plasma. Sum of* collection force due to ions impinging on grain and orbit force due to ions deflected by graiins.

u_d = dust velocity, v_T = gas thermal speed, ρ = grain density, ρ_g = gas density, δ=scattering coeff., κ=thermal conductivity of gas, u_i=ion drift speed, u_s=mean ion speed, b_c=collision impact parameter, b_{90}=impact parameter for 90 deg. Collisions, Λ=function of Debye length and collision parameters.

Figure 18: Examples of forces acting on cloud.

10.1.3 Cloud Gravito-electrodynamics

Gravito-electrodynamics,[40] and[12] refers to the interaction between a gravitational field and an electromagnetic field. To gain some insight into the physics of the problem, we can for the time being consider the dynamics of one grain and of a collection of grains separately. The equation of motion of one grain around planet rotating at p:

$$\ddot{\mathbf{r}} = -\frac{\mu \mathbf{r}}{\mathbf{m}|\mathbf{r}|^{\mathbf{3}}} + \frac{\mathbf{Q}(\mathbf{r})}{\mathbf{mc}}[\dot{\mathbf{r}} \times \mathbf{B}(\mathbf{r}) - (\mathbf{\Omega_p} \times \mathbf{r}) \times \mathbf{B}(\mathbf{r})] + \mathbf{F}(\mathbf{r}) \tag{2}$$

from which the resulting natural frequencies are

$$\Omega = \frac{\Omega_B}{2}\{1 \pm [1 + 4(\frac{{\Omega_K}^2}{{\Omega_B}^2} - \frac{\Omega_p}{\Omega_B})]^{\frac{1}{2}}\} \tag{3}$$

where Ω_B is the plasma gyro-frequency, Ω_p is the planet rotation rate, and Ω_K is the Keplerian frequency, indicating that gravity, electromagnetic fields are coupled and interact with local plasma.

As an example, consider a one-dimensional cloud. Consider the simple case of circular orbit with $R_o = (0, 0, R_o)F_o$ and $\Omega_o = (\omega_0, 0, 0)F_o$. The components of the gravitational gradient tensor are $\Gamma_1 1 = -{\omega_0}^2$ and $\Gamma_3 3 = 3{\omega_0}^2$, which imply that the motion along x (along normal to orbital plane) is compressive, the motion along y (along velocity vector) experiences no force, and the motion along z (along local vertical) is tensile. This is shown in Figure 19.

10.1.4 Dusty plasmas

If we want to thoroughly understand how the aerosol cloud behaves in space, we need to understand the interaction of the grains with the local space plasma environment, i.e. the physics of the resulting dusty plasma. A dusty plasma,[80],[40] and[58] is a system of particles suspended in a background plasma. This is shown in Figure 20. Sometimes called a complex plasma, the particles are typically tens of micrometers or smaller and are charged. This results in a variety of fascinating phenomena that can be observed with a simple CCD camera or even the naked eye. Dusty plasmas are found in space (comets, planetary rings, as shown in Figure 21), are a concern in fusion plasmas, and are considered an important impurity that must be controlled in plasma processing. Dusty plasmas are interesting[83] because the presence of particles

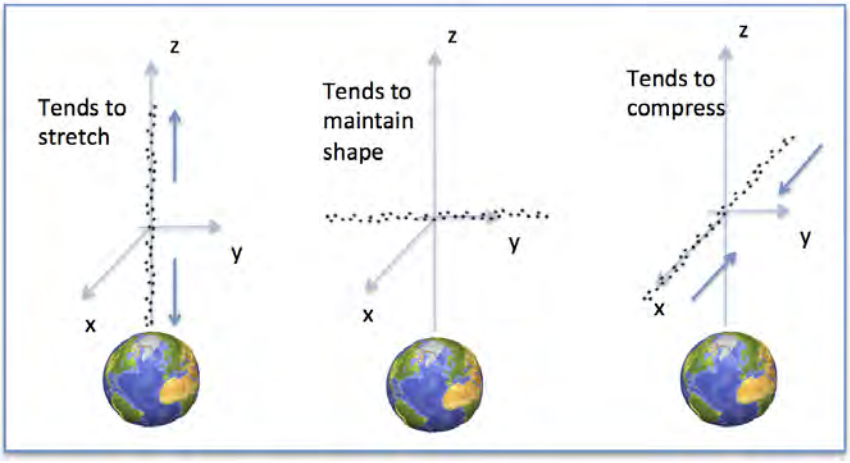

Figure 19: Effect of gravity gradient on linear cloud.

significantly alters the charged particle equilibrium leading to different phenomena. It is a field of current research. Electrostatic coupling between the grains can vary over a wide range so that the states of the dusty plasma can change from weakly coupled (gaseous) to crystalline. Such plasmas are of interest as a non-Hamiltonian system of interacting particles and as a means to study generic fundamental physics of self-organization, pattern formation, phase transitions, and scaling. The interaction between a dust grain and the surrounding plasma is an extremely complicated two-way process. For instance, an obvious manifestation of this interaction is the charging of the dust grain, which happens very rapidly. The charge depends on the fluxes of ions and electrons from the plasma onto the grain surface, and those fluxes, in turn, depend on the charge. Furthermore, the charged grains will modify their plasma environments by, for instance, setting up space charges and electrostatic fields. Regarding the strength of the various forces (gravitational, electric, thermophoretic, ion drag) acting on a dusty plasma, for micron-sized dust particles, the dominant forces are gravity and electric field force. The ion drag force is smaller than the electric field force and gravity under the chosen conditions. For dust particles well above 1 micron in diameter and with small temperature gradients only electric field force and gravity are important. For nanometer-sized dust particles gravity is negligible, as is for micron-sized dust under microgravity conditions. Then, ion drag force becomes the dominant

force which has to be balanced by the electric field force. Depending on the relative strength of the Coulomb energy vs. the thermal energy (the coupling parameter) and of the mean particle separation vs. the plasma Debye length (the structure parameter), very regular structures of macroscopic size can be generated with enormous potential for space applications. There are the "plasma crystals". Dusty Coulomb Crystals are highly organized structures with great potential for aerosol optics. Some experimental results relevant to this research are shown in Figure 25. In typical laboratory experiments on fundamental aspects of colloidal plasmas monodisperse spherical particles of 1 to 10 micrometer diameter are trapped in gas discharges. Figure 22 shows the components of a dusty plasma confinement device, where the thermophoretic force,the electric field force, and the gravitational force interact to form regular structures. The microspheres attain high negative charges of the order of 10^3 to 10^5 elementary charges due to the inflow of plasma electrons and ions. Due to the very low charge-to-mass ratio the spatial and time scales for particle motion are ideal for studying the dynamics of complex plasmas by video microscopy, e.g. interparticle distances are of the order of hundreds of microns, typical frequencies of the order of a few Hertz. Due to the high charges the electrostatic potential energy of the dust particles by far exceeds the thermal energy of the microspheres which are effectively cooled to room temperature by the ambient neutral gas: the system is said to be strongly coupled. The strong-coupling regime is hardly reached in ordinary plasmas. In colloidal plasmas, the dust particles can arrange in ordered crystal-like structures, the plasma crystal,[2],[54] and.[81] Figure 23 shows a detail of a regular configuration arising in a typical confined dusty plasma, and Figure 24 shows a photograph of a Yukawa ball. As we have seen above, typically, the cost of a space observatory is driven by the size and mass of the primary aperture. Generally, a monolithic aperture is much heavier and complex to fabricate (hence more costly) than an aperture of the same size but composed of much smaller units. Formation flying technology, as applied to swarm systems in space, is an emerging discipline, and we want to explore the potential of using formation flying technology as applied to swarms of grains in space to realize large apertures in space. In close proximity to the Earth, the interaction of the grains with the ambient plasma becomes a dominant effect. Hence, the solution that we propose uses a method to construct an aperture in space in which the nonlinear optical properties of a cloud of micron-sized particles, shaped into a specific surface through the interaction of light pressure, electromagnetic confinement fields, and the properties of the

local ambient plasma, allow to form a very large and lightweight aperture of an imaging system, hence reducing overall mass and cost. We envision a disk of the order of centimeter or more in diameter composed of small micron-sized grains locked into a plasma crystal via electromagnetic fields. More disks can be held together in formation, for example in a Golay array, to form a larger segmented aperture. Modulations of the confining electromagnetic field would be use to control coarse rigid body motions of the disk, for instance, piston, tip, and tilt of the disk, and retargeting of the line-of-sight. Optical manipulation technology, using laser beams, would be use for fine control within the disk, to correct for optical figure aberrations and for precise wavefront control. Formation flight technology would be used for sensing and control of the entire group of disks to remain tightly aligned to form a precise optical figure (spherical, paraboloid). Reflective, refractive, or diffractive imaging architectures are possible, depending on the properties of the grains (reflective, refractive). Since a granular medium in space is tightly coupled to the local plasma, the "cloud" of grains becomes a dusty plasma. As discussed above, dusty plasmas have self-organizing properties, and can form very regular arrangements of the grains which are easy to reproduce in the lab and in space, and very promising to form macroscopic structures in space. Examples are centimeter-sized Coulomb crystals, Yukawa balls, and similar regular crystalline structures which result from the balance between the charged micron-sized grains and the electric or magnetic potentials used to confine these structures in a volume where an ionized gas (a plasma) exists. Figure 26 shows a candidate architecture of a multi-scale aperture (f) in which the "segments" (c,d) of the "segmented aperture" (e) are composed of collections (c) of confined plasma crystals (b), held together by an appropriate confining device (a). More details of this novel application of dusty plasmas to synthesize apertures for NASA missions will be developed in Phase II.

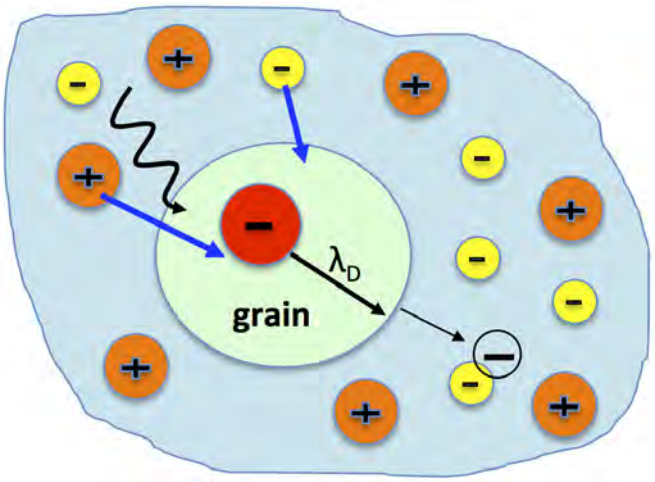

Figure 20: Components of a dusty plasma.

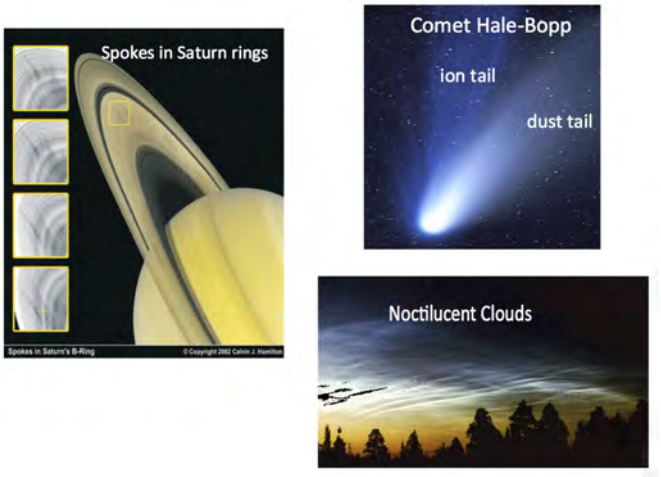

Figure 21: Dusty plasmas in Nature.

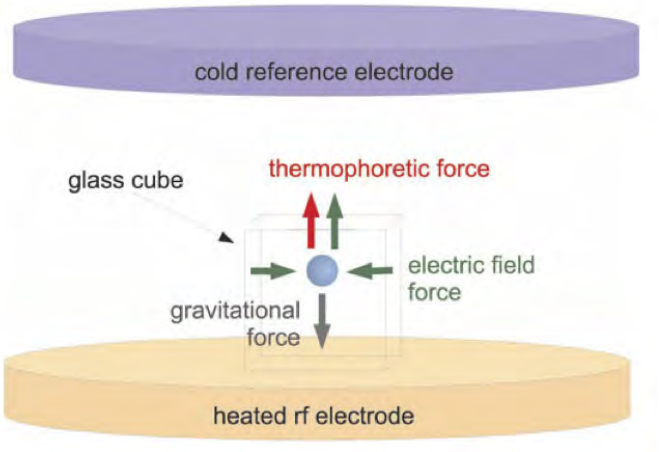

Figure 22: Components of a dusty plasma confinement device.

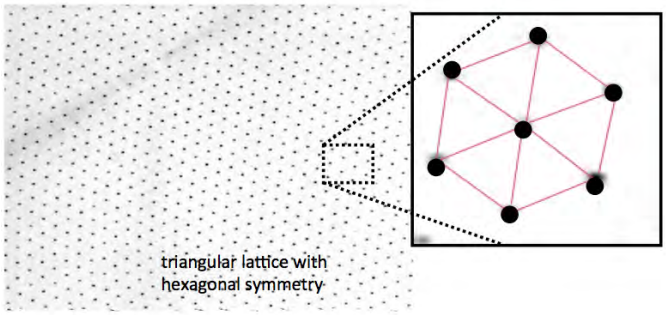

Figure 23: Regular configuration arising in a confined dusty plasma.

Figure 24: Example of a dusty plasma Yukawa ball.

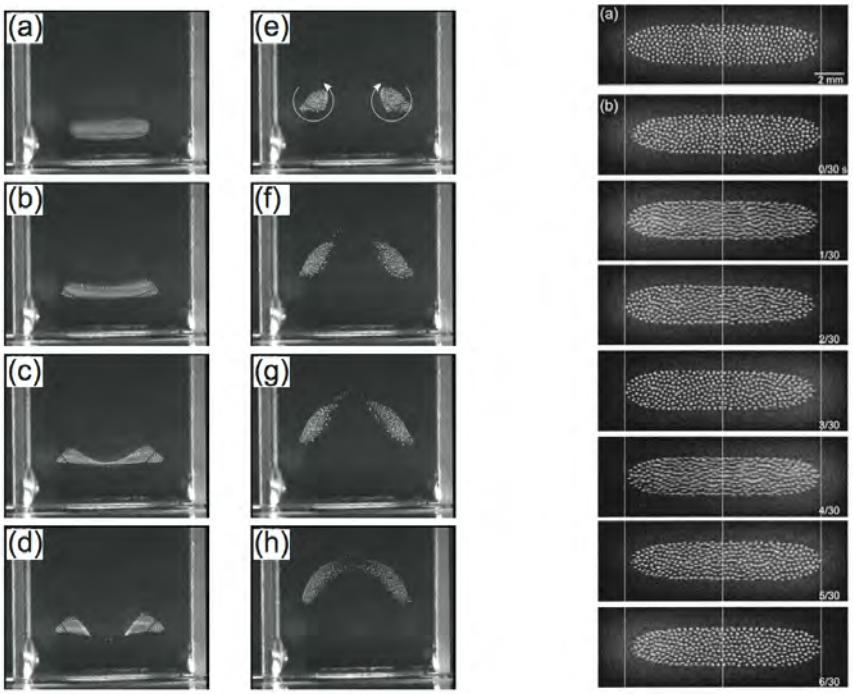

Figure 25: Example of large scale electrostatically confined dusty plasma cloud.

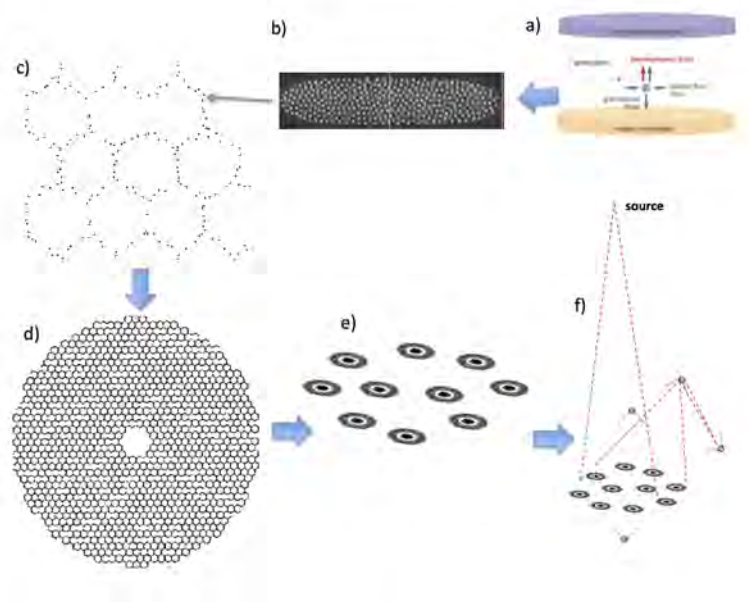

Figure 26: Example of synthesizing a multi-scale aperture from a cloud of confined dusty plasma.

10.1.5 Cloud Optics

In this section, we address the optics of granular assemblies in space.

The diffraction pattern from disordered assembly leads to a strong focusing potential. For some applications, the synthesis of large apertures made of large numbers of emitters/receivers placed with structural disorder is desirable.[14] Figure 27 is taken from Born and Wolf, and shows the comparison of the diffraction pattern between a regular and a random array. The random array shows a much more collimated central lobe, which implies the ability to focus more than the regular array. For a disordered array, focusing of the antenna is achieved by modulating the phase of the distributed radiators so as to obtain a conic phase surface. It was observed that the side lobes are suppressed by randomizing the emitter positions, and that the amplitude of far side lobes is inversely proportional to the number of the emitters. For these type of distributed systems, the intensity of the signal is more collimated when the distribution of apertures is randomized, the separation between apertures increases, or the number of apertures increases. Array configurations having irregular instead of periodic inter-element spacing have been discovered to have many useful properties:

- Interferometer lobes, or multiple periods of the periodic diffraction pattern appearing in the visible range, which are an inevitable consequence of the periodic array, are suppressed;
- Aperture dimensions can be realized with large number of radiators N on the basis of the periodic spacing;
- Focusing of the antenna is achieved by modulating the phase of the distributed radiators.
- Array properties such as side lobe levels persist over broader frequency ranges and are less sensitive to phasing errors than periodic arrays spatially tuned to one wavelength.
- The incentive to investigating thinned (sparse and disordered) arrays was the discovery of the fact that the removal of very large numbers of elements not only left the array performance virtually unaffected at the design wavelength, but extended the usable frequency range by suppressing the grating lobes present in a periodic lattice, with

the advantage of less elements and less coupling due to greater inter-element spacing.

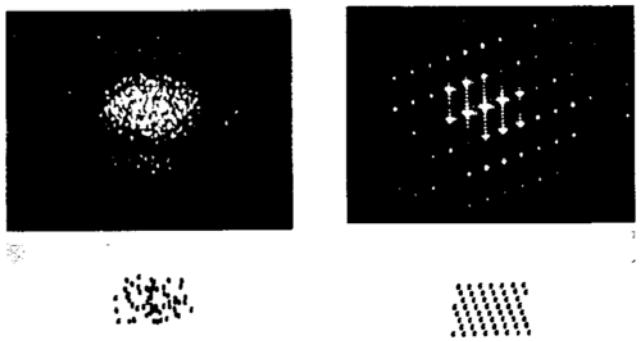

Figure 27: Effect of randomness on diffraction pattern.

Figure 28 shows a simulated raw image of an exo-earth at 10 light years, using a 150 apertures regularly distributed over 150 km. This image is taken from Labeyrie's book,[46] and shows the troublesome surrounding halo around the central lobe in the diffraction pattern of the regular, circular array. Figure 29 shows the optical point spread function for 20 randomly spaced circular apertures of diameter D within a circle of radius 20D, again showing the beneficial effect of randomness in removing the troublesome halo.

In Figure 30, we compare the Optical Transfer function and Modulation transfer function for a filled aperture (top) and a cloud aperture (bottom), confirming the presence of the halo around the central lobe, of much higher intensity.

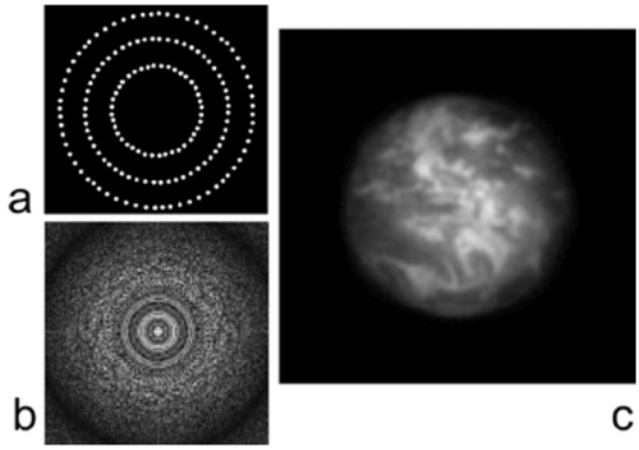

Figure 28: A simulated raw image of an exo-earth at 10 light years, using a 150 apertures regularly distributed over 150 km.

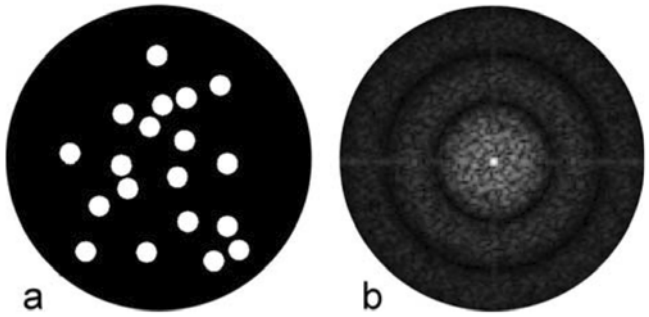

Figure 29: Point spread function for 20 randomly spaced circular apertures of diameter D within a circle of radius 20D.

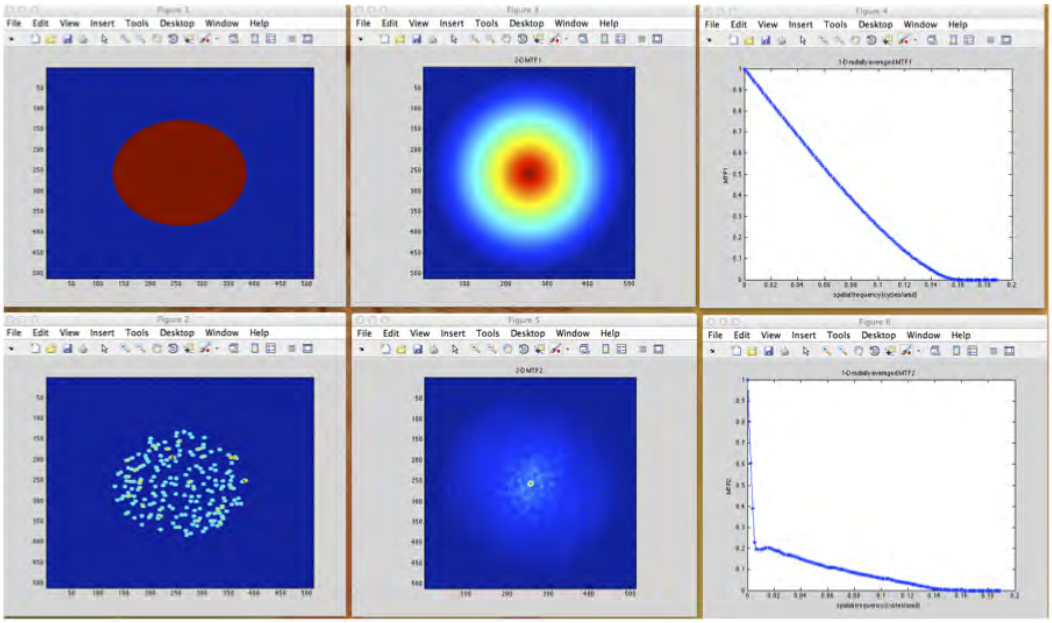

Figure 30: Comparison of Optical Transfer function and Modulation transfer function for filled aperture (top) and cloud aperture (bottom).

The use of a distribution of micron to millimeter-size spheres as a nonlinear optical medium is most easily accomplished in the absence of gravity, where the forces from the optical fields themselves at saturation power levels can provide a volumetric potential well capable of confining the cloud to a fixed region of space. In a 1-g field, levitation of the cloud can be easily accomplished either via suspension in an upward-directed flow field of a viscous medium, or by electrostatic or magnetic levitation. In space, the application of a cloud of dielectric (glass) spheres to the construction of large optical collectors/reflectors relies on the dynamic balance of laser light pressure, solar radiation pressure, gravitational forces and gradients, cloud self-gravity, and dissipation forces such as Poynting-Robertson drag. In space, the cloud will acquire the shape of the first fringes of the standing surface wave generated by two interfering counter-propagating coherent laser beams. Laser radiation pressure locks the granular material onto one of the nodal surfaces of constructive interference. Ideally, the dielectric particles should have 50% transmissivity and 50% reflectivity, no absorption, and to avoid diffraction they must be smaller than the wavelength of light. This giant, but tenuous, optical assembly has to be maintained either continuously or intermittently via separated free-flying pulsed lasers, which must have enough power, continuous operation capabilities, and adequate pointing capability to maintain the cloud stably in orbit. As shown in Figure 1, a multiple aperture collector/corrector could be used to reduce positioning requirements on the cloud utilizing multi-scale lens design.[15] This would have the additional benefit of increased field-of-view of the optical system and allow for less movement of the cloud when changing the line of sight of the system. Controlling the polarization of light may be one of the means to produce differential rotation in the particles in order to improve the reflectors surface accuracy, ultimately enabling precision optical applications.

10.1.6 Opto-mechanical Interactions at grain level

In,[3],[4],[5] a three-dimensional gradient-force optical trap for microscopic dielectric particles was demonstrated in 1986. They showed that low-absorbing, dielectric spherical particles with an index of refraction higher than that of a surrounding liquid could be trapped in three dimensions by use of a strongly focused Gaussian laser beam. This phenomenon was suggested earlier for moving atoms and more recently has led to biomedical and related applications involving micromanipulation of living cells, chromosomes, and motor

proteins. However, the conventional gradient-force trap based on the design of,[3],[45] has some limitations. Trapped particles are susceptible to optical damage by absorptive heating because the center of the trap is located in the high-intensity focal region of the beam. Another limitation is that multiple particles may be attracted into the same trap; thus isolating a single particle requires dilute samples. Furthermore, the trapping of low-index particles such as bubbles and droplets or of absorbing particles such as metallic fragments requires a rotating beam when a conventional gradient-force trap is used. To circumvent such limitations various schemes have been proposed, including the use of higher-order Gaussian mode beams and unusually shaped particles, but the most promising one is the trapping of low index particles with an optical vortex,[75].[74]

Generic particles illuminated by a Gaussian laser beam experience two optical forces: a scattering (levitation) force and a gradient force. The gradient force on a Rayleigh Particle ($r << \lambda$) can be written as:

$$F_{grad} = -\frac{1}{2}\alpha(\nabla E)^2 = \frac{4\pi\alpha}{c}\nabla I \tag{4}$$

where

$$I = (c/8\pi)|E|^2 \tag{5}$$

is the laser irradiance, and the polarizability is

$$\alpha = r^3(\frac{n^2-1}{n^2+2}) \tag{6}$$

The scattering force can be written as

$$F_s = \frac{I\sigma}{c} \tag{7}$$

with

$$\sigma = \frac{8}{3}kr^4(\frac{n^2-1}{n^2+2})^2\pi r^2 \tag{8}$$

where n is the refractive index, λ the wavelength, and $k = 2\pi/\lambda$. For a particle of any size and shape, the electromagnetic energy is minimized when the particle is in the brightest region of the beam, as shown in Figure 32.

Figure 31 show the type of particle that we are considering in this study. One side is highly reflective, and one side id convex, to enable the gradient force to act more effectively.

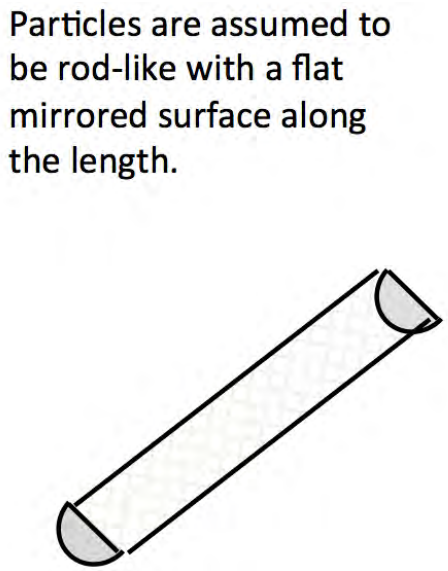

Figure 31: Grains considered in this study.

A spherical particle in the presence of light will experience both a scattering force in the direction of the beam axis, which is proportional to the irradiance, and a gradient force that may be expressed as $F_{grad} = -\frac{1}{2}\alpha(gradE)^2$, where α is the polarizability of the particle.[3] The gradient force is the direction of the beam axis is negligible unless the beam is tightly focus. Beam shaping of a cloud of particles is possible by molding the cloud in with the gradient force, say in the x-y plane, and by further molding the cloud in the z-direction by the combined optical scattering force and gravitational forces arising from the orbital dynamics (tidal forces). At the moment of release the velocity distribution of the cloud may be represented by a probability distribution such as the Maxwell-Boltzmann distribution. Without intervention, the cloud will diffuse to a rarified state where the particles move ballistically. The gradient force required to freeze the distribution in the x-y plane must then be of the order of $F_{grad} = m\sqrt{(2k_BT/m)}/\delta t$, where δt is the beam exposure time, T is the temperature, m is the particle mass, and k_B is Boltzmanns constant. The expansion of a rarefied gas cloud in vacuum expands as $exp(-\tau^2/t^2)$ where $\tau^2 = mR^2/2k_BT$, and R is a diffusion length.[57] The required irradiance, I, may therefore be estimated as $I = 4k_BT/\alpha\eta$, where $\eta = 377[\Omega]$ is the impedance of free space, and $\alpha = 4\pi\epsilon_0 a^3$, where a is the radius of a grain, and $\epsilon_0 = 8.910^{-12}$ [F/m]. For a radius of 1 micron, the irradiance becomes of the order of 13 kW/m^2, a CW laser power level which is within the range of commercial lasers in the visible band, including Nd:YAG laser at 532 nm. Although the radiation pressure force on a macroscopic body is weak, a few milliwatts of focused laser power are sufficient to achieve a force in the piconewton range. For a micron-sized body, the laser power is in the nanowatt range. Figure 33 depicts the estimates of orbital forces as function of grain size, that have to be compensated at an altitude of 1000 km to allow for cloud trapping, and Figure 34 shows the laser irradiance as function of grain diameter.

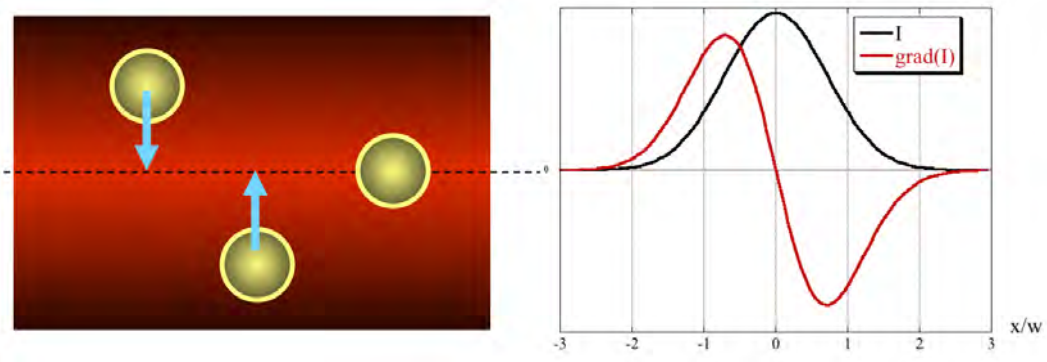

Figure 32: Electromagnetic gradient force

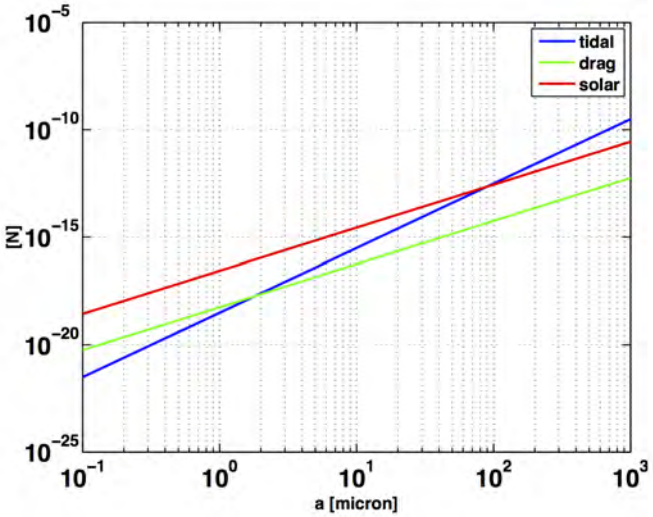

Figure 33: Estimates of orbital forces as function of grain size, that have to be compensated at an altitude of 1000 km to allow for cloud trapping.

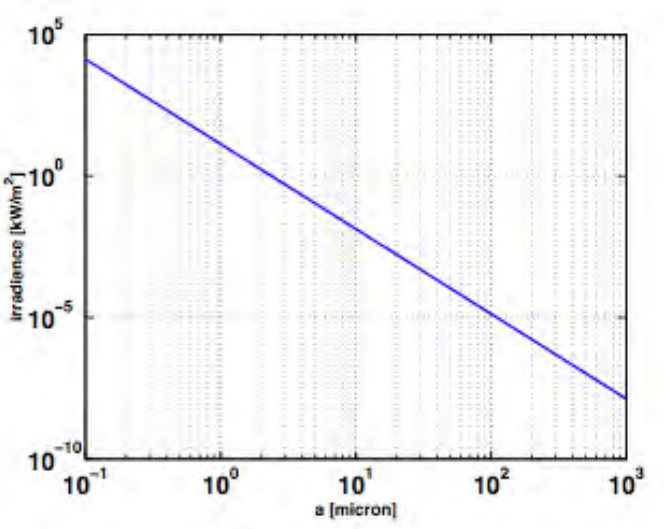

Figure 34: Laser irradiance vs. grain diameter.

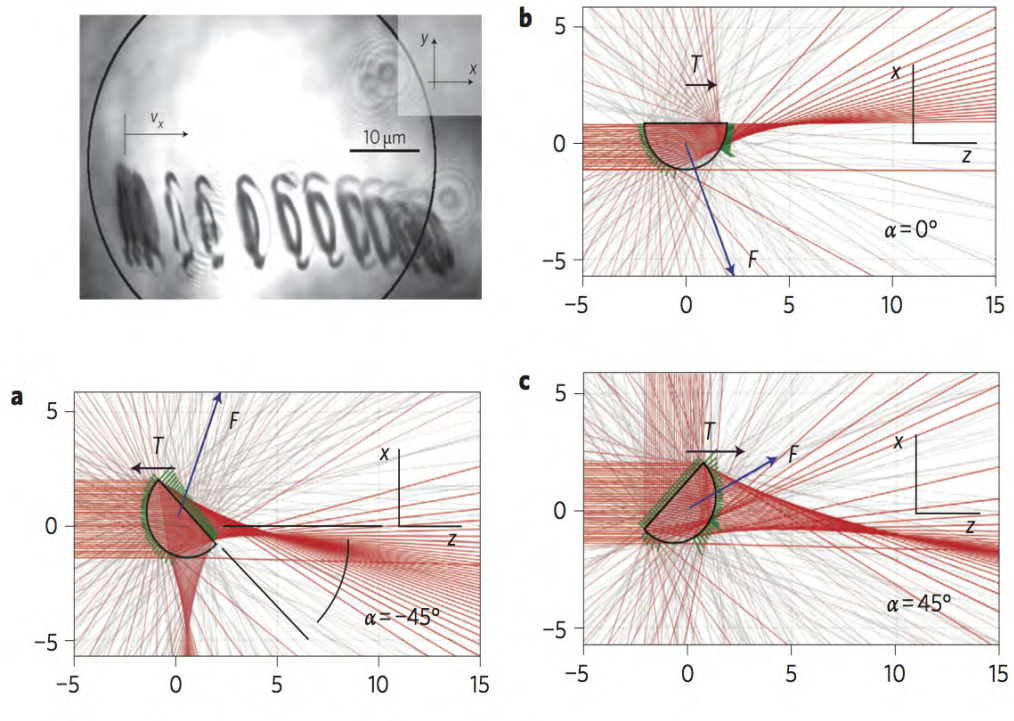

Figure 35: Optical Lift

G. Swartzlander et al.[75] discovered and demonstrated in 2010 that a uniform stream of light could create not only a stable push, but also a force named optical lift. This discovery has the potential to revolutionize micro- and nano-manipulation of objects in much the same way that the discovery of optical tweezers, now routinely used for DNA manipulation, did forty years ago. Although the radiation pressure force on a macroscopic body is weak, a few milli-watts of focused laser power are sufficient to achieve a force in the pico-newton range. This is shown in Figure 35.

10.1.7 The cloud as an adaptive system

The adaptive properties of the cloud emerge by virtue of the local anisotropy that can be induced by light, electric, magnetic, and gravitational fields, and combinations thereof. A stable configuration will likely be reached if the cloud is allowed to settle in the natural local coherent optical field, but a differential change of the surface reflectivity or emissivity of the grains may be able to change the cloud directional properties anisotropically, possibly causing a resultant macroscopic displacement or rotation as a reaction to the light. See Figure 36 for a summary of actuation mechanics that can be considered. A modulation of the scattering field of the grains would enable varying optical properties of the entire system. Controlling the polarization state of light may be one of the means to produce relative phase coherence of the grains in order to improve reflectors surface accuracy, and induce torques on the grains to control their attitude motion. With properly chosen material properties of the grain, a portion of the cloud may then behave as a refractive lens, and another portion as a reflective aperture. Other options could be: a hologram, a diffraction grating, or Fresnel lens.

10.1.8 Granular spacecraft modeling and simulation

Two simulations are currently being developed for systems engineering evaluations of proof-of-concept: one simulation of gravito-electrodynamics and control of cloud of grains subject to environmental disturbances and field control, i.e., electromagnetic, optical, gravitational (SIM1), and one simulation of dynamics and control of virtual truss model of imaging system in formation (SIM2). SIM2 is only in its infancy, and will be further developed in Phase II. A block diagram of SIM2 is shown in Figure 37. In SIM2, at each simulation step, the simulation flow follows this sequence. First, it generates

Degree of freedom	Actuation mechanism
Grain translation	Optical lift
Grain rotation	Light polarization, scattering
Cloud translation	Optical lift, gravity, solar pressure
Cloud rotation	Differential light pressure
Transmission/ Reflection	Varying grain index of refraction
Diffration Grating/ Hologram	Varying relative orientation between grains

Figure 36: Options for cloud control and adaptivity.

the granular spacecraft dynamic model, generates disturbances acting on the spacecraft, stabilizes the cloud dynamics at low frequency assuming it is in formation with the rest of the system, adds the effect of representative sensor and actuator noise models to the response, stabilizes the wavefront at high frequency, computes the overall response (low + high frequency), and goes to the next step.

A block diagram of SIM1 is shown in Figure 38, and it is discussed next. The SIM1 cloud simulation software is based on building a model of a large number of identical grains. This simulation environment allows trade studies for autonomy selection, trade studies for orbit selection for different applications, testing of autonomy algorithms at grain level and cloud level, development and testing of modeling and propagation algorithms. The grain model involves fully nonlinear dynamics with sensors/actuator models. One level of control for cloud shape maintenance, drift control, and another level of control is for cloud attitude stabilization. The cloud model involves an equivalent rigid body with coupled micro/macro motion. The disturbances modeled are Gravity, Third-Body, Drag, solar, EM field, thermal balance. The assumptions we used to model the dynamics are as follows: 1) The inertial frame is fixed at Earths center. 2) The orbiting Frame ORF follows

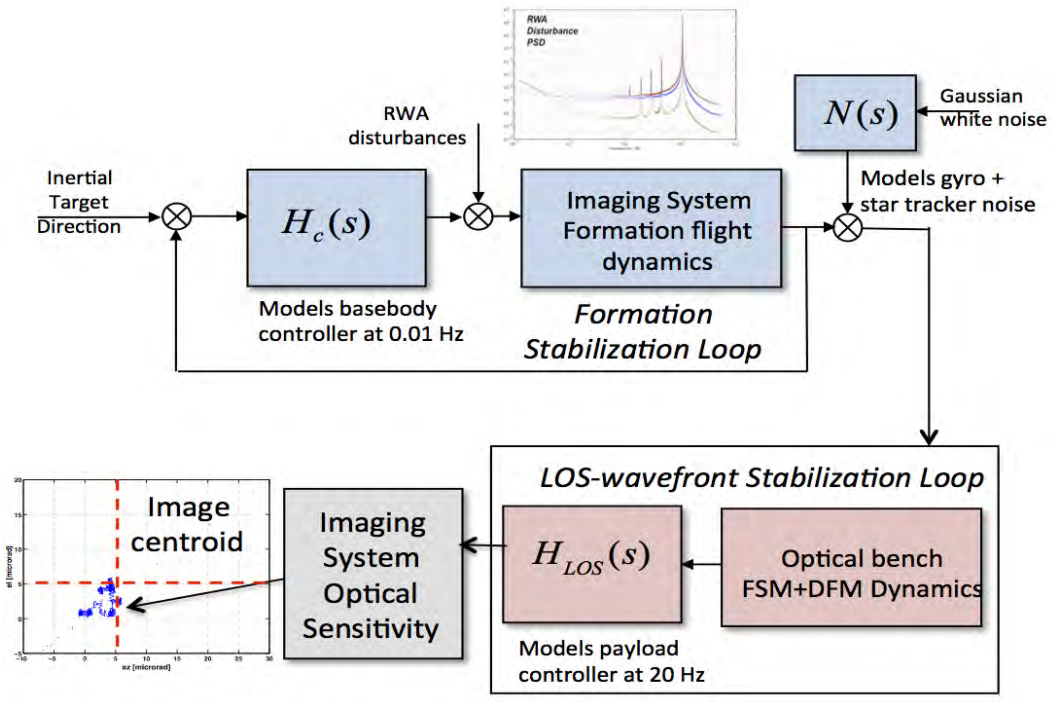

Figure 37: Simulation number 2

Keplerian orbit. 3) the cloud system dynamics is referred to ORF. 4) the attitude of each grain uses the principal body frame as body fixed frame. 5) the atmosphere is assumed to be rigidly rotating with the Earth. Regarding the grains forming the cloud: 1) each grain is modeled as a rigid body; 2) a simple attitude estimator provides attitude estimates, 3) a simple guidance logic commands the position and attitude of each grain, 4) a simple local feedback controller based on PD control of local states is used to stabilize the attitude of the vehicle. Regarding the cloud: 1) the cloud as a whole is modeled as an equivalent rigid body in orbit, and 2) an associated graph establishes grain connectivity and enables coupling between modes of motion at the micro and macro scales; 3) a simple guidance and estimation logic is modeled to estimate and command the attitude of this equivalent rigid body; 4) a cloud shape maintenance controller is based on the dynamics of a stable virtual truss in the orbiting frame. Regarding the environmental

perturbations acting on the cloud: 1) a non-spherical gravity field including J_0 (Earths spherical field) zonal component, J_2 (Earths oblateness) and J_3 zonal components is implemented; 2) atmospheric drag is modeled with an exponential model; 3) solar pressure is modeled assuming the Sun is inertially fixed; and 4) the Earths magnetic field is model using an equivalent dipole model. The equations of motion are written in a referential system with respect to the origin of the orbiting frame and the state is propagated forward in time using an incremental predictor-corrector scheme. Figure 39, shows the kinematic parameters of a 1000 element cloud in orbit.

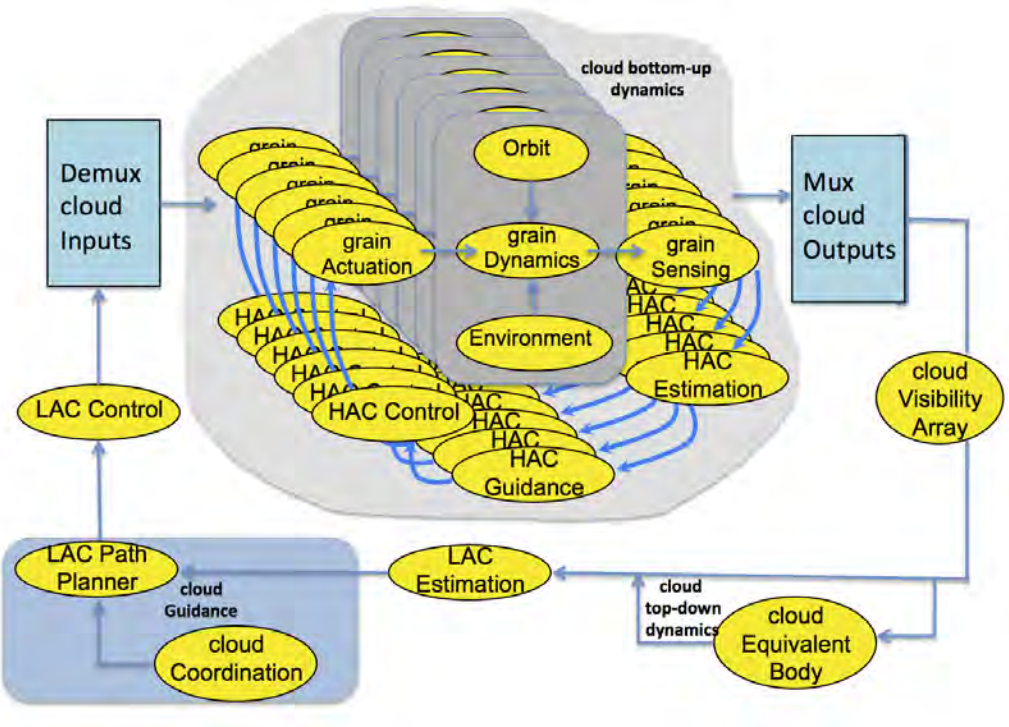

Figure 38: Simulation number 1

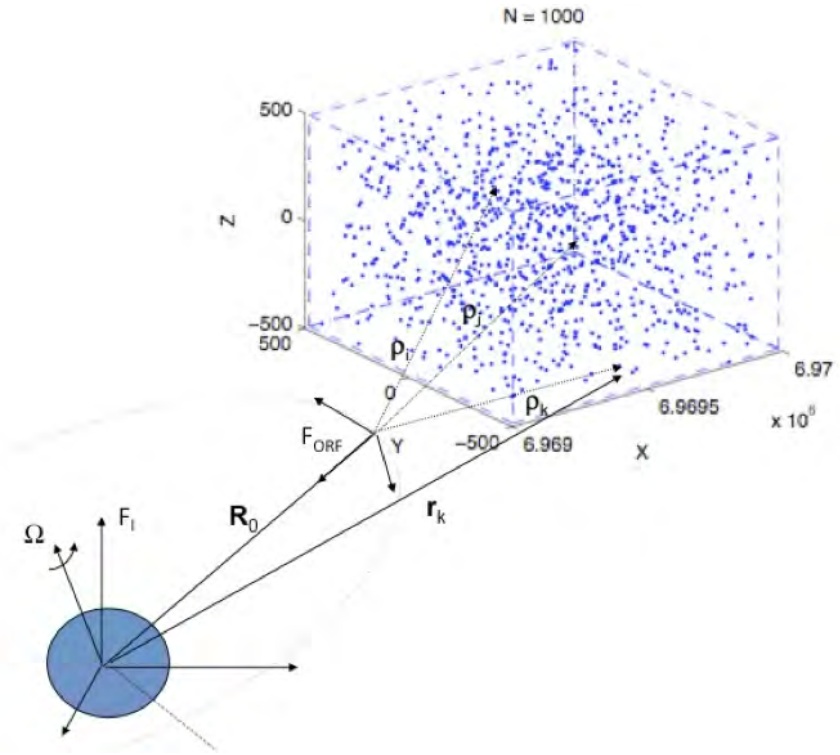

Figure 39: The kinematic parameters of a 1000 element cloud in orbit.

10.2 Cloud Engineering

In this section, we deal with the engineering applications of orbiting rainbows.

10.2.1 Applications in Remote Science

For relevant science applications of a cloud as a remote sensing random array, the following criteria must be met: a) high ground resolution, b) high sensitivity in the frequency band of interest, c) possibly frequent revisit, d) flexible scan area or continuous dwell on the spot of interest, and e) capability for large coverage. To accomplish these goals, spatial coherence at low frequency, or the aperture rigidity in orbit, must be achieved, by relative grain control. The system libration dynamics in orbit must be stable, i.e. the attitude dynamics of the aperture must be stable with respect to the local orbiting frame. This can be achieved by a favorable orbital distribution of the agents. In addition, large swaths of the earth could be continuously monitored with an extremely fault-tolerant system. Also, spatial coherence at high frequency must be achieved, and could be obtained by containing the cloud dispersion electromagnetically. Finally, the signal transmitted or received by the aperture must exhibit spatiotemporal phase coherence so that intensity at the maximum peak lobe of the array pattern is maintained. This could be achieved by limiting the differential effects of orbital perturbations. The incoming signal must be also in phase to within the diffraction limit to add coherently (this amounts to approx. 1 cm of relative grain motion within the cloud at 1.4 GHz). The motion of elements near the symmetry axis will cause de-focus, and higher order aberrations (coma, astigmatism) result from motion of the off-axis elements from the figure plane. Consequently some form of figure control (i.e. wavefront control) is necessary. Also, to accommodate multiple look angles (i.e., boresight control), the plane of the aperture must be able to tip/tilt as an equivalent rigid aperture. The determination of the effective aperture size and cloud density to fill the aperture, will depend strongly on the chosen wavelength, the noise-equivalent temperature at the detector, the diffraction limited ground resolution, surface reflectivity, dwell time, ground spot diameter, and source temperature. For Remote science applications, the spacecraft will be in close proximity to the Earth, hence in LEO or GEO. These are environments where the dusty plasma environment, including charging and ionization, are important. Therefore, as in a dusty plasma crystal, an aerosol aperture will require a combination of both opti-

cal manipulation for fine grain positioning, and electrostatic or magnetostatic confinement trap to contain and control the aperture at a coarser level.

10.2.2 Application to a Representative Optical Imaging System for Astrophysics

Resolution and aperture sizes for astrophysical optical systems are ever increasing in demand,[43].[55] With near-term plans to build 30 meter ground-based telescopes for astronomy, the demand for higher resolution optics in space continues to grow not only for exo-planet detection, but also for earth-based science, including hyper-spectral imaging and for monitoring of the oceans and land masses (e.g. seismic monitoring). ATLAST, still several decades away, is the largest practical space telescope designed using state-of-the-art light-weight segmented mirror technology: it may have an aperture up to 18 m. The aperture formed by the granular spacecraft cloud does not need to be continuous. Used interferometrically, for example, as in a Golay array,[15] imagery can be synthesized over an enormous scale. As part of our investigation, we have considered refractive, reflective and diffractive systems and outlined optical correction and collection systems. In addition to forming a single monolithic optical element with the cloud, we also considered forming smaller self-coherent patches, similar to segments in a segmented aperture, but not required to be phased with respect to each other. The segments can be continuous or separated by large amounts to form a sparse array. A corrector is then used to compensate for phase differences between each segment. A Fizeau interferometer is a straightforward corrector for a reflective system. A more advance corrector would be a multiple aperture system utilizing multi-scale lens design, as described by [4]. The multi-scale lens design has the additional benefit of an increased field of view of the optical system and will allow for less movement of the entire collection of sub-apertures when changing the line of sight of the system.

We designed an optical imaging system for multiple aerosol optics that combines several layers of sensing and control to adapt to possible misalignments and shape errors in the aerosol. The design also combines the light from several of these clouds to synthesize a large, multiple-aperture system to increase light throughput and resolution. A two-dimensional version that includes two separate patches, clouds, or aerosol reflectors, is shown in Figure 40. The entire system is represented in the diagram on the left. Starlight enters from the left, reflects off the two separate patches, and is slowly focused

toward the formation-flying spacecraft that collects, corrects, and combines the light from individual patches to a single detector. The diagram on the right is a enlarged drawing of the spacecraft/optical bench that contains all the optics to perform line-of-sight and mid- to low-spatial frequency wavefront sensing and control for the optical system.

The reflective concept design is shown in Figure 40. The sequence of optics is as follows: the starlight is focused by granular spacecraft optic patch, creating a spherical wavefront. Light from all patches converges at an intermediate focus, which can be seen in the left portion of Figure 40. The light then reflects off secondary mirror (Gregorian) and the light from each patch becomes collimated. The collimated light from each patch then continues to a separate adaptive optics system. A fast steering mirror and a deformable mirror correct pointing and low to mid-spatial frequency aberrations. An optical delay line is used to correct phasing difference between the patches and enables Fourier transform spectroscopy. A beam-splitter is included to allow some of the light to go to a Shack-Hartmann sensor to measure aberrations in the system and provides a feedback mechanism to the deformable mirror. The Shack-Hartmann placement can be seen in Figure 41 in blue. The light continues to the collector system, which consists of a Cassegrain telescope that combines and focuses the light from all the patches onto the science detector. Figure 42 shows a three dimensional solid picture of the optics. It includes eight optical patches arranged symmetrically in the right figure. The corrector and collector optics are shown on the left figure. Figure 43 summarizes the state of the art in deformable mirror technology, compared with the needs of the aerosol optics element.

For this system, the selected approach for cloud management, sensing, and control is multistage, with an outer stage for formation stabilization, and an inner stage for telescope wavefront sensing and correction, relegating fine adaptive optics to a deformable/fast steering mirror stage in the optical bench. The systems relative range/bearing sensing and metrology is based on virtual telescope formation flying, in which distributed relative sensing is accomplished using Ka-Band transceivers/patch antennas, and a centralized laser metrology system, relying on a single laser source on the main light-collecting spacecraft, while single reflecting target are on other free-flying elements except granular spacecraft.

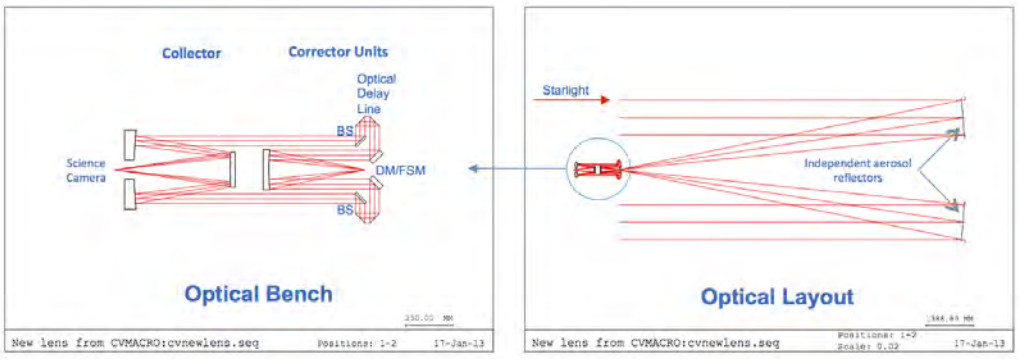

Figure 40: A two-dimensional slice of a multi-patch reflective system, with optical rays shown in red, is displayed on the right. An expanded view of the Optical Bench is displayed on the left.

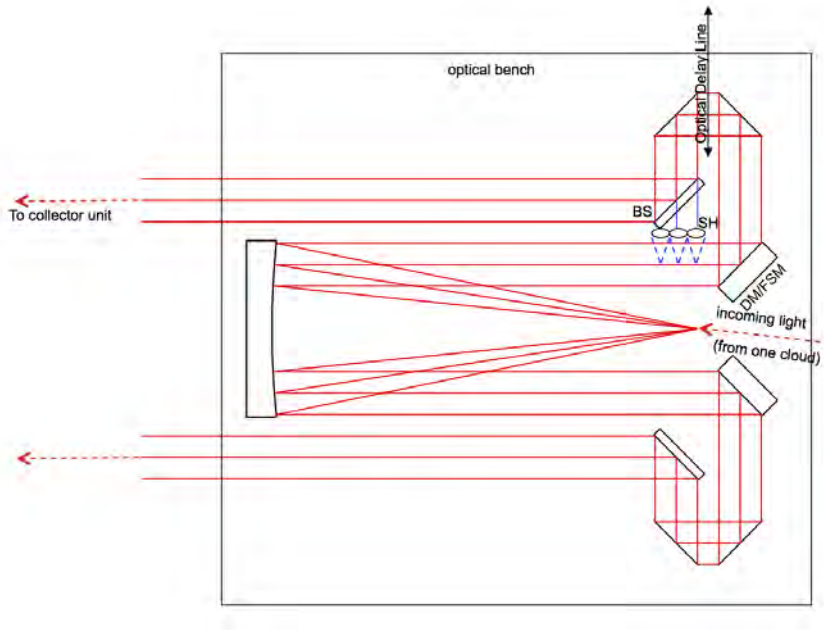

Figure 41: An expanded view of the corrector part of the optical bench that explicitly show the Shack-Hartmann wavefront sensor in blue. The SH sensor will be below the main optical path to avoid vignetting.

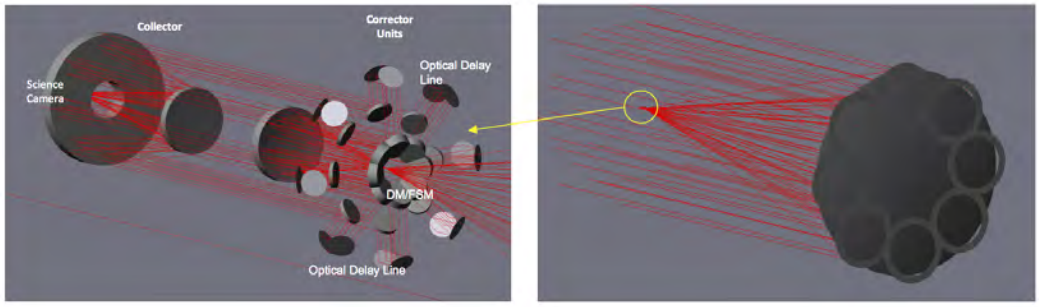

Figure 42: Three-dimensional solid optics view of the reflective imaging system concept design with 8 cloud patches forming the aperture.

Metric	Conventional Mirror SoA	Light-Weight Mirror SoA	Aerosol Objective
Mass Areal Density	**40-100 kg/m2**	**10-20 kg/m2**	**<1 g/m2**
Surface Figure Error	**10 nm RMS**	**14 nm RMS**	**100 nm RMS**
Surface microroughness	**<5Å**	**<10Å**	**<100Å**
First free-free mode	**>100Hz**	**>100Hz**	**TBD**
Size	**0.1 to 2.4m and larger**	**0.3 to 1.35m and larger**	**1 to 10m**
Deployable	**No**	**No**	**Yes**
Thermal stability	**Low CTE**	**Thermally controlled**	

Figure 43: State of the art of deformable mirror technology.

10.3 Other applications of granular spacecraft

In Figure 44, we can think of separate and independent clouds, separate and cooperative clouds, or distributed and cooperating clouds, opening up immense possibilities for a variety of space mission scenarios. In the case of separate, independent cloud, each cloud as a spacecraft, there is coherence only within a cloud, and each cloud acts independently. In the case of separate and cooperating cloud, each cloud acts as a separate spacecraft, there is coherence within as well as between clouds, and multiple clouds can act as one. In the case of distributed cooperative clouds, the swarm is distributed globally, and it establishes a truly distributed spacecraft. There is coherence between any or all the elements, and this solution creates multiple independent beams, thereby supporting multiple simultaneous functions.These applications represent the future of granular spacecraft, but can still be enabled by the concepts explored in this report.

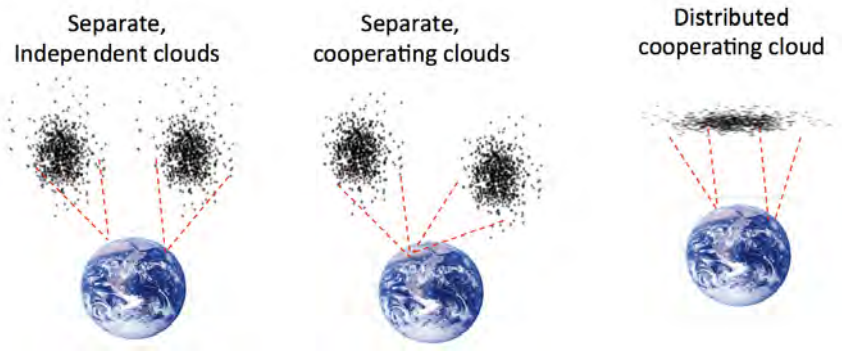

Figure 44: Future possibilities of using clouds in space.

10.3.1 Control, Sensing and Metrology at the formation level

This section deals with the macro-scale. While the focus of this Phase I study was to investigate the properties of the orbiting cloud, ultimately this system will have to be part of a larger system, for instance, the reflecting element of a telescope. Hence, ways need to be considered to autonomously maintain the alignment between the cloud and the other components of the telescope in space (a sunshade, relay elements, focal plane system, and others). Adding intelligence and autonomy to these large optical systems may be accomplished in multiple ways. One approach is to use formation-flying technology to maintain the relative distances and orientations of the elements of the optical system with high precision with respect to the cloud, hence creating the equivalent of a virtual truss. Systems of large focal length are then possible without a structure to hold them in place. On large scales (km-size apertures and focal lengths), the same formation-flying principles can be applied to steering and stabilizing very large structures, such as orbiting antennas and reflectors[1]and they could enable the synthesis of focused random electromagnetic arrays in the visible, IR, and microwave bands with the necessary system autonomy. Recent work on autonomy of distributed systems for planetary exploration,[65] and[66] indicates that an alternative centralized approach to managing the information flow is more robust than a decentralized approach. In,[67],[47] a promising probabilistic approach has been proposed for modeling of distributed robotic systems, which could be used to study the stochastic properties of the cloud dynamics. If the cloud is part of a larger system, issues such as obtaining knowledge of the inertial state of the cloud or of the relative motion of a portion of the cloud with respect to another become important. Also, it becomes necessary to investigate how would a local parabolic curvature of the cloud be realized, if relative motion (edge effects) are important, and if the whole cloud can be slewed to acquire a new target without losing the optical accuracy.

The cloud sensing approach is based on imaging/laser scanning, relying on custom or commercial stereo vision or laser scanning systems which can create precise 3-D model of complex objects. As in the previous JPL study, we baseline our cloud sensing and control approach on the following key features:

- Centralized relative optical/laser metrology, as shown in Figure 45
- Decentralized relative RF metrology and absolute celestial-inertial ref-

erencing

- Centralized formation state estimation, and onboard telescope model-based optics module location prediction and positioning reference
- Telescope Commanding and Control methodology from acquisition to precision targeting
- Primary mirror shape sensing and formation vector metrology
- Telescope element(s) positioning error allocations, and analysis of metrology error sensitivities

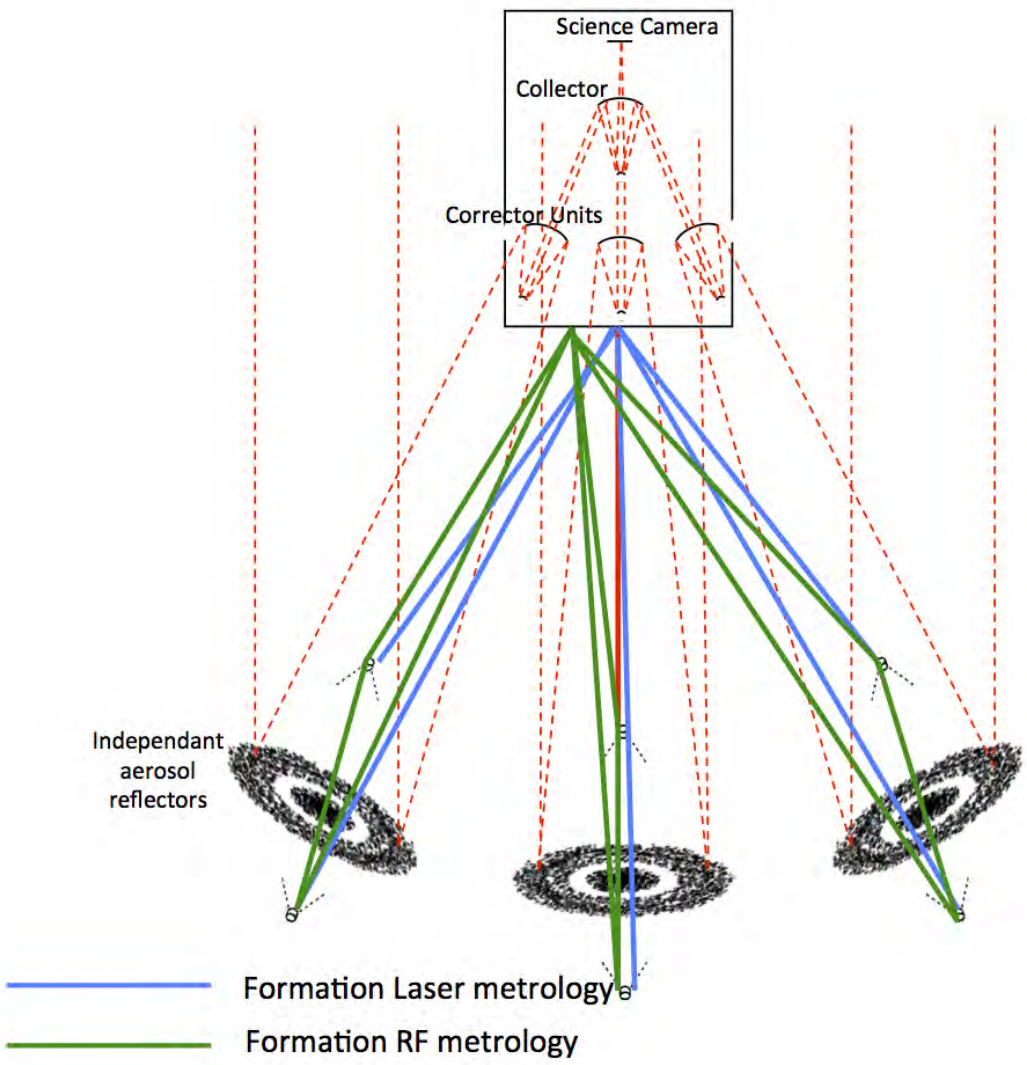

Figure 45: Laser and RF metrology

10.3.2 Orbital control of cloud and estimates of complexity

A representative cloud with varying number of grains is simulated to identify the limitations in computation time as the number of grains grows. We can derive a control law to track a desired surface in the ORF (equivalently to maintain a reference cloud shape) as follows,[72].[26]

Define the tracking error

$$e = q(x, y) - q_d(x, y) \tag{9}$$

where $q_d(x, y)$ are the desired surface, and $q(x, y)$ the current position of the agent with respect to the origin of ORF. By imposing an exponentially stable error dynamics in the form:

$$\ddot{e} + 2\zeta_n \omega_n \dot{e} + \omega_n^2 e = 0 \tag{10}$$

or

$$\ddot{q}(x, y) + 2\zeta_n \omega_n \dot{q}(x, y) + \omega_n^2 [q(x, y) - q_d] = 0 \tag{11}$$

we can make sure the error e is driven to zero. Therefore, using the equations of motion expressed in ORF coordinates, the control law with components in ORF becomes:

$$u = -f_{pert} + f_{gyro} + m\ddot{q}_{des} - K_d \dot{e} - K_p e \tag{12}$$

where f_{pert} is the resultant of J_2 and J_3 forces on the agent, f_{gyro} are the Coriolis and centrifugal forces acting on the agent, K_d is a derivative gain, and K_p is a proportional gain. Both f_{pert} and f_{gyro} can be modeled, act on a time scale which is very long, and can be canceled out by the feed-forward control scheme. These control forces are applied by the laser scanning system, coupling mechanically with the grains via opto-mechanical interaction. The control gains are selected to limit the transient to a fraction of an orbit period. The results of the preliminary simulation study are shown in the next section.

10.3.3 Results of system-level simulation

The simulation results shown in Figure 46 were obtained by commanding the grains to conform to a prescribed optical surface. The cloud is first shaped into a disk, then into a paraboloid of specified focal length and diameter. The numerical results indicate that the force required to shape 1 meter diameter disk into parabola is of the order of 10^{-8} N. Assuming a grain shape which is asymmetric to incoming light, the torque required to align 1 micron grain is of the order of 10^{-15} Nm. For the computation time as a function of the number of grains N, preliminary results indicate an order $N^{1.43}$ scaling on a 8Gb, 1067 MHz RAM MacOSX computer with a 3.06 GHz Intel Core 2 Duo processor. With this metric, the same simulation for a system of N=1000 grains takes 5.4 hours, and 146 hours (i.e., 6 days) for a system with N=10,000 grains. Therefore, efficient ways to simulate this complex system, where not only the time scales of natural system dynamics, but also the sampling times of the Guidance, Navigation, and Control are included, remain to be fully explored. These methodologies would include GPU acceleration and multigrid solvers for the cloud dynamics, and will be the subject of future investigations,[31].[64] Figures 47, 48, 49, 50, and 49 show various snapshots of the simulations of the entire imaging system with the cloud as an aperture.

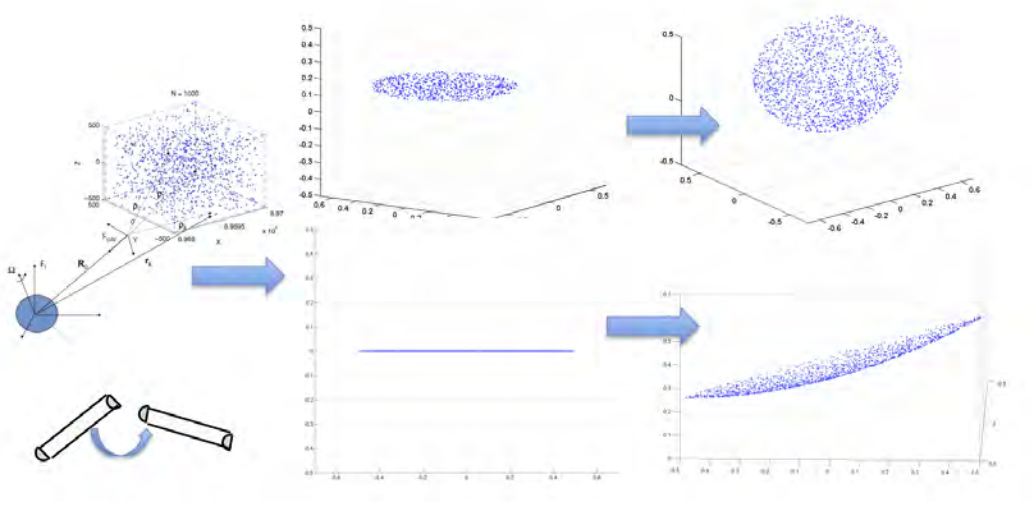

Figure 46: Shaping of a disk into a paraboloid

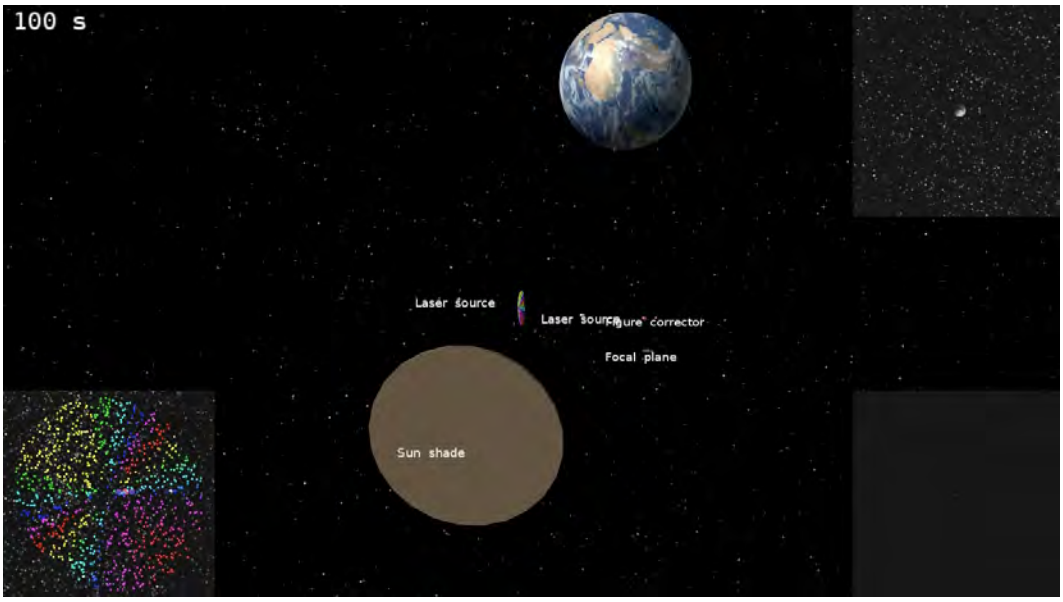

Figure 47: Snapshots of simulation.

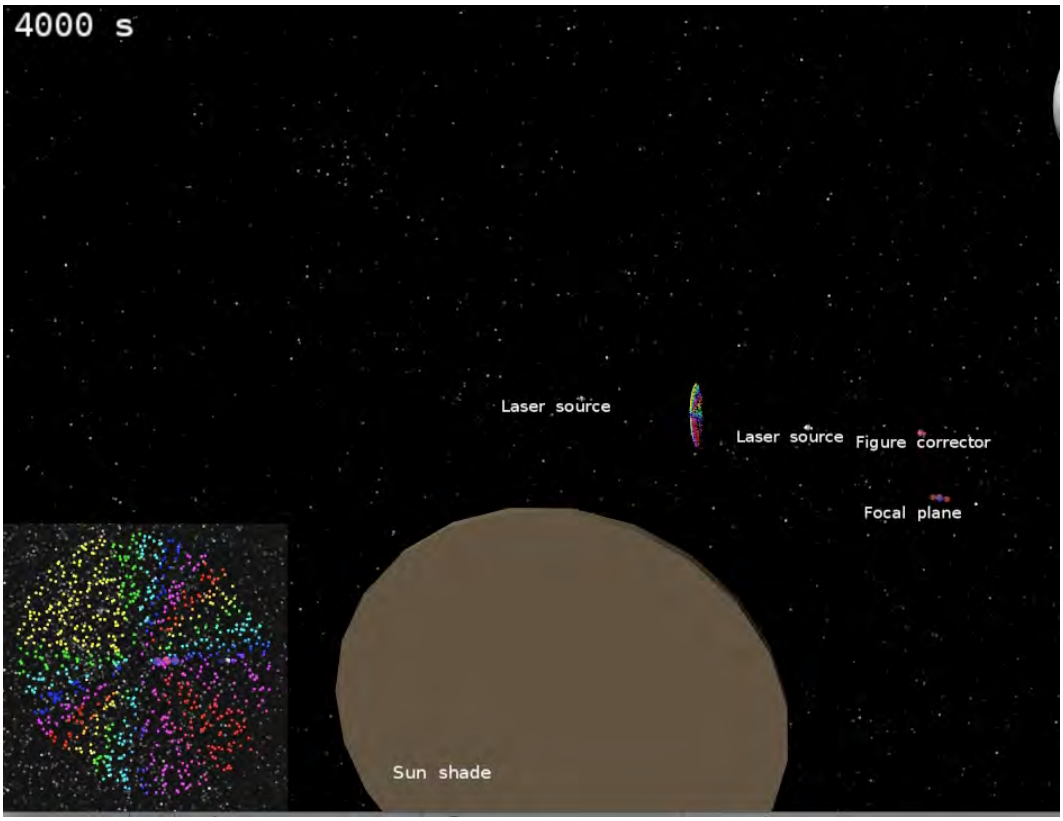

Figure 48: Snapshots of simulation.

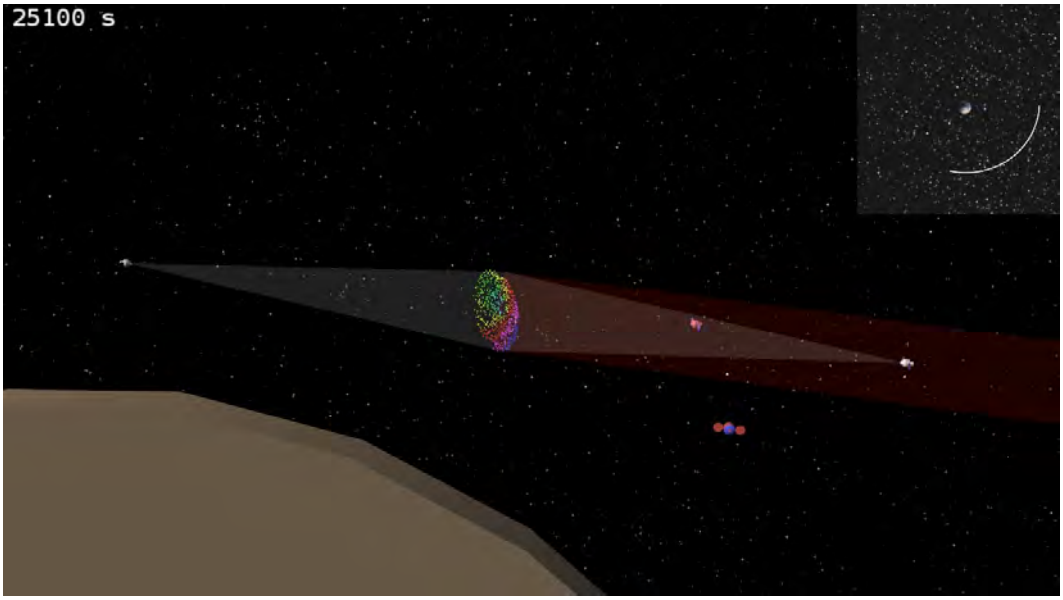

Figure 49: Snapshots of simulation.

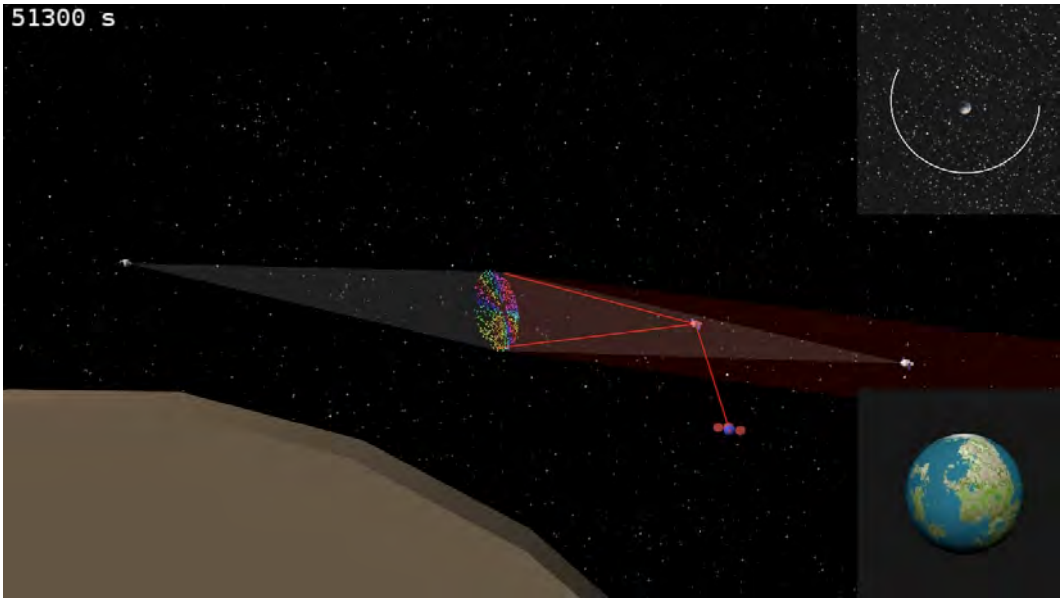

Figure 50: Snapshots of simulation.

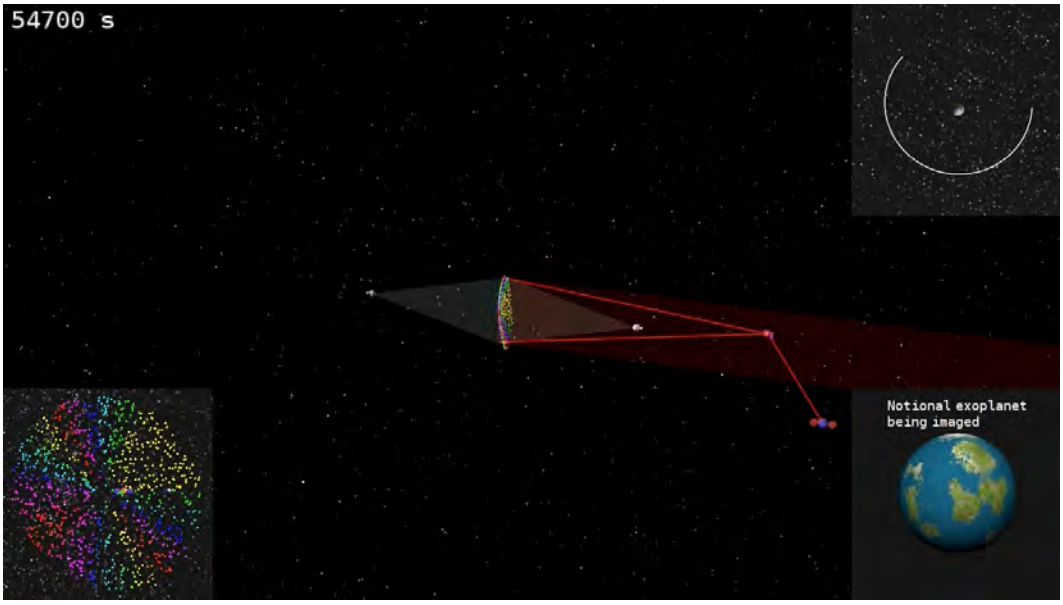

Figure 51: Snapshots of simulation.

10.3.4 Approach to cloud flight operations

We envision a multi-stage approach for the assembly and containment of the aperture. See Figure 52. First, the cloud is deployed. In the 1980s, AMPTE (a prior NASA mission of upper atmospheric aerosol investigation) released sodium aerosol in the ionosphere. We could leverage this and similar missions for aerosol sprayer design. The cloud then needs to be trapped to avoid leakage and diffusion. A pair of counter-propagating laser beams could trap the cloud at the interference fringe, as originally proposed in.[?] Once the cloud is trapped, we need a coarse control stage to create a roughly two-dimensional carpet from the cloud. Besides using light pressure, magnetic or electrostatic field might help this process. The carpet does not need to involve the entire cloud, only part of it. Once we have the carpet, we need a fine control stage for figure control. The approach involves the use of tight, large-scale, formation flight technology for precision alignment of the cloud aperture with the remaining optical system elements, but specific optical lift technology for coarse and fine cloud control and shaping. Electrostatic charging might cause undesired aggregation and clustering that might counteract the optical lift force. For this reason, combinations of optical, magnetic, electric, and gravitational forces will have to be considered to control and manipulate the cloud. The cloud will experience very small gravity gradient forces if deployed at a Lagrange point (for example, the Sun-Earth L2 point), which will not disrupt the clouds stability over time, and only infrequent orbital correction maneuvers would be necessary to maintain the system in orbit. Once the observation campaign is over, the system can be decommissioned, and the same force fields can be used to de-orbit the cloud, or used advantageously to clean other orbital debris.

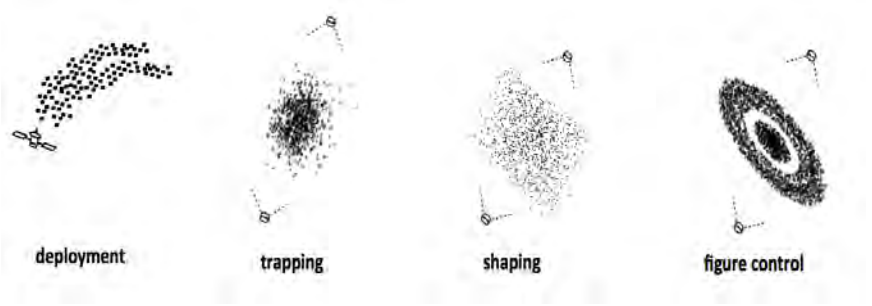

Figure 52: Mission phases to ultimately achieving an optical aperture from a cloud.

The approach to cloud maintenance is to make sure that in all phases the cloud is stabilized, all sensors/actuators, control loops, communication, collision avoidance have been checked-out prior to science operations, cloud containment and maintenance maneuvers are done periodically once the system has been deployed.

In general, the timeline is phased as follows:

- Mother-SC checkouts/calibrations
- Orbit injection cleanup
- Cloud deployment
- Cloud-level checkouts/calibrations
- Science validation and calibration.

and Figure 53 presents a proposed sequence of mission operations to enable a science observational campaign. Note that optical figure corrections, formation corrections, and cloud shape corrections must take place simultaneously to enable a stable system.

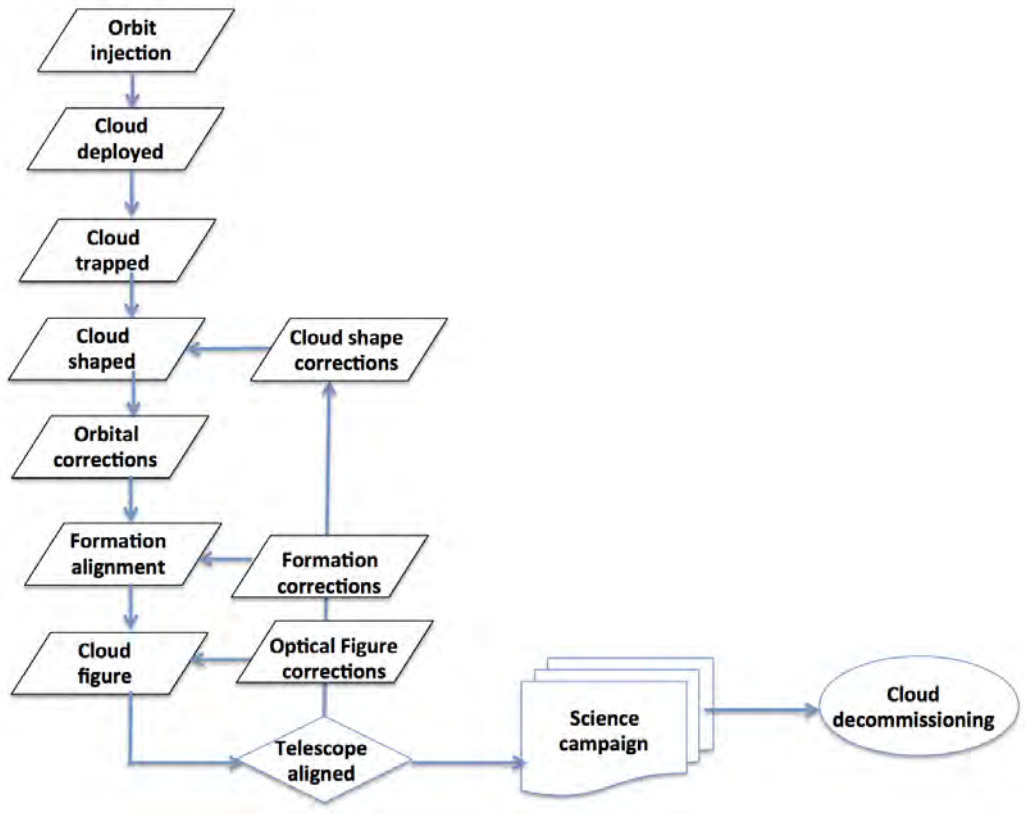

Figure 53: Proposed sequence of mission operations.

10.3.5 System cost modeling

We started an effort on the preliminary evaluation of total system cost, based on existing cost models available in literature (NASA Advanced Mission Cost Model, developed by Stahl[73]). Related work is derived in.[20] If N is the number of aerosol clouds, M the total mass, λ the wavelength, the dollar amount is in billion, and we introduce difficulty levels DL as: -2=very low, -1=low, 0=average, 1=high, and 2=very high, the cost model is written as:

$$Cost = \$2.25 \times (M/10,000kg)^{0.654} \times 1.555^{DL} \times N^{-0.406} \times \lambda^{-0.5} \qquad (13)$$

We assumed 10^7 grains per aerosol patch, a grain density of 2500 kg/m^3, 3 patches of diameter 1 meter, difficulty level 2, cloud thickness 1 micron. Figures 54 and Figure 55 show the preliminary results of these computations for a wavelength of 0.3 micron, i.e. the effective aperture mass and imaging system cost vs. effective diameter, for monolithic and cloud apertures, demonstrating the enormous cost reduction for the orbiting cloud, compared to a monolithic system. This cost model, however, does not include the cost of the laser manipulation system, or the impact of utilizing a system in formation flight, only the cost of the equivalent aperture compared to a monolithic aperture.

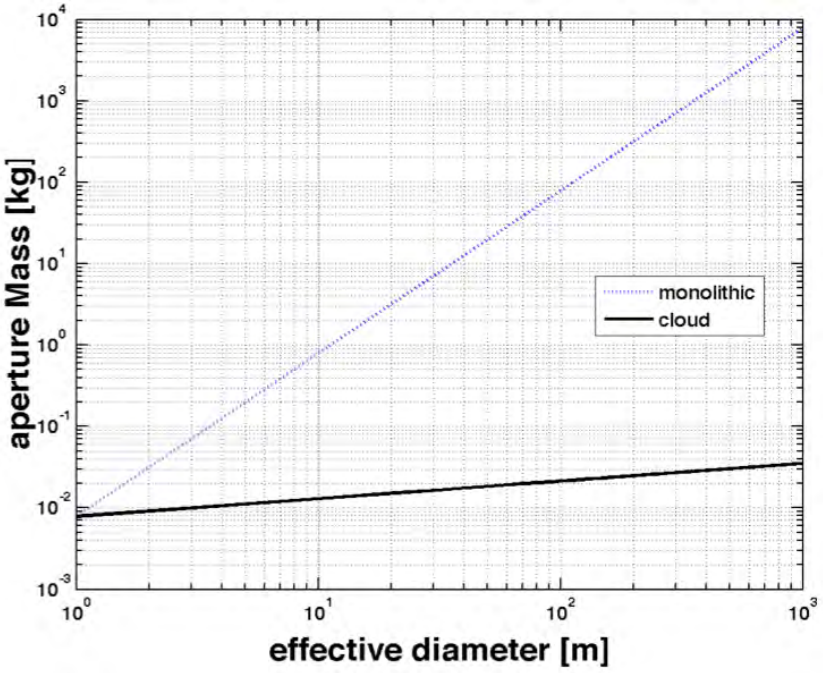

Figure 54: Effective aperture mass vs. effective diameter, for monolithic and cloud aperture.

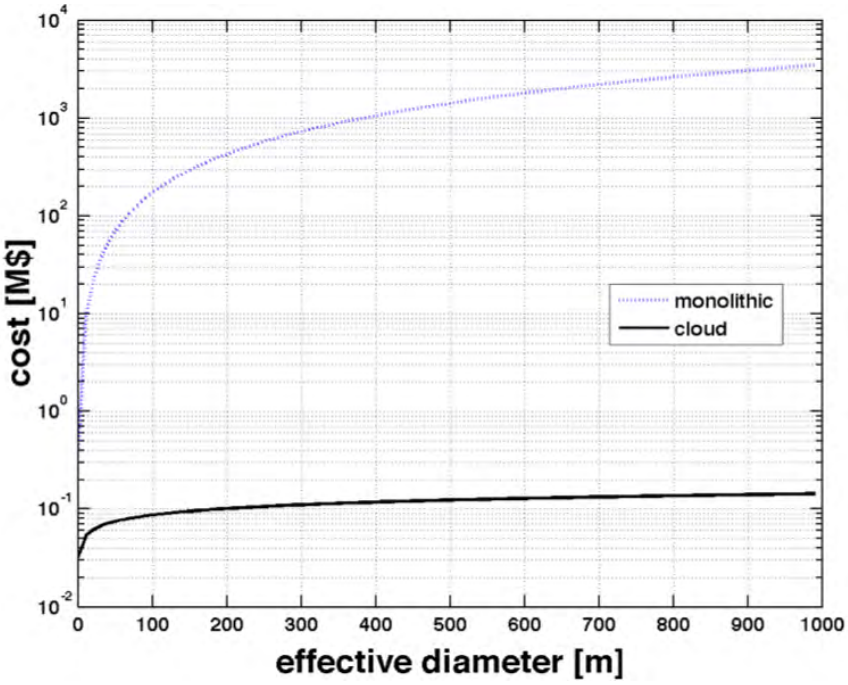

Figure 55: Effective imaging system cost vs. effective diameter, for monolithic and cloud aperture.

10.4 Exploring New Optical System Options

10.4.1 Reflective system optical considerations

For the system design outlined in the Cloud Engineering Section, that utilizes the aerosol cloud as a reflective optic, or primary mirror, the front surface of the optical cloud is all that matters to the light path. Height variations of the optical surface must be less than $\lambda^2/\Delta\lambda$, where $\Delta\lambda$ is the bandwidth of light, to achieve meaningful imagery. Longer wavelengths (e.g. $10\mu m$) and smaller optical bandwidths make this requirement achievable with micron-sized particles for the cloud.

Creating and maintaining a perfectly continuous surface is not likely to be achieved using the techniques we are considering in our approach, therefore sophisticated image processing algorithms will be required to synthesize an astronomical image. For example, taking several short exposures and using speckle imaging techniques would allow for weaker tolerances on the reflective surface. Instead of correcting for atmospheric instabilities, as is typical for speckle imaging, we would correct for the small changes of the mirror surface due to particles being constantly in motion,[45].[10] Multiframe blind deconvolution[8] is a related technique to process multiple imperfect images to obtain a better estimate of the object. Utilizing multiple clouds would be a natural extension that would be applicable to speckle interferometry and increase the effective resolution of the system inversely proportional to the separation of clouds,[82].[23]

In addition to the techniques mentioned above, the addition of a diversity mechanism to the optical path would allow for phase diversity[63]techniques to be used. We plan to use a MEMS-based microshutter array as a programmable coded aperture in a pupil plane. This would be a feasible technique to inject a known diversity in the pupil plane of our optical system. Using optimized patterns in the coded aperture, and taking multiple images, would allow phase diversity to reconstruct the phase of our reflective surface as well as obtain an enhanced estimate of the object (or image). Multiframe blind deconvolution and phase diversity are discussed in more detail in a later section.

10.4.2 Refractive system optical considerations

In addition to the system design we created for treating the cloud as reflective optical surface, discussed in the Cloud Engineering Section, we also designed

an optical system for treating the cloud as a refractive optic, or lens, to maintain maximum flexibility of the cloud physics for future work. One such system design is shown below in Figure 56. The diagram on the left shows light from an object passing through a medium (our cloud). The cloud causes the light to come to a focus and is then relayed to our separated spacecraft that contains the rest of the optical system, shown on the diagram on the right. The corrector/collector design is identical to the reflective system. The solid optics view on the bottom left shows 8-apertures, each consisting of one aerosol optic, forming an equivalent lens. The solid optics view on the bottom right shows a three-dimensional view of the corrector/collector system.

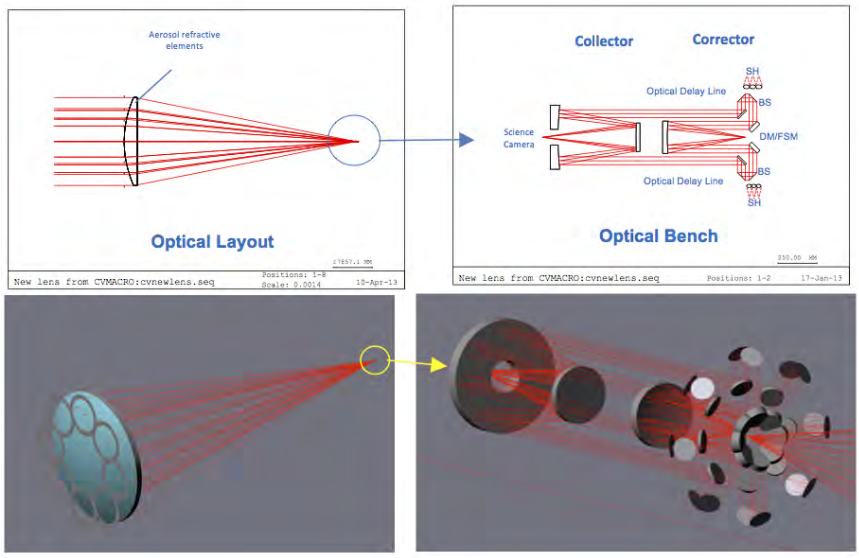

Figure 56: Refractive optical system design, both 2-D and solid views.

10.4.2.1 Bruggeman effective medium One approach for creating a refractive optic using aerosols is to assume very small particles dispersed evenly throughout a volume and use Bruggeman effective medium theory to compute the focusing power of the volume of particles. The containment mechanism of the particles could be as simple as a thin transparent bladder that is released and filled in space. Other approaches could include a laser containment system.

The following computations assume particles with a refractive index approximating that of glass, for example, n = 1.5.

According to Bruggeman effective medium theory, the focal length would be roughly:

$$f = \frac{2R}{(n_e - 1)} \tag{14}$$

where

$$(n_e - 1) = \frac{3}{2} F \frac{(n^2 - 1)}{(n^2 + 2)} \tag{15}$$

F is the fill fraction, and n is the refractive index of the particles.

If we have cloud of diameter 2R = 10 meters, a fill fraction of 10^{-3}, and particles with an index of refraction of n = 1.5 then the focal length of the cloud is f = 23 km. The f-number would be $f/D = 2.310^3$. The Airy disk ($1.22\lambda f/D$) would then be 1.4 mm (at $\lambda = 0.5$ micrometers), there the camera pixels would ideally be about this size to have a reasonable Q.

The f-number is inversely related to the fill fraction as can be seen from

$$\frac{f}{D} = \frac{f}{2R} = \frac{1}{(n_e - 1)} \tag{16}$$

The angular resolution (λ/D) is independent of the fill fraction. If n = 1.5 is replaced with $n \approx 1$, the focal length tends toward infinity.

This represents a very slow optical system, however, since our plan is to have a separate spacecraft to collect the light, separation of several kilometers is not unreasonable, especially assuming we utilize an alignment optical metrology system as discuss in the Cloud Engineering section.

10.4.2.2 Luneburg lens We have also considered creating a Luneburg lens using aerosols. This type of lens is a form of gradient-index lens that is

spherical in shape. The indices of refraction are spherically symmetric, with a higher index in the center of the sphere and lower index at the outer edge. This idea came about while considering particle containment and noting that we could possibly produce a spherical volume of particles that would be more dense near the center and more diffuse the farther from the center the particles are. Figure 57 shows an example of the focusing properties of a Luneburg lens. A Luneburg lens has an enormous field of view since it can accept light from any angle. The only limitation on its field of view is caused by the placement of detectors.

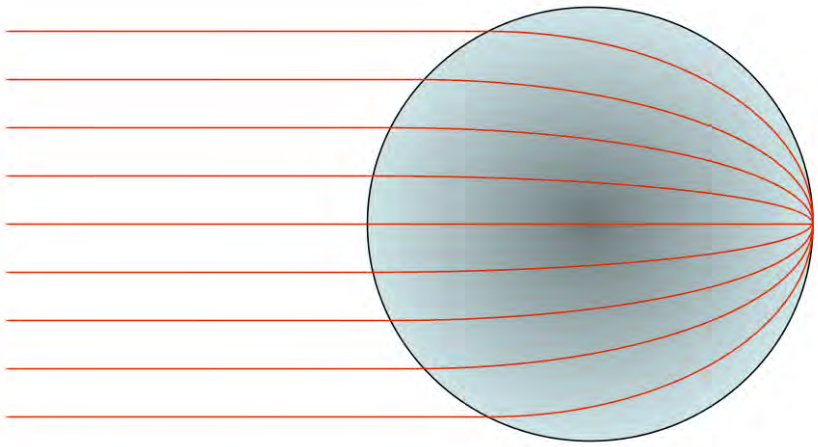

Figure 57: Crude drawing of a Luneburg lens. Light enters from the left and is focused on the opposite side of the sphere.

10.4.3 Diffractive system optical considerations

Another application of our orbiting aerosol that we have considered is to create a holographic, or diffractive, optic for our system. Projects such as DARPAs Membrane Optic Imager Real-Time Exploration (MOIRE) are striving to create a Fresnel Lens in space using a thin membrane. The goals of that program are similar to ours, to develop a space-based telescope with apertures larger than 10 meters. It would rely on a separate spacecraft for with a chromatic corrector. Laboratory demonstrations of a 50 cm class diffractive primary mirror with long f-numbers (f/50) have been published.[9] Lawrence Livermore National Laboratory, through the Eyeglass program, has created a 5 meter diameter f/50 transmissive diffractive optic composed of 50 cm segments.[35]

Palmer[60] considered using the nonlinear optical index of glass beads or aerosol droplets to organize the particles and trap them into fresnel-like three-dimensional holographic gratings. Extrapolating from this concept, we have designed a third optical system that has a diffractive optical element (DOE) as its primary lens. The system design is shown in Figure 58 and is nearly identical to the other two systems we designed.

A diffractive lens is inherently monochromatic, it only brings light to a focus for the wavelength it was designed for. However, it is straightforward to design an all-refractive chromatic correction system that provides a diffraction limited system with a 10% bandwidth. Meinel and Meinel published a basic design for such a system,[51],[52].[53] M. Rud at JPL designed such a system pictured below in Figure 59 for a concept for the MOIRE project. More complex correctors that include a reverse fresnel lens have also been proposed for space telescope applications.[49]

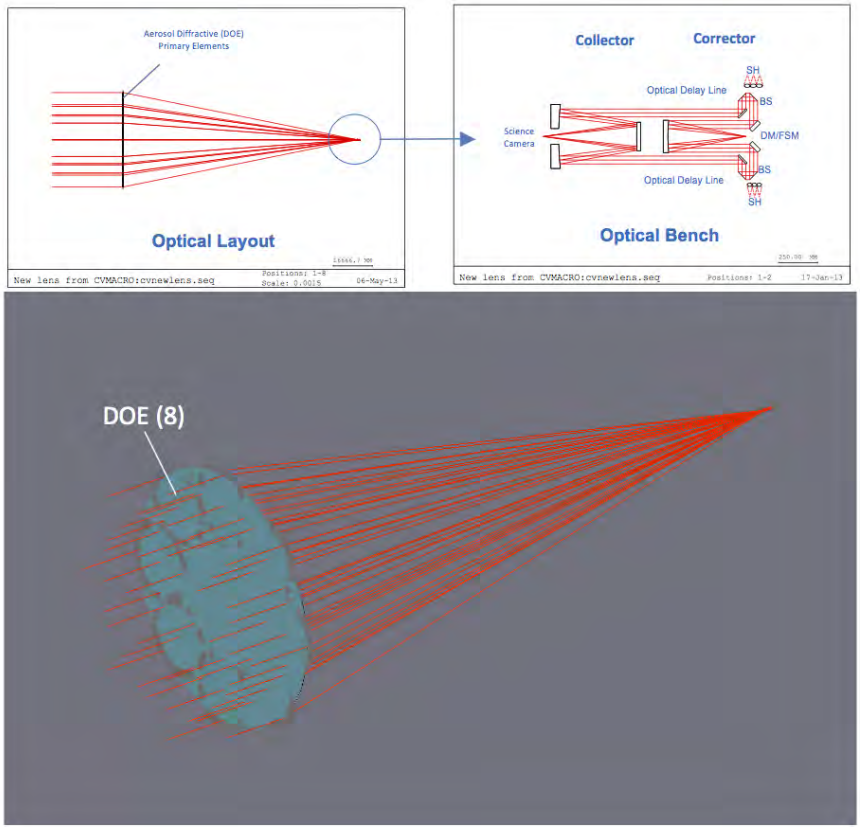

Figure 58: Eight 10 m F/10 Diffractive Patches Concept Design. The DOE is optimized for a wavelength of 633 nm.

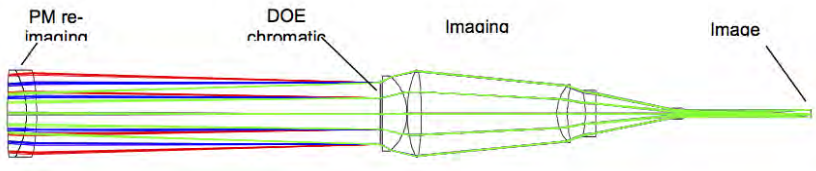

Figure 59: Diffractive Optical system chromatic corrector (courtesy M. Rud, JPL)

10.5 Wavefront Sensing and Control

10.5.1 System Description

Wavefront Sensing (WFS) is the measurement of the optical aberrations in an imaging system, such as a space telescope. Phase Retrieval is an image-based WFS tool, taking as its input data defocused images of an unresolved object such as a star or an optical pinhole or fiber. It computes a WF map a 2-dimensional array of Optical Path Difference values showing the deviation of the actual wavefront from its spherical ideal. For telescopes equipped with actuated optics, such as deformable or movable mirrors, this WF map provides the information needed for control of WF errors, and it does so in the actual science cameras, without requiring a dedicated WFS instrument. A detailed description of a simple iterative phase retrieval algorithm is given in the next section.

Phase Diversity is a superset of Phase Retrieval that attempts not only to estimate phase errors in a system, but also an object that forms an image. Therefore, it is not limited to an unresolved point source, but utilizes an extended scene. There are many methods for performing phase diversity, one of which, multiframe blind deconvolution, is described in detail in the following section.

Phase retrieval and phase diversity generally need to know the relative intensity across the entrance pupil of the system. If the illumination source is an unresolved point source, then the pupil amplitude, and therefore intensity, can be assumed to be constant over the entrance pupil. However, it is generally conceivable that there will be features in the exit pupil that are underdetermined, such as obscurations caused by objects in the optical path (support struts for example). When one begins to image resolved sources, or scenes, the pupil amplitude will be even less well known and it may become necessary to include the estimation of the pupil amplitude as part of the wavefront sensing methodology. Several different groups have reported results of estimating the amplitude and phase using phase diversity,[37].[70]

We have done a comprehensive search of various phase retrieval and phase diversity approaches. We plan to explore several ourselves in the next phase of our research. For example, Fienup and his research group at the University of Rochester have had tremendous success using nonlinear optimization techniques with numerous kinds of diversity to solve for phase errors and object estimates. They solve for the full complex pupil function using phase-diverse

data.[15] They have invented a new kind of diversity, called transverse translation diversity, which uses a shifting pupil mask to provide image diversity.[34] Our idea of using a microshutter array in the pupil plane is similar to this technique. Thurman and Fienup described an algorithm that can handle random misregistrations of the PSFs collected for a single image data set,[76] a situation which our ever-shifting aerosol optic may find itself needing to exploit. To combine data from several apertures, a piston diversity technique was also developed.[13]

Shack-Hartman wavefront sensing does utilize a dedicated instrument, which includes a lenslet array at a pupil to convert wavefront slope to centroid offsets on a separate detector. Therefore, part of the light from the science path must be picked off, typically using a beamsplitter, for this instrument. The advantage of a Shack-Hartman wavefront sensor is that is has a relatively high dynamic capture range and the image processing requirements are low. Therefore is can make rapid phase estimates (typical systems run at 500 Hz or greater, including corrections on a deformable mirror). However, the spatial frequencies that it can measure are limited to the number of lenslets and it does not work across discontinuities, such as a segmented telescope system will have. Our system is not segmented, and therefore we will utilized this kind of wavefront sensor to interrogate and keep aligned individual aerosol clouds. When combining imagery from multiple apertures, or clouds, we plan to investigate using phase diversity.

10.5.2 Multiframe blind deconvolution

Phase diversity[29] is a technique to jointly estimate an object, i.e. extended scene, and phase errors in an optical system. The phase errors are typically used to deconvolve a better estimate of the measured object. This technique requires a set of diverse images to be taken nearly simultaneously. The most common form of diversity is phase diversity, and the phase is most commonly a focus term. In other words, a set of imagery, each with different focus terms, can be used to create a better overall estimate of the scene under interrogation. Other types of diversity are just as useful, as long as something is known about the diversity. Multiple techniques exist to solve for phase errors, including iterative[27] and using global optimization. If the diversity between images is not known or not known well, then other techniques are used such as blind deconvolution.[42] Multi-frame Blind Deconvolution[?] was developed for speckle imaging, where a precise measurement of a stellar object from

the ground is not possible due to the changing index of refraction caused by the Earths atmosphere. Schulz developed the technique for ground-based imaging of finite extent objects and Van Kampen and Paxman extended the technique to infinite extent objects, or objects that extend beyond the field of view.[39]

In general, multi-frame blind deconvolution works by taking multiple images through the optical system. Ground-based techniques assume that the effect of the atmospheric effects are not known exactly, or not measured. However, certain information, such as measuring the Fried parameter (r_0) and relying on Kolmogorov statistics, are used in the algorithm. Recent work[68] has shown that high-order aberrations can be estimated and compensated for computationally. In our Phase II report, we will discuss simulating the cloud physics, and will explore using multi-frame blind deconvolution to determine the quality of imagery that can be reconstructed using these advanced computational optics techniques.

Another form of diversity that can be exploited for post-processing of multiple images to better estimate the object is wavelength diversity. This was discussed by[30] and a blind-image deconvolution approach was developed and tested more recently by.[36] Assuming our system is polychromatic, we plan to pursue this technique as well.

In our design we stated that we plan to exploit a micro-shutter array (MSA)[48] in the pupil plan to create different aperture masks. This will allow us to essentially block out, or ignore, portions of the cloud optic while interrogating others. One of our initial goals for this system was to make it extremely fault-tolerant. This implies that the particles that make up the optic could be constantly shifting depending on the trapping scheme that is implemented. If so, then different parts of the cloud may contain more densely packed particles than others and being able to dynamically block out less-dense portions of the aperture and concentrate on sweet spots becomes important.

Figure 60 compares the three optical systems considered until now, namely a refractive, reflective, and diffractive, and their implications regarding optical bandwidth and control needs at the grain level.

10.5.3 Expansion of Wavefront Sensing Conceptual Description

Consider the simple parabolic mirror imager sketched in Figure 61. Ideally, this mirror takes a collimated beam of light from an infinitely distant star,

Characteristic	Reflective	Refractive	Diffractive
Each particle needs to be precision controlled	Yes	No	Yes
Optical Bandwidth	Very high	Constrained	Very constrained

Figure 60: Comparison of three optical systems.

and brings it to a sharp focus at a single point on a detector. If we think of the starlight in simplified wave-optics terms, monochromatic, coherent light emitted from the star arrives at the mirror in a series of planar wavefronts (WFs), all of which are perfectly flat and perpendicular to the line of sight between the star and the mirror. The WFs can be thought of as surfaces where all of the coherent light has the same complex amplitude and phase. The mirror collects all of the light that hits it, converting the sequence of planar wavefronts to a sequence of concentric spherical wavefronts, whose shared center of curvature is a single point on the surface of the focal plane the image spot. These spherical wavefronts compress and concentrate as they approach the focal plane. If one places a detector at the focal plane, the detector will see a tight spot image, with a bright central core (and dim, diffused sidelobes due to diffraction). If one places a detector away from focus, at the locations indicated in the figure, the detector will see a blurred top hat image an outline of the aperture of the mirror, blurred by diffraction, but radially symmetric and smooth. Now consider the effect of a small bump on the mirrors surface. Such a bump will induce wavefront error (WFE) or deviation of the wavefront from a perfect sphere. The radius of the light that hits the bump will change, shifting the point at which that patch of light comes to a focus away from the common focal plane. Now a detector at the focal plane will see a degraded spot, with less light in the core and a blob in the sidelobes. Defocussed images will show a strong signature of the bump, as sketched in the figure. The intrafocal image in this example has less light in the area of the bump, so that patch of the defocused image is dimmer; the extrafocal image has more light in that patch, so it shows up as a bright spot compared to the rest of the top-hat image. Physics tells us that the complex amplitude field at the pupil and image planes are related by Fourier transforms. If we know the one, we can

compute the other. The image intensity gives us the magnitude part of the complex amplitude matrix, but not the phase at least not directly. The images can give us the phase indirectly, however, as was first described by Gerchberg and Saxton.[27] Iterative processing of multiple defocussed images correlates the intensity variations in each, providing a means to compute a common WF phase map. Our MGS algorithm uses just such an approach. Its inner loop (Figure 62) iterates between the image plane and the pupil plane using Fourier transforms. At the image plane, we replace the magnitude part of the complex amplitude matrix with the square root of the image, so that the complex amplitude is at least half right. Then the amplitude is propagated to the pupil plane. Here the square root of the pupil image replaces the magnitude part of the complex amplitude matrix, and again we are half right. The iterating phase (initialized randomly) is not replaced. It is propagated through the iterations, quickly evolving to be consistent with both images. Basically, any phase that is not consistent with an image is thrown out when we overwrite the magnitude of the propagated amplitude with the measured intensities. After a few iterations, the iterating phase becomes a reasonable estimate of the WF phase.

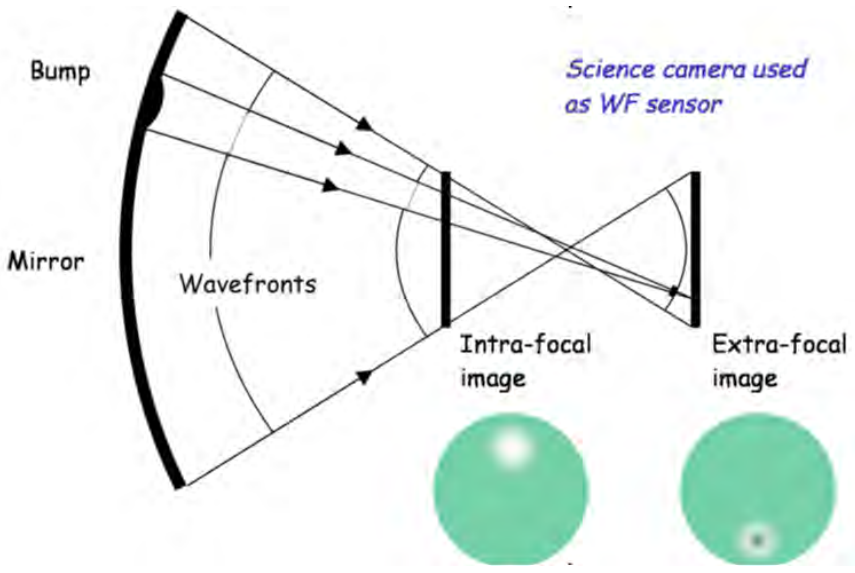

Figure 61: Sketch of how WF errors influence defocused images.

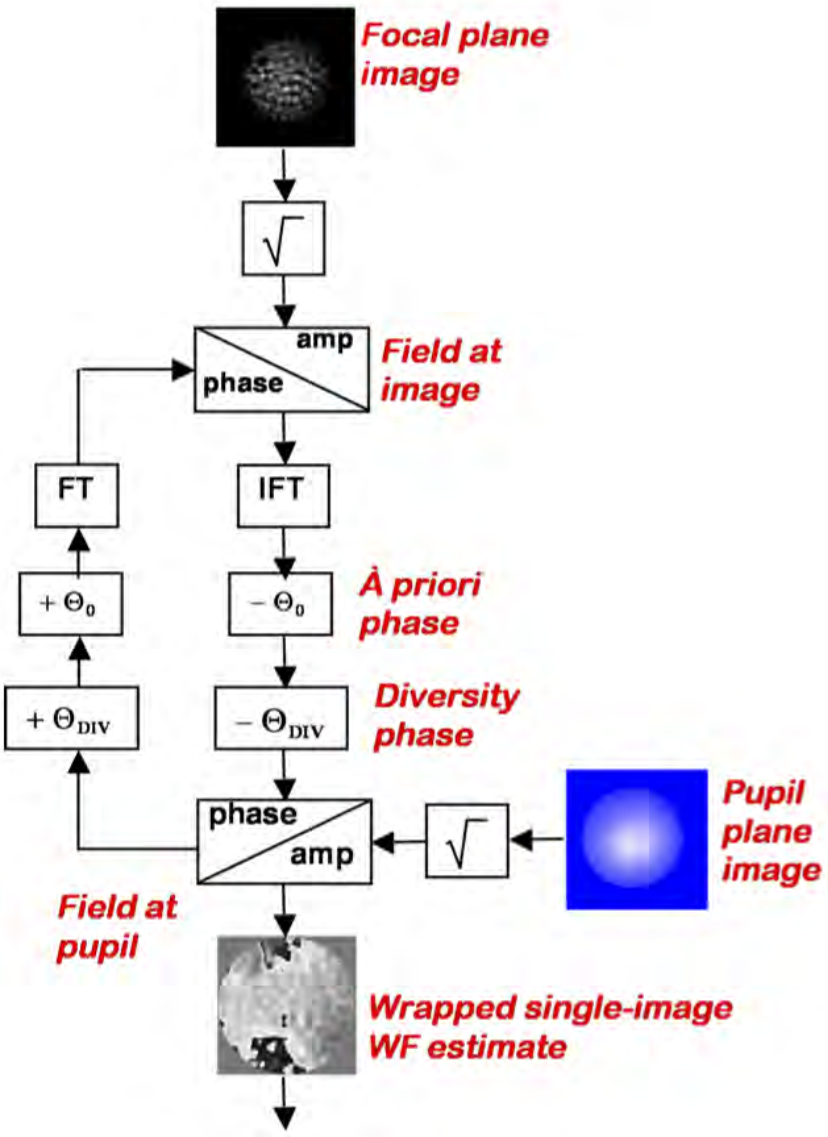

Figure 62: The MGS inner loop.

10.6 Novel techniques for deployment, cooling, and reforming the cloud

The advantages of distributed space systems have been explored in many contexts. For an imaging system such as a space telescope, there are both cost and performance advantages owing to reduced mass and a larger effective aperture.[53] The fractional degree of thinning allowable for incoherent imaging in principle is inversely proportional to the square root of the number of elements in the full array".[77]

Previous studies, including NIAC ones (see section on prior NIAC studies), have struggled to position and orient the optical sub-systems to achieve a good surface figure. Woolf proposed ways to correct surface errors of 100 m in-space reflectors. Bekey explored a swarm of station-keeping adaptive-optically controlled primaries, each positioned with precision micro-thrusters, having an effective aperture of 30 m. A real-time holographically corrected 1 m low thermal expansion polymer membrane telescope was proposed by Palisoc. Motivated by the laser-controlled pellicle of Labeyrie,[43] McCormack explored the possibility of trapping refractive particles along a parabolic shaped interference fringe. Making use of reversible trans-cis photoisomerization, Ritter proposed using a UV light source to correct the figure of a large space optic film. Combining tethers with radiation pressure, Bae proposed nanometer scale accuracy of formation flying spacecraft.

In recent years however, advances in optical imaging have combined computer algorithms with measured irradiances to achieve good imaging performance from sparse (even random) systems. Early examples date back to 1970 when Antoine Labeyrie demonstrated near diffraction limited imaging under poor atmospheric seeing conditions.[45] More recent examples include phase-shifted interferometry to recover tomographic images,[19] and using disordered optical elements to achieve sharp images.[79] In all these cases, the seemingly poor optical system was empirically characterized so that a numerical algorithm could use the information to enhance the image quality. With a proliferation of such techniques in the modern literature, we can trade optical figure (which is difficult and expensive) with computing power (which is proven and inexpensive). In this report we therefore explore means to achieve a good enough optical system that will afford the use of advanced image reconstruction algorithms.

10.6.1 Deployment

We start by considering a swarm of reflecting optical elements distributed in an ideal space environment free of gravity, drag, radiation pressure, solar winds, plasma charging, and other disturbances. Let us assume each element has a reflective area, A_0, and all together, they constitute a net reflective area A_{net}. The elements are distributed throughout a volume of space, which we assume takes the form of a sparsely populated pancake of diameter D. The elements may be released, one by one, from a spinning spacecraft, such that each particle has its own axis of rotation, but a common angular velocity, ω_0. The attitude of the releasing craft may be controlled to allow the rotation axis of each particle to vary across the swarm. For example, the particles at the center of the swarm will be aligned with an imaginary line that constitutes the optical axis of the imaging system. For convenience we define this as the z-axis of the system. As the craft spirals azimuthally and radially outward, the rotation axis of each particle will lie along an extended line that passes through the radius of curvature, R, of the optical imaging system. In this way the swarm represents a dilute segmented mirror of focal length $f = R/2$. It is unrealistic to expect the craft to place each element on an imaginary spherical or parabolic surface. Such control ideas dating back to Labeyrie have met with extreme difficulty in achieving and maintaining the required interferometric precision. Rather than trying to control the swarm to achieve an ideal optical figure across meters of space, we ask what control is good enough to achieve, with the aid of computer algorithms and measured characterizations of the swarm, an sufficiently good image. Addressing the imaging problem in this way provides a roadmap for advancing the image quality via three routes: better control of the swarm, better characterization of the swarm, and better imaging algorithms.

Each i_{th} reflective element is ejected from the spinning craft with a linear velocity equal to the instantaneous velocity of spacecraft at the time of release: $v_i(r) = v_{SC}(t)$. An outrigger on the craft may be used to provide a momentary burst of light that exerts radiation pressure on the element. This is done to effectively freeze the swarm so that the relative motion between the elements is minimized. The radiation pressure force is linearly related the reflected laser power: $F \approx Power/c$, where c is the speed of light. For an optical element of mass m_0, we can estimate the energy that must be delivered by the laser using the relation $F = m_0 v_x/\Delta t$. That is, $Energy = (Power)\Delta t = m_0 c v_{SC}$. Clearly this approach of freezing the

cloud benefits from low mass elements. For example, if $m_0 = 1$ [mg] and $v_{sc} = 1$ [cm/s], then 3 [J] of energy must be illuminate the element. A 100 [W] diode laser, for example, would necessitate an exposure time of 30 [ms]. Over this duration the relative displacement of the spacecraft and element would be roughly than 3 [mm]. The laser bars may be hinged to prevent a collision with the released optical element. A schematic diagram of the system is shown in Figure 63.

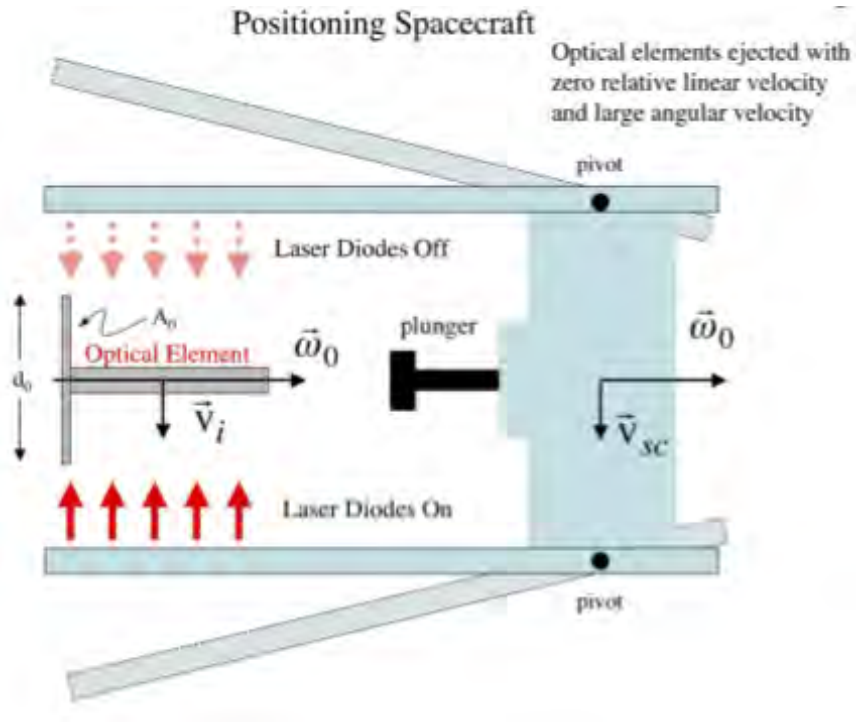

Figure 63: Elements of a delivery system for spinning optical elements. Laser diode illumination of the element is synchronized with the spin rate so that the radiation pressure acts to stop drift.

The elements are composed of a low mass reflective film, which is unfurled from a higher mass reflective cylindrical tube. The purpose of the cylinder is to (1) stow the film before it is unfurled, and (2) provide rotational stability. The spin-up and controlled release of cylindrical objects is a mature mechanical process.

As shown in Figure 64, the elements tend to focus light toward a com-

mon focal point, acting as a distributed segmented mirror. In fact, however, the optical figure cannot be controlled with optical precision. However, if the inter-element spacing does not change rapidly, then one may record a speckle pattern, assuming starlight is sufficiently coherent. So-called speckle interferometry[?] is a well-known area of astronomical imaging that was developed to achieve near diffraction limited performance under poor seeing. Figure 65 shows a numerical example showing the reconstruction of a binary light source from speckle images. The summation of all irradiance distributions in the image plane is Fourier transformed to recover an image. To obtain a good image, the number of samples may number in the hundreds. Here the poor seeing is attributed to the random relative phase of the reflected beamlets. If the reflective area, A_0, is too small, the reflected beamlet will diffract in the focal region, and the collected irradiance will be too weak. The radial diffracted beam size may be expressed as $q_0 = 1.22\lambda f/d_0 = 1.08\lambda f/{A_0}^{1/2}$where we have assumed an element having a circular reflective surface of diameter d_0: $A_0 = \pi(d_0/2)^2$ and $f > (\pi\lambda)(d_0)^2$. For example, if $\lambda = 1$ [μm], $f = 100$ [m], and $d0 = 1$ [mm], then $2q_0 = 0.24$ [m]. The speckles will therefore tend to be concentrated across this region. The diameter of each speckle is expected to be roughly $2q_s = 2.44\lambda f/D$. For $D = 10$ [m] this provides as many as $(q_0/q_s)^2 = (D/d_0)^2 = 108$ speckles across the beam focal area, each of diameter 24 [μm]. The number of recorded speckles is expected to scale with the effective number of elements taking part in the interference, N_{eff}, which may be as high as the actual number of elements, N, if they are well aligned. The sparsity of speckles scales with the sparsity of reflecting elements.

Significant image enhancements may be achieved by determining the point spread function of the quasi-stationary swarm of reflectors. We proposed a reverse guide star approach for this purpose. On Earth, a laser may be used to create an artificial guide star from atmospheric scattering (e.g., from the sodium layer). Lacking such scatterers in space, we propose a formation-flying laser, aligned directly between the desired astronomical body and the swarm. At a sufficient distance the laser will flood the swarm with bright collimated light. The measured laser speckles will coincide with those from the astronomical target, assuming the wavelengths are roughly the same. By electronically masking the areas of the detector where the laser speckles are absent or weak, one may, after switching the laser off, eliminate light scattered toward the detector from other sources (noise sources). This masking technique may be applied even if the swarm is slowly evolving, since

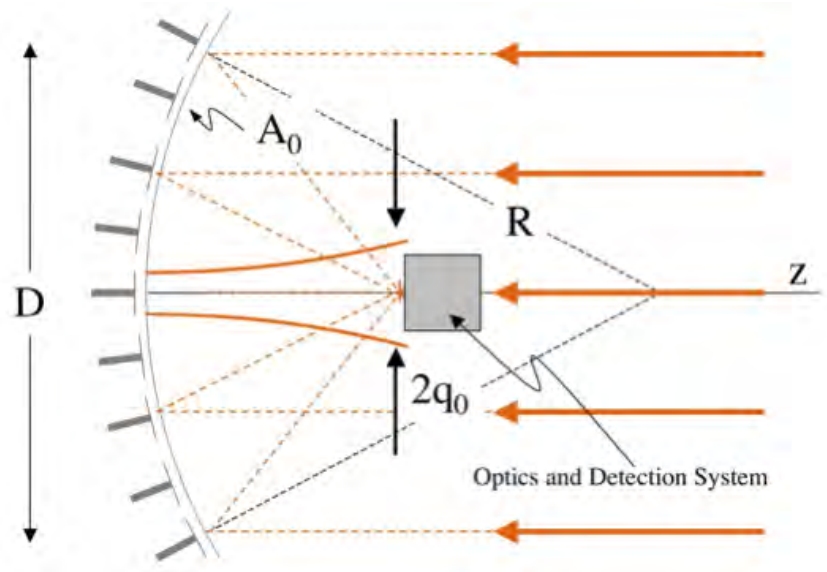

Figure 64: Schematic of optical elements roughly positioned along a spherical or parabolic surface to form an optical concentrator.

speckles may evolve in a deterministic wave if the swarm perturbations are regular.

10.6.2 Precession Cooling

Owing to disturbances in the space environment or intentional perturbations, the spinning optical elements may exhibit precession about the rotation axis. This may cause the speckle field to scintillate, requiring a short exposure time for each speckle image. An understanding of this effect is needed to establish a control mechanism to slow the rate at which the speckles change. Toward this goal we consider radiation pressure induced torque in the following section. Assuming the attitude of the optical element is close to a state of rotational equilibrium, an undamped restoring torque will exist. Lacking any damping, the system may exhibit complicated dynamics. Negative feedback mechanisms will be explored in Phase II to restore the attitude to the rotational equilibrium state. For simplicity, the system may be first treated as a one-dimensional harmonic oscillator in a rotating frame.

In free space and ignoring all external forces, a material particle may

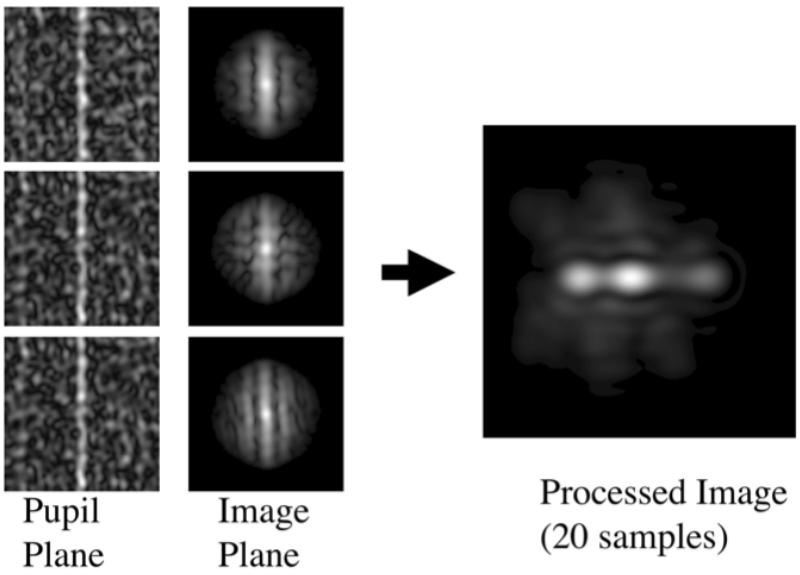

Figure 65: Numerical example showing the reconstruction of a binary light source from speckle images. The summation of all irradiance distributions in the image plane is Fourier transformed to recover an image. To obtain a good image, the number of samples may number in the hundreds.

be translated and rotated by means of a beam of light. Radiation pressure forces produce scattering and gradient forces on the particle. If the particle is non-spherical, the forces will not be uniformly distributed along the particle interface, and therefore the particle may experience a torque about the center of pressure. What is more, a polarized beam may be used to exert a torque on a particle owing to the birefringence. Here we examine mechanical properties of an arbitrary rod-shaped particle, assuming a restoring radiation pressure torque. See Figure 66.

Let us first describe the system when the turntable is stationary ($\Omega = 0$). Assuming the rod experiences a linear restoring torque toward the equilibrium angle, $\theta = 0$, the natural frequency of oscillation may be expressed $\omega = (k/I)^{1/2}$, where k is the torsional stiffness and I is the moment of inertia. The rocking rod may be conceptually replaced by a simple linear harmonic oscillator having an equivalent natural frequency. The linear oscillator is

constrained to the x-axis.

In the rotating reference frame there is an effect centrifugal force, as well as a harmonic restoring force so that the conceptually equivalent equation of motion may be expressed:

$$\ddot{x} = (\omega^2\Omega^2)x = -g^2x \tag{17}$$

where $g = (\omega^2\Omega^2)^{1/2} = \pm i(\Omega^2\omega^2)^{1/2} = \pm i\gamma$. When $\omega > \Omega$ solutions of Eq. (1) may be expressed for the displacement and velocity as harmonic functions:

$$x(t) = x_0 cos(gt) + (v_0/g)sin(gt) \tag{18}$$

$$v(t) = v_0 cos(gt) - gx_0 sin(gt) \tag{19}$$

The phase space trajectory (v(t) vs x(t)) maps out an ellipse $g^2x(t)^2 + v(t)^2 = g^2{x_0}^2 + {v_0}^2$:

However, when $\omega < \Omega$ solutions of Eq. (1) become hyperbolic, as may be seen by writing $g = \pm i(\Omega^2\omega^2)^{1/2} = \pm i\gamma$, where $\gamma = (\Omega^2\omega^2)^{1/2}$ is a real quantity, assumed to be positive. Direct substitution into the above solutions, using the identities $cos(i\gamma) = cosh(\gamma)$ and $sin(i\gamma) = isinh(\gamma)$, provides the following:

$$x(t) = x_0 cosh(\gamma t) + (v_0/\gamma)sinh(\gamma t) \tag{20}$$

$$v(t) = v_0 cosh(\gamma t) + \gamma x_0 sinh(\gamma t) \tag{21}$$

The parametric equation in phase space may be written

$$\gamma^2 x(t)^2 + v(t)^2 = (\gamma {x_0}^2 + {v_0}^2)(cosh^2(\gamma t) + sinh^2(\gamma t)) + 4\gamma x_0 v_0 cosh(\gamma t)sinh(\gamma t) \tag{22}$$

Unlike the harmonic case ($\omega > \Omega$), the hyperbolic case ($\omega < \Omega$) provides *a means to decay a point in phase space toward the origin.* This is satisfied for an initial point (x_0, v_0) if the following relation is obeyed: $v_0 = -\gamma x_0$. This condition may be satisfied in quadrants II and IV of phase space. The displacement and velocity tend to zero as t approaches infinity. In this special case, we write

$$x(t) = x_0(cosh(\gamma\, t) - sinh(\gamma\, t)) \tag{23}$$

$$v(t) = v_0(cosh(\gamma\, t) - sinh(\gamma\, t)) \tag{24}$$

The phase space trajectory is a straight line of slope $v(t)/x(t) = v_0/x_0 = -\gamma$. On either side of this line the phase space trajectories are hyperbolic, diverging away from the origin, as graphically illustrated in Figure 65. In comparison, all points satisfying $v_0/x_0 = +\gamma$ (e.g., in quadrants I and III) have trajectories that diverge away from the origin along a straight line. The set of lines $v_0/x_0 = \pm\gamma$ represent separatrices for the hyperbolic orbits for a given origin along a straight line. The set of lines $v_0/x_0 = \pm\gamma$ represent separatrices for the hyperbolic orbits for a given value of γ .

Since only a small region of phase space may be decayed to the zero point for a given control value of Ω, this approach is not efficient. A feedback mechanism or loss is need to actively bring large regions of phase space toward the origin, $(x, v) = (0, 0)$.

To attract a larger region of phase space toward the origin, let us consider loss. The mechanism of loss may come, for example, from the conversion of mechanical energy into heat that dissipates. Let $2\alpha > 0$ be the loss coefficient.

$$\ddot{x} = (\omega^2\Omega^2)x - 2\alpha\dot{x} = -\gamma^2 x - 2\alpha\dot{x} \tag{25}$$

Solutions can be found in terms of the initial conditions, with $\gamma = (\omega^2\Omega^2)^{1/2}$ and $s_0 = (\gamma^2 - \alpha^2)^{1/2}$ as:

$$x(t) = (x_0 cos(s_0 t) + \frac{v_0 + \alpha x_0}{s_0} sin(s_0 t)) \exp(-\alpha t) \tag{26}$$

$$v(t) = (v_0 cos(s_0 t) - v_0(\alpha/s_0) sin(s_0 t) - x_0(\alpha^2/s_0 + s_0) sin(s_0 t)) \exp(-\alpha t) \tag{27}$$

Hyperbolic case: If $\omega^2 < \Omega^2 + \alpha^2$ then $s_0 i(\alpha^2 + \Omega^2 - \omega^2)^{1/2}$ and

$$x(t) = (x_0 cosh(st) + \frac{v_0 + \alpha x_0}{s} sinh(st)) \exp(-\alpha t) \tag{28}$$

$$v(t) = (x_0 s sinh(st) + (v_0 + \alpha s) cosh(st)) \exp(-\alpha t) - \alpha x(t) \tag{29}$$

Finally we note the special case $\gamma = (\Omega^2 - \omega^2) = 0$, then $s = \alpha$:

$$x(t) = (x_0 + \frac{v_0}{2\alpha})(1 - \exp(-2\alpha t)) \tag{30}$$

$$v(t) = v_0 \exp(-2\alpha t) \tag{31}$$

This is remarkable because as t tends toward infinity, the velocity becomes zero valued for all points in phase space. The asymptotic value of position tends toward $x0 + v0/2\alpha$. The phase space trajectories are straight lines having the slope 2α, and the equation for the line is

$$v(t) = 2\alpha x(t) - (2\alpha x_0 - v_0) \tag{32}$$

All points in the system simply decays to the point $(x, v) = (x_0 + v_0/2\alpha, 0)$ as t tends toward infinity. To ensure that x tends toward zero, the following condition is required for the decay constant: $2\alpha = -v_0/x_0$. Thus, for a low loss system having a small decay constant, the initial velocity must be relatively small.

Figures 67, 68, and 69, respectively, depict representative results of the numerical simulation of the cooling process.

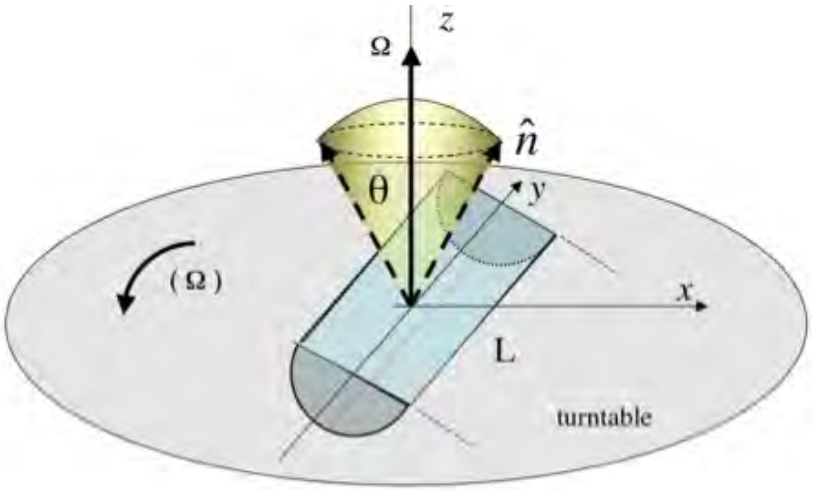

Figure 66: Semicylindrical rod of length L and radius R aligned with the y-axis of a rotating turntable having angular velocity ω. The rod swings to an angle $\theta(t)$ about z-axis in the x,z plane. The x,y,z axes are fixed to the turntable. In this rotating system the equation of motion is given by Eq. (1). In the laboratory frame the normal vector of the rod, **n**, swings throughout a cone (demarked by yellow region).

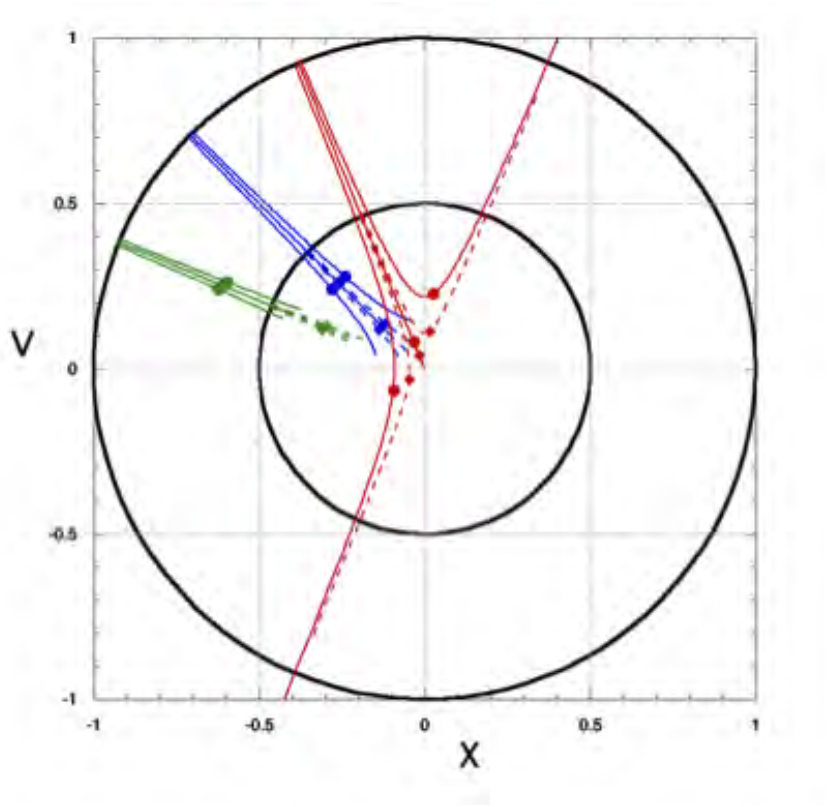

Figure 67: Hyperbolic phase space curves for three different values of γ, and for initial points 1% away from the initial points that satisfy $v_0/x_0 = -\gamma$. The blue lines correspond to $\gamma = -1$. The red (green) line correspond to $\gamma = -2.4(0.4)$. Time ranges from zero to $T = 2$. The red case nearly reach the origin at T, whereas the blue and green cases do not. Solid (dashed) lines correspond to initial points on the unit (half-unit) circle. Initial points not satisfying $v_0/x_0 = -\gamma$ diverge. Therefore, a small region of phase space may be decayed toward $(x, v) = (0, 0)$.

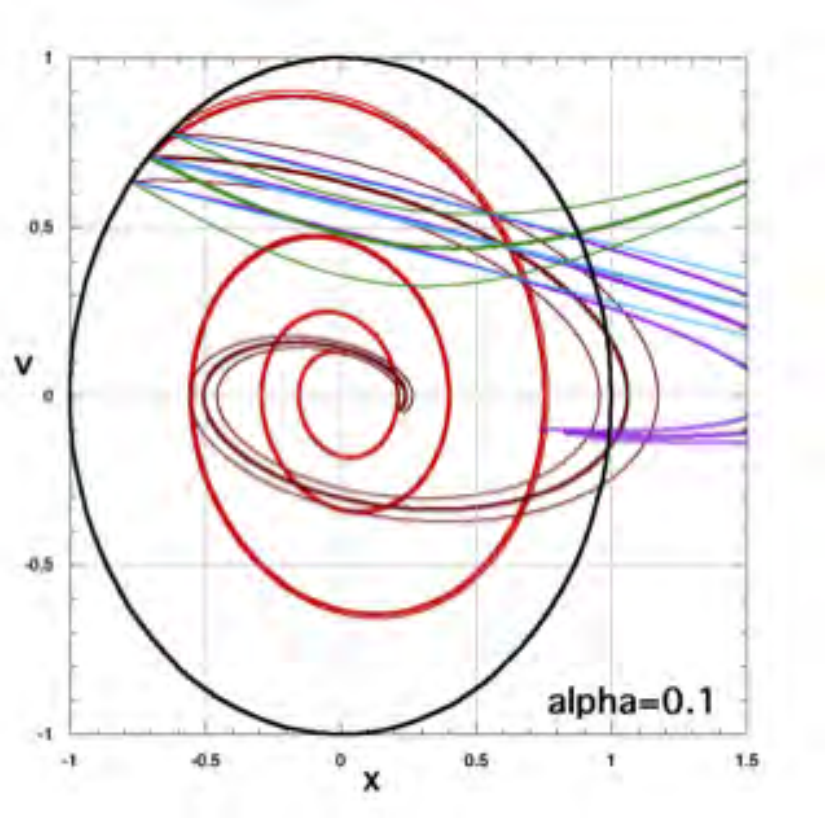

Figure 68: Phase space plots for $\alpha = 0.1$ and various values of Ω/ω, ranging from 0.5 (bright red), 0.9 (dark red), 0.99 (purple), 1.0 (cyan), and 1.1 (green). The initial point is at 135 degrees on the unit circle (black).

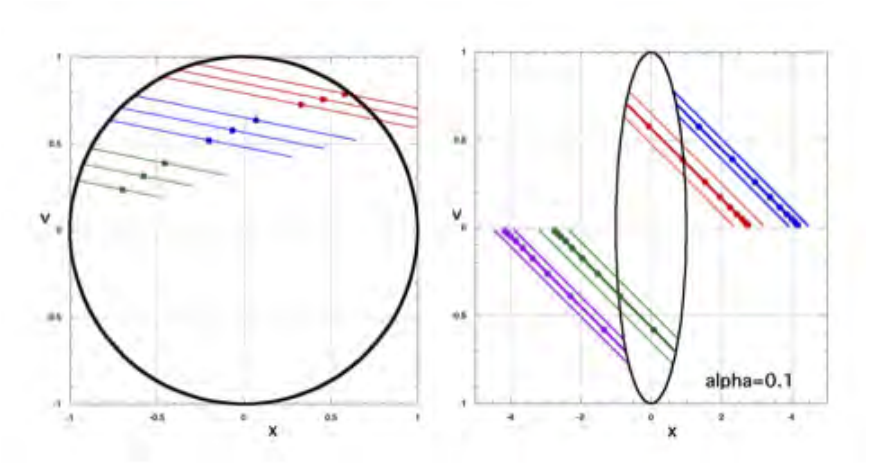

Figure 69: Hyperbolic case for $\Omega = \omega$ so that $s = \alpha$. The slope of the lines are equal to the loss, 2α.

10.6.3 Reforming the Cloud

This section deals with the Control, Sensing and Metrology at the cloud level, i.e., assuming that the formation flying loop has already taken care of the gross translations and rotations of the cloud as a rigid object. hence, we deal with the micro-scale and the meso-scale.

The approach for cloud control is multistage, based on laser cooling, and involves three levels: a) Trapping (corralling) through gradient forces to provide containment against cloud diffusion due to thermal, radiation, and gravity and cloud cooling; b) shaping/alignment through laser pressure, to change amorphous cloud into disk or rectangular carpet; and c) alignment of grains to wavefront direction, which implements wavefront/boresight control through adaptive optics in order to maintain optical figure. Related work is presented in[32] and.[33] For any size/shape particle, the electromagnetic energy is minimized when the particle is in the brightest region of the laser beam, and this is the basis for light-induced control. Corralling assumes mechanically releasing the cloud with low ejection velocities, then applying 3-axis laser illumination to corral the cloud via optical gradient forces. The cooling approach can be achieved by means of gradient forces, which involves rotating the linear polarization direction of the control laser at the rocking frequency. This effectively freezes the oscillations in a rotating reference frame. By adiabatically slowing the rotation of the polarization axis, some population of particles can be made to assume the same orientation, e.g., with the flat mirrored side of the rod facing the center of curvature. Cloud shaping is carried out via raster scanning of the beam across granular patch. An optimization is needed of the time dependent beam power and beam velocity to capture the most particles, and will be subject of future work. Grain alignment for phase coherence is achieved by applying linearly polarized control laser to orient particles along dominant polarization axis (long axis of rod), so that the particles will rock under the influence of polarization torque and radiation pressure torque.

In the event that the delivery vehicle can not place the reflecting elements on an imaginary spherical or parabolic surface in space, or if disturbance forces from the space environment disrupt the swarm, we must consider reforming the swarm. If the individual elements are too small to support their own thrust mechanisms, then external forces may be applied. The reflecting or refracting properties of the elements afford an opportunity to use radiation pressure to corral the swarm into a pancake shaped structure, and optical

polarization to affect the attitude of each particle. Compact diode-pumped lasers with powers up to the 100 kW range have been developed and may suitable for use in space, assuming solar arrays and heat radiators can handle the load. This approach benefits from the advances made in laser ballistic missile defense, including targeting, system integration, and wavefront control.

As seen in a previous section, radiation pressure forces can be decomposed into two components: a scattering force that acts in the direction of the incident beam of light, and a gradient force that in our case is directed perpendicular to the incident beam. The magnitude of the scattering force may be expressed as $F_s = \eta IA/c$ where η is a dimensionless efficiency factor, I is the incident irradiance, A is the cross-sectional area of the illuminated object, and c is the speed of light. As an example, the solar irradiance near the earth ($1.3kW/m2$) produces a force as high as 10 pN on a 1 mm^2 object. Using the density of water ($1g/cc = 10^3kg/m^3$) as a guide, the mass of a $1mm^3$ object (10^6kg) would accelerate at $10^5m/s^2$. In contrast a 100 kW beam having a 0.1 m diameter would produce a larger force by a factor of 13 $MW/m^2/1.3kW/m^2 = 10,000$. (Note: for comparison the long exposure damage threshold for an aluminum mirror is $1GW/m^2$.) A 10 second exposure of such a beam would produce a change of velocity: $\delta v = 1m/s$. To prevent unwanted scattering forces, counter-propagating beams may be employed. With the swarm positioned between the opposing lasers, and with the lasers mutually incoherent, the elements would experience a zero net force along the direction of the beams. (The lasers would employ optical isolators to reduce the risk of damage and instability.)

Having effectively eliminated the scattering force, the gradient force may be used to control the swarm. For an uncharged dielectric particle having a polarizability α, the gradient force may be expressed as $F_g = (4\pi\alpha/c)\nabla I$, where $I(x, y, z)$ is the irradiance. For a quasi-collimated Gaussian beam of light, assumed here, the direction of force is transverse to the optical axis of the beam, and the particle is attracted into the beam. Similarly, for a reflecting particle, the net force scales as the gradient – except the particle is repelled by the laser beam, as shown below in Figure 70. This scenario is preferable, as it lessens problems associated with laser heating. The gradient force for the reflecting particle may be written as $F_g = -\eta_g RA\nabla I/c$ where η_g is a dimensionless efficiency parameter. Note that if the particles develop a charge, the resulting ponderomotive force will also tend to repel the elements from the beam. To achieve a strong gradient, a large value of the peak

irradiance and a small beam width is desired. The maximum gradient of intensity for a Gaussian beam of power P is $|\nabla I|_{max} = I_0/w$ where $I_0 = 2P/\pi w^2$ is the peak irradiance and w is the beam radius. For a 100 kW beam. If for example the peak irradiance is 1/10th the damage threshold and the beam power is 100kW, then a beam size of $w = 2.5$ cm is required. This may be achieved by focusing the output of the laser, or by adaptive optic control.

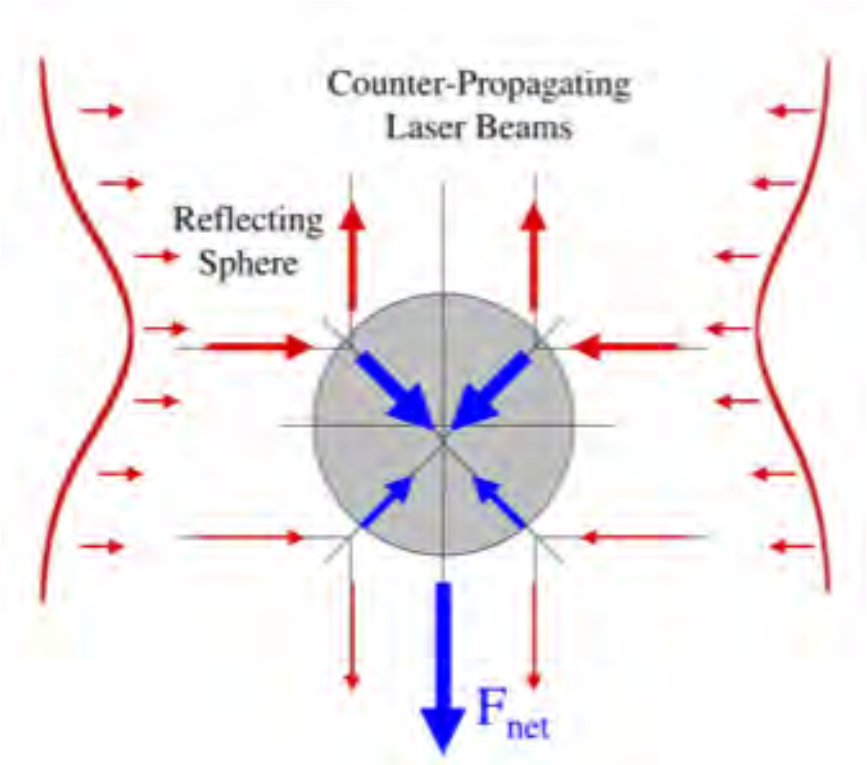

Figure 70: Counter-propagating laser beams incident upon a reflecting sphere produce a net repulsive force away from the beam.

If we consider a Maxwell-Boltzmann velocity distribution across the swarm (see Figure 71), a spatially localized group of elements will expand into a Gaussian distributed cloud after a time T. As the swarm expands it loses its ability to concentrate high intensity speckles in the focal region.

To remedy this we suggest using a push-broom mechanism, which is applicable for both reflective and refractive elements. Co-linear counter-

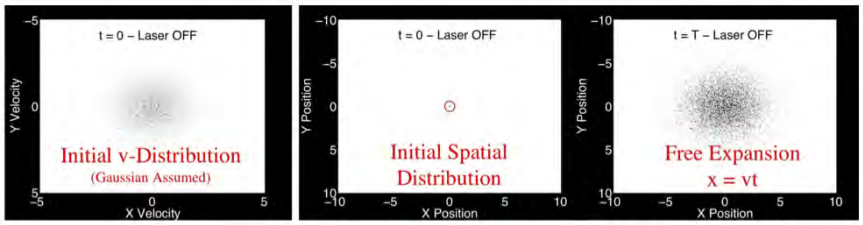

Figure 71: Simplified depiction of an expanding swarm in free space owing to a Maxwell-Boltzmann velocity distribution.

propagating beams are used to sweep the particles toward a desired central location, as depicted in Figure 72. The beam is raster scanned to effectively form a sheet-beam. Like bookends, two sets of sheets may be using to confine the particles into a central layer. Orthogonal sets of sheet beam may be used confine the particles from escaping in the other two directions. Particles having a kinetic energy greater than the trapping potential barrier, $U_g = \eta_g R A I_0 / c$, will escape the swarm. To estimate the velocity of such particles, let us assume a 1 mm3 particle having the density of water (1 kg/m^3) and a 100 kW laser beam having a wavelength $\lambda = 1\mu m$ focused to a radial size of 2.5 cm. A beam of this focal size will remain roughly collimated over a distance $z_d = \pi w^2/\lambda = 2.0km$. The peak irradiance is given by $I_0 = 2P/\pi w^2 = 10^8\ W/m^2$ (1/10th the damage threshold). Equating the kinetic and potential energies and solving for the relative escape velocity, one finds $v_{esc} = \sqrt{2\eta_g I_0/\rho c} = 1.0$ m/s, where an efficiency of 1.5% has been assumed. Although this figure does not account for the actual shape of the particle and the raster rate of the beam, it provides a useful order of magnitude estimation that can be compared against disturbances in the space environment. This also sets on upper limit on the transverse speed of the sweeping beam, v_{beam}. At this upper limit no particles would be swept.

The orientation of the particles must be set after this corralling process. If the corralling and disturbance forces take are applied adiabatically, then the precession of the spinning particles may be controlled by introducing loss or a feedback mechanism.

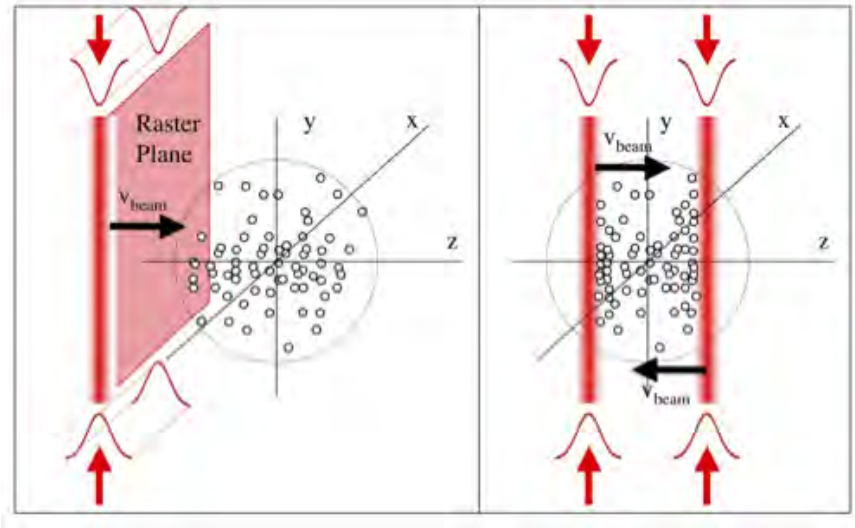

Figure 72: Push-broom optical corralling mechanism whereby counter-propagating laser beams (here parallel to the y-axis) are simultaneously dragged across the swarm (here in the z-direction) at a speed v_beam. The beams are also raster scanned in the x-direction to collect the entire swarm. Reflecting (refracting) particles are repelled by (attracted to) the beam, causing the particles to translate through space.

11 Phase I Accomplishments

The work in Phase 1 was distributed among the following tasks:

- Task 1: Kick-off activity
- Task 2: Optical manipulation requirement definition
- Task 3: Imaging system requirement definition
- Task 4: Integrated mission scenario requirement definition
- Task 5: Prepare and coordinate report and close-out activity

To accomplish these tasks, we had identified the following milestones:

- M1, at Start of Study: Kick off meeting for initial coordination between team members, and subcontract initiation.
- M2, at end of Task 2: Cloud manipulation requirements developed
- M3, at end of Task 3: Imaging system requirements developed
- M4, at end of Task 4: Autonomy requirements developed
- M5, at Study Completion: Final report completed

Our initial plan was to address the overall mission design, find one or more candidate system architectures for the aerosol imaging system (for example: optical imager, hyper-spectral remote sensing), and identify technology gaps by addressing one or more of the following areas:

- a) Identification of practical methodologies to deploy and maintain an active cloud in space,
- b) Determination of requirements for extrapolation of optical lift technology to manipulation of macroscopic cloud,
- c) Determination of conditions required by aperture to function as either a transmitter, receiver, or lens, as a single or multiple aperture,
- d) Determination of key material/thermal properties of cloud,

- e) Determination of key miniaturization requirements to enable a minimum of autonomy (power, GNC, data transfer) at the grain level,
- f) Assessment of risk areas and mitigation plans for areas such as excessive scattering, loss of phase coherence, and orbital debris generation.
- g) Summary of findings and layout of plan forward to Phase II.

Of this ambitious list, we have successfully addressed a), b), c), f), g). Points d), e), and partially f) (orbital debris mitigation) were left for Phase II, as we realized that they depended of a specific system architecture, yet to be developed at the time of the Phase 1 report. Furthermore, Milestone M2 (Cloud manipulation requirements developed) has been met, and is discussed in the section on Novel Techniques for Deployment, Cooling, and Reforming the Cloud of this report, Milestone M3 (Imaging system requirements developed) has been met, and is discussed in the section Exploring New Optical System Options of this report, and Milestone M4 (Autonomy requirements developed) has been met, and is discussed in the section on Cloud Engineering of this report. In summary, we have conducted a preliminary assessment of the initial feasibility of the concept, will have identified credible system architectures, and determined the crucial design parameters of the system. The current TRL at completion of Phase I is TRL 1-2.

12 Publications and Patents

This final report will be made available as a NIAC report in the public domain. In addition, we produced the following reports:

- Dynamics and Control of a Disordered System In Space, submitted to the AIAA SPACE 2013 Conference and Exposition, San Diego, CA, Sept. 10, 2013.
- Multi-scale Dynamics, Control, and Simulation of Granular Spacecraft, submitted to ECCOMAS Multibody Dynamics Conference, Zagreb, Croatia, 1-4 July 2013.
- Scheduled presentation at 2013 Sagan Exoplanet Summer Workshop, July 29 to August 2, 2013. We plan to display a poster at the JPL Open House, Fall 2013. We have also submitted a NASA Technical

Brief package NTR 48950, titled Engineering applications of controllable granular matter in space, on February 23, 2013.

13 Summary and Next Steps

In this section, we summarize our achievements, and lay out the plans for continuation of the work in Phase II. Figure 73 shows a comparison of tasks accomplished or initiated in Phase I and some of the tasks proposed for Phase II.

Task	Phase I	Phase II
Identification of practical methodologies to deploy and maintain an active cloud in space	✖	
Determination of conditions required by aperture to function as either a transmitter, receiver, or lens, as a single or multiple aperture	✖	✖
Determination of key material/thermal properties of cloud		✖
Determination of key miniaturization requirements to enable a minimum of autonomy (power, GN&C, data transfer) at the grain level		✖
Assessment of risk areas and mitigation plans for areas such as excessive scattering, loss of phase coherence, and orbital debris generation	✖	✖
Determination of the crucial design parameters for system deployment, orbit selection and maintenance, autonomous optical system stabilization, and cloud optical manipulation.	✖	✖
Preliminary assessment of simulation needs	✖	
Demonstration of system performance in simulation		✖
Identify technology gaps for selected architectures	✖	✖
Proposed experimental efforts		✖

Figure 73: Tasks in Phase I and Phase II.

13.1 Cloud physics

We have insight on physics of disorder system and dominant forces that perturb cloud, and discovered that the forces involved in the cloud gravito-

electrodynamics leads to self-organization. **An in-depth characterization of material and electromagnetic properties of the grains, of the self-organizing properties of the cloud in space, of the attainable coherent vs. incoherent imaging, ambiguity, resolution, and imaging sensitivity, will be carried out in Phase II using an integrated structural, thermal, optical, controls, and gravitational (STOPCG) analysis effort using simulation.**

13.2 Cloud sensing and control

The proposed cloud sensing approach is based on imaging/laser scanning, relying on custom or commercial laser scanning systems which can create precise 3-D model of complex objects. The proposed multistage approach for cloud control based on laser cooling, and involves three levels: Trapping (corralling) through gradient forces to provide containment against cloud diffusion due to thermal, radiation, and gravity and cloud cooling; shaping through laser pressure, to change amorphous cloud into disk or rectangular carpet; and alignment of grains to wavefront direction, which implements wavefront/boresight control through adaptive optics in order to maintain optical figure. The cloud cooling can be achieved by means of gradient forces, which involves rotating the linear polarization direction of the control laser at the rocking frequency. This effectively freezes the oscillations in a rotating reference frame. **Simulation studies will be conducted at JPL and Rochester showing the system-level dynamics of the cloud in orbit, and experiment design as well as preliminary experimental work to be conducted in Phase II, will be based on demonstrating the trapping and grain alignment approach on an optical bench at Rochester Institute of Technology.**

13.3 Supporting simulations

Two simulation efforts were initiated in Phase I for systems engineering evaluations of proof-of-concept: one simulation of dynamics and control of virtual truss model of imaging system in formation, and one simulation of gravito-electrodynamics and control of cloud of grains subject to environmental disturbances and field control (electromagnetic, optical, gravitational). **These simulations constitute the basis of a more complex simulation to be developed in Phase II, which will include the multi-scale behavior**

of the entire system, and will have the ultimate goal to demonstrate that light focusing from the cloud can be attained, and in which system level requirements will be verified and validated.

13.4 Imaging system architectures in the visible and radar bands

In Phase I we have developed an optical design for multiple aerosol apertures involving a reflective, refractive, and diffractive aperture. The refractive design would alleviate the forward scattering problem that makes the reflective aperture more challenging. For this imaging architecture, which will apply to astrophysical missions, the selected approach for cloud management/sensing/control is multistage. It involves an outer stage for formation stabilization. It also involves an inner stage for telescope wavefront sensing and correction, relegating the fine adaptive optics to a deformable and fine steering mirror corrective element in the optical bench. It relies on relative range/bearing Sensing between the elements of the formation, and the metrology is based on a virtual telescope formation flying approach, in which distributed relative sensing using Ka-Band transceivers/patch antennas, and centralized laser metrology, relying on single laser source on main SC, for the basic elements. **Together with these architectures (reflective, refractive, diffractive) in the visible band in a Sun-Earth L2 point, Phase II will also consider an innovative architecture in the radar band in GEO, and explore the self-organizing properties of the dusty plasma to synthesize the aperture in the more demanding environment close to Earth.**

13.5 Sequence of mission operations

In Phase I we have proposed a sequential approach for flight operations. The selected orbit for the astrophysical system is such that the system is placed in a halo orbit at Sun-Earth L2, where the system is much less sensitive to gravitational disturbance. The system can be kept at constant temperature by a sun-shield, flying in formation with the cloud. The approach is to make sure that in all phases the cloud is stabilized, all sensors/actuators, control loops, communication, collision avoidance have been checked-out prior to science operations, and cloud containment and maintenance maneuvers are

done periodically once the system has been deployed. **For the selected architectures (reflective vs. refractive/diffractive, visible vs. radar), this timeline constitutes the basis of a more detailed mission timeline to be investigated in Phase II, which will include the selection of the best cloud deployment scheme, and the selection of the specific laser types and power to be used for optical manipulation.**

13.6 Orbital debris mitigation plan

Our preliminary approach to debris mitigation is that since light-induced forces are manipulating the grains, in the decommissioning phase the illuminated system can just be turned off. Since we are at Sun-Earth L2, the micron-sized grains will remain in the halo orbit and over a long period of time will very slowly separate from each other on account of weak perturbations and mostly due to solar radiation. We discussed using the optical lift technique conceived by one of us (Swartzlander, 2012 NIAC Phase 1 study on Solar Sails with Optical Lift) to propel the grains as a miniature solar sail, where one of the lasers could actually illuminate the cloud with strong intensity, which will push the grains away indefinitely. **In Phase II, we will consider alternative orbital debris mitigation plans to accommodate geostationary orbit scenarios, where the cloud could operate in the radar band for remote sensing applications.**

13.7 Cost model

In Phase I, we started an effort on the preliminary evaluation of total system cost, based on existing cost models available in literature (NASA Advanced Mission Cost Model, developed by in Stahl, H. P., Survey of Cost Models for Space Telescopes, Optical Engineering, Vol. 49, No. 5, May 2010.). The preliminary results of these computations, i.e. the effective aperture mass and imaging system cost vs. effective diameter, for monolithic and cloud apertures, demonstrate the enormous cost reduction for the orbiting cloud, compared to a monolithic system. **This preliminary effort constitutes the basis of a more detailed cost-benefit analysis to be conducted in Phase II, which will culminate in a detailed assessment of cost and technology gaps for the selected system architectures.**

14 Acknowledgment

This research was carried out at the Jet Propulsion Laboratory, California Institute of Technology, under a contract with the National Aeronautic and Space Administration under the NASA Innovative Advanced Concepts Program. Thanks to: Steven Myint (JPL), Mayer Rud (JPL), Bob Balaram (JPL), Adrian Stoica (JPL), Andrew Shapiro-Scarlotta (JPL), Barbara Wilson (JPL), Liz McCormack (Bryn Mawr College), Tomasz M. Grzegorczyk (Delpsi LLC.), Jean-Marc Fournier (Swiss Federal Institute of Technology), David Brady (Duke Univ.), James Fienup (Univ. of Rochester), and everyone else that was enthusiastically supportive of this effort.

References

[1] Andersen, T., and Enmark, A.: Integrated Modeling of Telescopes, Springer Astrophysics and Space Science Library, vol. 377, 2011.

[2] O. Arp, D. Block, A. Piel and A. Melzer, "Dust Coulomb balls: Three-Dimensional Plasma Crystals", Phys. Rev. Lett. 93 (2004) 165004.

[3] Ashkin, A.: Acceleration and trapping of particles by radiation pressure, Phys. Rev. Lett. 24. 156-159, 1970.

[4] Ashkin, A.: Trapping of atoms by resonance radiation pressure, Phys. Rev. Lett. 40. 729-732, 1978

[5] Ashkin, A., Dziedzic, J.M., Bjorkholm, J.E., and Chu, S., Observation of a single-beam gradient force optical trap for dielectric particles, Optics Letters 11(5), pp. 288290, 1986.

[6] P.D. Atcheson, C. Stewart, J. Domber, K. Whiteaker, J. Cole, P. Spuhler, A. Seltzer, J.A. Britten, S.N. Dixit, B. Farmer, L. Smith, MOIRE initial demonstration of a transmissive diffractive membrane optic for large lightweight optical telescopes, Proc. SPIE 8422, Space Telescopes and Instrumentation 2012.

[7] Axelrad, D.R.: Micromechanics of Solids, Elsevier Scientific Publishing Company, Amsterdam, 1978.

[8] G.R. Ayers, J.C.Dainty, Iterative blind deconvolution method and its applications, Optics Letters Vol. 13 No. 7 (1988)

[9] I.M Barton, J.A. Britten, S.N. Dixit, L.J. Summers, I.M. Thomas, M.C. Rushford, K. Lu, R.A. Hyde, M.D. Perry, Fabrication of large-aperture lightweight diffractive lenses for use in space, Applied Optics, 40(4) 447-451 (2001).

[10] W.I. Beavers, D.E. Dudgeon, J.W. Beletic, and M.T. Lane, Speckle Imaging through the Atmosphere, The Lincoln Laboratory Journal, Vol. 2, Number 2 (1989).

[11] Bekey, I.: An extremely large, yet ultra-lightweight space telescope and array, NIAC Phase I report, 1999.

[12] Bliokh, P., Sinitsin, V., Yaroshenko, V.: Dusty and Self-Gravitational Plasmas in Space (Astrophysics and Space Science Library), Springer, 1995.

[13] M.R. Bolcar and J.R. Fienup, Sub-aperture piston phase diversity for segmented and multi-aperture systems, Appl. Opt. 48, A5-A12 (2009).

[14] Born, M., and Wolf, E.: Principles of Optics, 2nd edition, Pergamon Press, 1964, pp. 400

[15] Brady, D.J., Hagen, N.: Multiscale lens design, Opt. Express 17, 10659-10674, 2009

[16] G.R. Brady and J.R. Fienup, Nonlinear optimization algorithm for retrieving the full complex pupil function, Optics Express, Vol 14, No. 2 (2006).

[17] O. Brzobohaty, V. Karasek, M. Siler1, L. Chvatal, T. Cizmar, and P. Zemanek, Experimental demonstration of optical transport, sorting, and self-arrangement using a tractor beam, Nature Photonics Vol. 7, 123-127 (2013).

[18] Choi et al: Overcoming the Diffraction Limit Using Multiple Light Scattering in a Highly Disordered Medium, PRL 107, 023902, 2011.

[19] W. Choi, C. Fang-Yen, K. Badizadegan, S. Oh, N. Lue, R. R. Dasari, and M. S. Feld, Tomographic phase microscopy, Nature Methods Vol. 4, 717-719 (2007).

[20] Chung, S.-J., and Hadaegh, F.Y. Swarms of femtosats for synthetic aperture applications. In 4th international conference on spacecraft formation flying missions and technologies. St-Hubert, Quebec. May 18-20, 2011.

[21] Dienerowitz, M.: Plasmonic Effects upon Optical Trapping of Metal Nanoparticles, PhD Thesis University of St. Andrews, U.K., 2010.

[22] Eringen ,C.: Microcontinuum Field Theories, Springer Verlag, 1999.

[23] J.R. Fienup, G.B. Feldkamp, Astronomical Imaging By Processing Stellar Speckle Interferometry Data, SPIE Proc. 243-16 (1980).

[24] Friedlander, S. K.: Smoke, Dust, and Haze, John Wiley and Sons, 1977.

[25] Fuchs, N.A.: The Mechanics of Aerosols, Dover Publications, 1989.

[26] Gazi, V., and Passino, K.: Stability Analysis of Clouds, Proc. Of the American Control Conference, Anchorage, AK, May 8-10, 2002, pp. 1813-1818.

[27] R.W. Gerchberg and W.O. Saxton, A practical algorithm for the determination of the phase from image and diffraction plane pictures, Optik 35, 237 (1972).

[28] Ghanem, R., and Spanos, P.: Stochastic Finite Elements, a Spectral Approach, Dover Publications, New York, 2003.

[29] R.A. Gonsalves and R. Chidlaw, Wavefront sensing by phase retrieval, in Applications of Digital Image Processing III, A.G. Tescher, ed., Proc. SPIE 207, 32-39 (1979)

[30] R.A. Gonsalves, Phase retrieval and diversity in adaptive optics, Opt. Eng. 21, 829-832 (1982).

[31] Greengard, L.: The numerical solution of the N-body Problem, Computers in Physics, March-April 1990, pp. 142-152.

[32] Grzegorczyk, T., Kemp, B. A., Kong, J.A.: Trapping and binding of an arbitrary number of cylindrical particles in an in-plane electromagnetic field, J. Opt. Soc. Am. A, 23(9) Sept. 2006.

[33] Grzegorczyk, T., Kemp, B. A., Kong, J.A.: Passive guiding and sorting of small particles with optical binding forces, Opt. Lett., 31(22), Nov. 2006.

[34] M.Guizar-Sicairos and J.R. Fienup, Phase retrieval with transverse translation diversity: a nonlinear optimization approach, Optics Express, Vol 16, No. 10, 7264-7278 (2008).

[35] R.A. Hyde, Eyeglass: Large Aperture, Lightweight Space Optics, LLNL Report UCRL-ID-151390 (2003).

[36] H.R. Ingleby and D.R. McGaughey, Real data results with wavelength-diverse blind deconvolution, Opt. Lett. 30 No. 5, 489-491 (2005).

[37] S.M. Jefferies, M. Lloyd-Hart, E.K. Hege, and J. Georges, Sensing wavefront amplitude and phase with phase diversity, Appl. Opt 41, 2095-2102 (2002).

[38] Kadowaki, H., and Liu, W.K.: A Multiscale Approach for the Micropolar Continuum Model, Computer Modeling in Engineering and Science, 2005, vol.7, no. 3, pp. 269-282.

[39] W. van Kampen and R.G. Paxman, Multi-Frame Blind Deconvolution of Infinite-Extent Objects, Proc. SPIE Vol. 3433, Propogation and imaging through the Atmosphere II (July 1998).

[40] Kikuchi, H.: Electrohydrodynamics in Dusty and Dirty Plasmas - Gravito-Electrodynamics and EHD (Astrophysics and Space Science Library, Volume 258), Springer, 2001.

[41] Kokhanovsky. A. A.: Cloud Optics, Springer, 2006.

[42] D. Kundur and D. Hatzinakos, Blind Image Deconvolution, IEEE Signal Process. Mag. 13, 43-64 (1996).

[43] Labeyrie, A.: Standing Wave and Pellicle: A Possible Approach to Very Large Space Telescopes, Astronomy and Atrophysics, 77, L1-L2, 1979.

[44] Labeyrie, A., M. Guillon and J.-M. Fournier, Optics of Laser Trapped Mirrors for large telescopes and hypertelescopes in space, SPIE Proc. 5899, 2005.

[45] A. Labeyrie, Attainment of Diffraction-Limited Resolution in Large Telescopes by Fourier Analysing Speckle Patterns in Star Images, Astron. Astrophy. 6, 85 (1970).

[46] Labeyrie, A., Lipson, S.G., and Nisenson, P.: An Introduction to Optical Stellar Interferometry, Cambridge Univ. Press, 2006.

[47] Lerman, K., Martinoli, A., Galstyan, A.: A Review of Probabilistic Macroscopic Models for cloud Robotic Systems, in cloud Robotics Workshop: State-of-the-art survey, edited by E. Sahin and W. Spears, LCNS 3342, Springer-Verlag, Berlin, 2005, pp.143-152.

[48] M. Li, et al, invited report Complex MEMS Device: Microshutter Array System for Space Applications, Micro (MEMS) and Nanotechnologies for Defense and Security, Proc. SPIE 6556, 2007.

[49] A.S. Lo, J. Arenberg, Architectures for space astronomical telescopes using Fresnel optics, Proc. SPIE 6265, Space Telescopes and Instrumentation I, (June 2006).

[50] McCormack, et al., Laser Trapping of Mirrors in Space, NIAC Phase I report, 2006.

[51] A.B. Meinel and M.P. Meinel, Large membrane space optics: Imagery and aberrations of diffractive and holographic achromatized elements of high diffraction order, Opt Eng 41(8), pp 1995-2007 (2002).

[52] A.B. Meinel and M.P. Meinel, Parametric dependencies of high-diffraction-order achromatized aplanatic configuration that employ circular or cross-linear diffractive optcal elements, AO 41(34), pp 7155-7166 (2002).

[53] A. Meinel and M. Meinel, Extremely large sparse aperture telescopes, Optics and Photonics News, 26-29, Oct. 2003.

[54] Melzer, Phys. Rev. E 67, 016411 (2003), and "Stereoscopy in dusty plasmas", Photonik International Nr. 2/2008, 56.

[55] Mettler E., Breckenridge W.G., and Quadrelli M.B.: Large Aperture Telescopes in Formation: Modeling, Metrology, and Control, The Journal of the Astronautical Sciences, vol. 53, no.5 October-December 2005, pp.391-412.

[56] Mogilner, A., Edelstein-Keshet, L.: A Non-local Model for a Cloud, Journal of Mathematical Biology, 1999, no. 38, pp. 534-570.

[57] Molmud, P., Expansion of a Rarefield Gas Cloud into a Vacuum, The Physics of fluids 3, 362-366 (1960).

[58] Morfill, G. E. (2009). "Complex plasmas: An interdisciplinary research field". Review of Modern Physics 81: 1353. doi:10.1103/RevModPhys.81.1353.

[59] Mugnier, L.M., Rousset G., and Cassaing F., Aperture configuration optimality criterion for phased arrays of optical telescopes, J. Opt. Soc. Am. A., vol. 13, no. 12, December 1996

[60] Palmer, A.J.: Nonlinear Optics in Aerosols, Optics Letters, vol. 5, no. 2, February 1980

[61] Palmer, A.J.: Plasmon-Resonant Aerosols for Space Optics, J. OP. Soc. America, vol. 73, no. 11, November 1983.

[62] Palmer, A.J.: Radiation-induced Orientation of Atmospheric Aerosols, J. OP. Soc. America A, vol. 8, no. 2, February 1991.

[63] R.G. Paxman, T.J. Schulz, J.R. Fienup, Joint estimation of object and aberrations by using phase diversity, J. Opt. Soc. Am. A, Vol. 9, No. 7 (1992).

[64] Pfalzner, S, and Gibbon, P.: Many-Body Tree Methods in Physics, Cambridge University Press, 1996.

[65] Quadrelli M.B., Zimmermann, W., Chau, S.: System Architecture for a Guided Herd of Robots for Surface/Sub-Surface Exploration of Titan, presented at the 2004 IEEE Aerospace Conference, Big Sky, MT.

[66] Quadrelli, B.M., and Chang, J.: Dynamics and Control of a Herd of Sondes Guided by a Blimp on Titan, presented at the 14th AAS/AIAA Space Flight Mechanics Meeting, Maui, Hawaii, February 8-12 2004.

[67] Reif, J.H., and Wang, H., Social Potential Fields: A Distributed Behavioral Control for Autonomous Robots, Robotics and Autonomous Systems 27 (1999) 171-194.

[68] G.B. Scharmer, M.G.Lofdahl, T.I.M. van Werkhoven, and J. de la Cruz Rodriguex, High-order aberration compensation with multi-frame blind deconvolution and phase diversity image restoration techniques, Astronomy and Astrophysics Vol. 521, A68 (2010).

[69] T.J. Schulz, Multiframe blind deconvolution of astronomical images, J. Opt. Soc. Am A, 10:1064-1073, 1993.

[70] J.H. Seldin and R.B. Paxman, Joint Estimation of Amplitude and Phase from Phase-Diversity Data, in Signal Recovery and Synthesis Topical Meeting of the Optical Society of America (June, 2005), report JTuB4.

[71] Shapiro, I.I., Jones, H.M., Perkins, C. W.: Orbital Properties of the West Ford Dipole Belt, Proceedings of the IEEE, May 1964.

[72] Siljak, D.D.: Decentralized Control of Complex Systems, Academic Press, 1990.

[73] Stahl, H. P., Survey of Cost Models for Space Telescopes, Optical Engineering, Vol. 49, No. 5, May 2010.

[74] Summers, M. D.: Optical Micromanipulation of Aerosols, PhD Thesis University of St. Andrews, U.K., 2009.

[75] Swartzlander G. A., Peterson, T. J., Artusio-Glimpse A. B., Raisanen A. D.: Stable optical lift. Nature Photonics, Nature Photonics 5, pp.4851, 2011.

[76] S.T. Thurman and J.R. Fienup, Complex pupil retrieval with undersampled data, J. Opt. Soc. Am. A, Vol 26, No. 12 (2009).

[77] D. Y. Tseng and B. H. Soffer, Analysis of image formation with thinned random arrays, AFOSR-TR-79-0894 (1979). www.dtic.mil/dtic/tr/fulltext/u2/a072512.pdf

[78] Van de Hulst, H. C.: Light Scattering by Small Particles, Dover Publications, 1981.

[79] Vellkhoop et al, Exploiting disorder for perfect focusing, arXiv:0910.0873v1.

[80] Vladimirov, S.V., Ostrikov, K., Samarian, A.A.: Physics and Applications of Complex Plasmas, World Scientific Publishing; 1 edition (Sep 7 2005).

[81] Wang, Juan, I : Physical Review E, vol. 62, no. 4, October 2000, pp.5667-5671.

[82] Weigelt, Gerd, Modified astronomical speckle interferometry speckle masking, Optical Communications 21 (1) 55 (1977).

[83] `http://en.wikipedia.org/wiki/Dusty_plasma`.

[84] Yavuz, D.: Frequency and Focal Region Properties of Random Sparse Arrays, IEEE Transactions on Antennas and Propagation, vol. AP-32, no. 5, May 1964.

[85] Zhao, F.: Development of high-precision laser heterodyne metrology gauges, SPIE Proc. Vol. 5634, 14 Feb. 2005, Advanced Sensor Systems and Applications II, Yun-Jiang Rao; Osuk Y. Kwon; Gang-Ding Peng, Editors, pp.247-259.

A Appendix

The following paper has been submitted to ECCOMAS Multibody Dynamics Conference, Zagreb, Croatia, 1-4 July 2013.

Multi-scale Dynamics, Control, and Simulation of Granular Spacecraft[1]

Marco B. Quadrelli[1], Scott Basinger[1], Grover Swartzlander[2]

[1] *Jet Propulsion Laboratory, California Institute of Technology, 4800 Oak Grove Drive, Pasadena, CA 91109-8099, Mail Stop 198-219,* Marco.B.Quadrelli@jpl.nasa.gov, Scott.Basinger@jpl.nasa.gov

[2] *Center for Imaging Science and Physics Dept., Rochester Institute of Technology, 54 Lomb Memorial Drive, Rochester, NY 14623,* grovers@mail.rit.edu

Abstract

In this paper, we present some ideas regarding the modeling, dynamics and control aspects of *granular spacecraft*. Granular spacecraft are complex multibody systems composed of a spatially disordered distribution of a large number of elements, for instance a cloud of grains in orbit. An example of application is a spaceborne observatory for exoplanet imaging, where the primary aperture is a cloud instead of a monolithic aperture. A model is proposed of the multi-scale dynamics of the grains and cloud in orbit, as well as a control approach for cloud shape maintenance and alignment, and preliminary simulation studies are carried out for the representative imaging system.

Keywords: *multibody dynamics, spacecraft, granular media, distributed systems*

1 Introduction

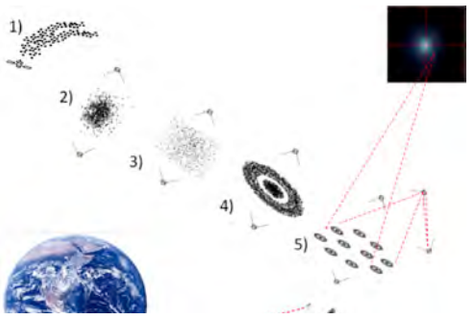

Figure 1. Scenario of application of a granular spacecraft.

The useful engineering properties of a cloud of granular matter in space are virtually unknown. Granular matter is considered to be the 5th state of matter (after solid, liquid, gaseous, and plasma) by virtue of its peculiar response characteristics (cohesiveness, fluid behavior, compactification, phase transformation capability, and others) [6]. However, it is a fact that the dynamics, controllable properties, and consequent benefits of engineering and manipulating granular matter such as dust grains, powders, and granular spacecraft is poorly known to the space exploration community.

In this paper, we present some ideas regarding the modeling, dynamics and control aspects of *granular spacecraft*. Granular spacecraft are complex multibody systems composed of a spatially disordered distribution of a large number of elements, for instance a cloud of N grains in orbit, with $N>10^3$. We address the modeling and autonomous operation of a distributed assembly (the cloud) of large numbers of highly miniaturized space-borne elements (the grains). A granular spacecraft can be defined as a collection of a large number of space-borne elements (in the 1000s) designed and controlled such that a desirable collective behavior emerges, either from the interactions among neighboring grains, and/or between the grains and the environment. The ultimate objective would be to study the behavior of the single grains and of large ensembles of grains in orbit and to identify ways to guide and control the shape of a cloud composed of these grains so that it can perform a useful function in space, for instance, as an element of an optical imaging system for astrophysical applications. This concept, in which the aperture does not need to be continuous and monolithic, would increase the aperture size several times compared to large NASA space-borne observatories currently envisioned such as ATLAST, allowing for a true Terrestrial Planet Imager that would be able to resolve exo-planet details and do meaningful spectroscopy on distant worlds. To accomplish this goal, we need to investigate the conditions to manipulate and maintain the shape of an orbiting cloud of dust-like matter so that it can function as an ultra-lightweight surface with useful and adaptable electromagnetic characteristics. Consider the following scenario, shown in Figure 1: 1) the cloud is first released; 2) it is contained by laser pressure to avoid dissipation and disruption by gravitational tidal forces, 3) it is shaped by optical manipulation into a two-dimensional object (coarse control), and 4) ultimately into a surface with imaging characteristics (fine control). The cloud shape has to be maintained against orbital disturbances by continuous figure control, also achieved optically. Applying differential light pressure retargets the entire cloud, so that a change of the optical axis can be induced. Selected parts of the cloud are reshaped when required for wavefront control, thus enabling higher quality optics. The entire imaging system is now in full operation, as 5) a multilens system searching for exo-planets, or 6) as a radio receiver engaged in remote sensing investigations. The potential advantages of the granular spacecraft concept are that: a) it can result in an ultra-lightweight system, made of very simple, very low cost, units; b) it can be very big: the cloud can distribute itself to kilometer scales, without the need to fill the aperture; c) the cloud is easy to package, transport and deploy; d) it is reconfigurable, and can be retargeted and repointed with non-mechanical means; e) the cloud is a highly fault-tolerant system with very low vulnerability to impacts. Other potential advantages offered by the cloud properties as optical system involve possible combination of properties (combined transmit/receive), variable focal length, combined refractive and reflective lens designs, and hyper-spectral imaging.

The study of granular spacecraft involves different disciplines, some of which are outlined in Figure 2: gravito-electrodynamics, optics, laser-matter interaction, disordered and distributed systems, multi-scale simulation, formation-flying, granular media, and plasma physics, among others. Because it is such a complex problem, this paper only scratches the surface and proposes a systemic view by first making some modeling considerations in section 2, discussing the physics of the problem in Section 3, a representative example in Section 4 and its numerical simulation in Section 5. A discussion of preliminary numerical results concludes the paper.

2 Modeling considerations

[1] This research was carried out at the Jet Propulsion Laboratory, California Institute of Technology, under a contract with the National Aeronautic and Space Administration.

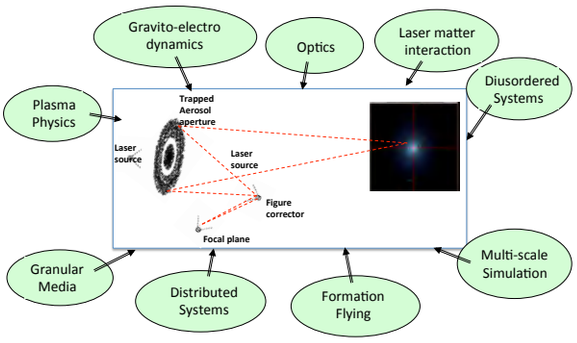

Figure 2. Multi-disciplinary elements of problem.

Modeling of granular spacecraft is more challenging than modeling of conventional space-borne vehicles because we are faced with a probabilistic vehicle composed of a large number of physically disconnected vehicles. First, different scales of motion occur simultaneously in a cloud: translations and rotations of the cloud as a whole (*macro-dynamics*), relative rotation and translation of one cloud member with respect to another (*meso-dynamics*), and individual cloud member dynamics (*micro-dynamics*). A major challenge is to incorporate these modes of motion into a reduced order model. There exist at least two time scales, as well as at least two space scales, in the description of the dynamics of a cloud. The dynamics of an individual vehicle begin to emerge when the time scale of a stimulus (internal or external to the cloud) is smaller than the time scale representative of the cloud dynamics itself. Similarly, in the opposite case the cloud behavior as an integrated unit is predominant. This behavior affects the stability of the system as cloud cohesiveness depends on the internal space and time scales. Furthermore, these effects become more complicated and nonlinear when the cloud undergoes large reconfigurations, both in relative translation and in attitude with respect to a reference configuration. These systems also display both a *local* and a *non-local* aspect. The local aspect pertains to the near-collocation represented by a sensor and an actuator located on the cloud. The non-local aspect appears when a sensor located on one end of the cloud feels the effect of an actuator mounted on another one at a different location. Second, the control design needs to be tolerant of the system complexity, of the system architecture (centralized vs. decentralized large scale system control) as well as robust to un-modelled dynamics and noise sources. Optimized sensor locations and robust dynamics estimation schemes are required to achieve full knowledge of the states of the system within a significant cluster of individual grains. Additionally, information processing on a granular spacecraft is inherently distributed by nature. Modeling of a cloud cannot dispense with the need to appropriately model the latencies and bandwidth limitations associated with inter-cloud communications. Single vehicle applications are immune to such considerations. Simulation of a cloud must also address a large range of spatial and temporal scales, in effect a multiple-scale problem, a solution to which will require a new class of numerical algorithms with special demands on accuracy, stability, and provision for coexisting multiple time scales. Table 1 shows a comparison of various requirements for simulation of single spacecraft vs. granular spacecraft, indicating the high degree of complexity that needs to be taken into consideration.

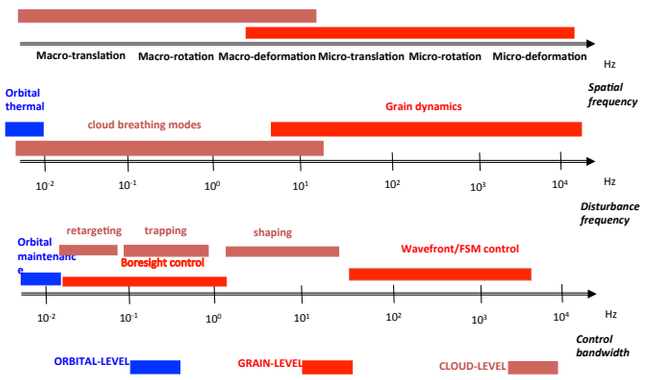

Figure 3. Spatial, temporal, and control scales involved in the granular spacecraft problem.

Three spatial and temporal domains can be identified: a) micro, at the scale of the individual vehicle; b) meso, at the scale of a cluster of vehicles within the cloud; and c) macro, at the scale of a very large number of vehicles. Figure 3 shows the different spatial and temporal scales involved in the system. While the micro-, meso-, macro-scales affect the spatial frequency distribution, depending on the disturbance frequency various parts of the system are excited differently. Furthermore, to be useful as an engineering system, the various control bandwidths of interest must be considered at the orbital level, grain level, and cloud level.

From the point of view of modeling the system, two main problems are identified. First, the Direct Problem, in which given the individual cloud elements, interconnectivity dictated by communication constraints, and local potential functions describing the interaction (or collision avoidance constraint) between adjacent elements, predict the global motion of the cloud and control it according to an optimality criterion. Second, the Inverse Problem: given a desired trajectory for the cloud, determine the interconnectivity and local potential functions between adjacent elements of the cloud that result in the desired motion. In this paper we deal only with the Direct problem.

By means of micro-continuum field theory ([2], [5], [12]), we can unify the deformation and dynamics modalities of a cloud. We use continuum mechanic constructs for this analysis. Each individual grain is endowed with a position vector, a rotation tensor, and a deformation gradient tensor, in the spirit of micromorphic kinematics. This means that each individual grain is capable of changing its configuration in response to stimuli originated either from the exterior of the cloud or within the cloud itself. The cloud is therefore treated as a continuum at the macroscopic level, with added extra structure at the micro-continuum, or particle, level. A set of balance laws for the cloud can then be derived, assuming invariance of the cloud energy functional to translations and rigid rotations. These balance laws include the conservation of the cloud mass, the balance of cloud linear momentum, the balance of macroscopic cloud angular momentum and of particle angular momentum, the cloud entropy inequality, and the boundary conditions at the boundary of the cloud. The description of the internal constitution of the cloud, i.e. the constitutive relation between internal reconfiguration kinematic variables (strains) and internal reconfiguration momenta, completes the mechanical description of the cloud. The internal reconfiguration momenta represent the generalized inertia and the generalized stresses that the individual grain experiences when a reconfiguration is taking place. The constitutive functional includes memory dependent terms and nonlocality in the cloud response [17]. That this must be included stems from the fact that the behavior of the cloud can be influenced both at the system level and at the individual grain level. Therefore, two time scales enter the picture, as well as two space scales. The individual grain dynamics begins to emerge when $(\lambda / L) \approx 1$, where λ is the time (or space) scale of the stimuli internal or external to the cloud, whereas L is a time (or space) scale representative of the cloud itself. When $(\lambda / L) << 1$, the individual grain behavior is predominant, and when $(\lambda / L) >> 1$, the cloud behavior as a unit is predominant. The spatial nonlocality occurs since one grain may respond to stimuli from another grain located far away from

Table 1. Comparison of requirements for simulation of single spacecraft vs. granular spacecraft.

	Single SC	cloud
Propagation model	Serial	Distributed/parallel
Workspace volume	Small	Very large
Input data structure	Small	Very large
Output data structure	Small	Very large
Significant digits	Many	few
Spatial scales of motion	Orbital/attitude/flex	Orbital/micro/meso/macro
Temporal scales of motion	Orbital/attitude/flex	Orbital/micro/meso/macro
Disturbance frequency	Orbital period	Orbital/micro/macro
Controller bandwidth	ACS+DV	ACS+DV+reconfiguration +containment
Computation on GPU	Not needed	Recommended

it in the cloud, and it occurs also at a global level, since each grain may respond to stimuli of the cloud as a unit. This multilevel behavior is reflected in the nonlocal constitutive functional. Memory dependence, also known as time nonlocality, enters the constitutive functional through time dependence of the current instant from previous instants. Since both the target location knowledge and the physical grain (and sensor) locations are stochastic in nature, we use the concept of random fields to set up an equivalent boundary value problem in the time domain where the coefficients of the differential operator are random processes. A description of the cloud dynamics within the spatial domain Ω can then be cast as a boundary value problem ([7], [8]) as

$$[\mathrm{B}(x,t) + \mathrm{G}(x,t;\omega)]\, u(x,t;\omega) = f(x,t;\omega) \tag{1}$$

together with the appropriate boundary conditions at the boundary of Ω, where x is the spatial scale, t is the temporal scale, ω is a random fluctuation, B is the deterministic operator describing the dynamics, G is the stochastic part whose coefficients are zero-mean random processes, and f is the vector of exogenous and control inputs. It is clear that, depending on the connectivity between the elements of the cloud, the B and G operators may be local or nonlocal operators derived from variational principles expressed in their weak form. This approach ensures a robust mathematical formulation since the stochastic nature of the states is reflected in the stochastic nature of the differential operators.

3 Cloud Physics

To address the engineering applications, we need to have insight on physics of disorder systems and the dominant forces that perturb the cloud. Related background can be found in refs [13], [19], [23]. Cloud gravito-electrodynamics leads to self-organization: for a cloud of particles released from an orbiting vehicle, the diffusion characteristics are important, as well as the tendency to form natural ring-like structures governed by the local gravity gradients, solar pressure, and radiation properties of each individual grain. The electrodynamic Lorentz coupling in LEO-GEO provides high degree of structural coherence which can be exploited in applicaitons. Once illuminated, the diffraction pattern from a disordered assembly leads to a strong focusing potential: the intensity of the signal is more collimated when the distribution of apertures is randomized, the separation between apertures increases, and the number of apertures increases. Focusing is achieved by modulating the phase of the distributed radiators so as to obtain a conic phase surface, and this leads naturally to the shaping a cloud in the form of a lens. In space, the cloud behavior depends on the dynamic balance of different force fields: Laser light pressure, as light can induce motion; Solar illumination radiation pressure, which carries momentum; Gravitational forces and gradients, resulting in orbital and tidal effects; Electrostatic Coulomb or dielectrophoretic forces, since the grains are charged; Electromagnetic Lorentz forces resulting from the interaction with local magnetic field; Cloud self-gravity caused by the cloud being an extended body; Poynting-Robertson drag, in which grains tends to spiral down towards the Sun; and Yarkovstky (YORP) effect, caused by the anisotropic emission of thermal photons, which carry momentum. In the next sections, we describe the gravito-electrodynamics coupling, and the opto-mechanical interaction.

3.1 Cloud Gravito-electrodynamics

To gain some insight into the physics of the problem, we can for the time being consider the dynamics of one grain and of a collection of grains separately. The equation of motion of one grain around planet rotating at Ω_p:

$$\ddot{\mathbf{r}} = -\frac{\mu \mathbf{r}}{m|\mathbf{r}|^3} + \frac{Q(r)}{mc}\left[\dot{\mathbf{r}} \times \mathbf{B}(\mathbf{r}) - (\Omega_p \times \mathbf{r}) \times \mathbf{B}(\mathbf{r})\right] + \mathbf{F}(\mathbf{r}) \cdot \tag{1}$$

from which the resulting natural frequencies are

$$\Omega = \frac{\Omega_B}{2}\left\{1 \pm \left[1 + 4\left(\frac{\Omega_K^2}{\Omega_B^2} - \frac{\Omega_p}{\Omega_B}\right)\right]^{1/2}\right\}. \tag{2}$$

where Ω_B is the plasma gyro-frequency, Ω_p is the planet rotation rate, and Ω_K is the Keplerian frequency, indicating that gravity, electromagnetic fields are coupled and interact with local plasma. For a cloud of particles released from an orbiting vehicle, the diffusion characteristics are important, as well as the tendency to form natural ring-like structures governed by the local gravity gradients, solar pressure, and radiation properties of each individual grain. As a system the orbital mechanics of a cloud can be modeled by the following equations:

$$\begin{aligned}
&\ddot{R}_0 - \dot{v}^2 R_0 = -\frac{\mu}{R_0^2}\left[1 + \frac{3}{2mR_0^2}\left(trace(J) - 3J_1 \sin^2\alpha - 3J_3 \cos^2\alpha\right)\right] - \frac{f}{m}\cos(\alpha + \theta) \\
&\dot{v} + 2\frac{\dot{R}_0}{R_0}\dot{v} = -\frac{3\mu}{mR_0^5}\left(J_3 - J_1\right)\sin\alpha\cos\alpha - \frac{f}{mR_0}\sin(\alpha + \theta) \\
&\ddot{\alpha} - \ddot{v} = \frac{3\mu}{R_0^3}\frac{\left(J_3 - J_1\right)}{J_2}\sin\alpha\cos\alpha + \frac{f}{J_2}\left(d_3 \sin\theta - d_1 \cos\theta\right)
\end{aligned} \tag{3}$$

These equations apply to an extended cloud of total mass *m* and moments of inertia J_1, J_2, J_3 in the baricentric frame. The equations of motion are nonlinear and non-homogeneous and apply to any type of orbit. The attitude dynamics and the orbital dynamics are, indeed, coupled through the pitch angle α, which is not necessarily small, and through the true anomaly *v*. When the orbit is circular, the cloud attitude dynamics is uncoupled from the orbital dynamics. The overallthrust direction (θ) and magnitude (*f*) affect both the orbital and attitude dynamics. The gravity gradient effect (represented by the terms in *sinα* and *cosα*) appears in all the equations. This state coupling has not yet been investigated in the literature. Now, let us consider the local vertical-local horizontal (LVLH) frame F_o, and let's look at the point located at $\rho = \begin{pmatrix} x & y & z \end{pmatrix} F_o$ from the origin of the moving coordinate system. Its relative acceleration in F_o *is:*

$$\ddot{\rho}_i = -\dot{\mathrm{V}}_0 - \left(\dot{\Omega}^{\times} + \Omega^{\times}\Omega^{\times}\right)\rho_i - 2\Omega^{\times}\dot{\rho}_i + a_{\mathbf{i}}(r_i, \dot{r}_i, t) \tag{4}$$

Then its gradient tensor can be computed in matrix form as:

$$\Gamma_{ij} = \frac{\partial \ddot{\rho}_i}{\partial \rho_j} = -\left(\dot{\Omega}^{\times} + \Omega^{\times}\Omega^{\times}\right) + \frac{\partial}{\partial \rho_j}\left[a_{\mathbf{i}}(r_i, \dot{r}_i, t)\right] = -\left(\dot{\Omega}^{\times} + \Omega^{\times}\Omega^{\times}\right) + \frac{\partial a_i}{\partial r_i} \bullet \frac{\partial r_i}{\partial \rho_j} + \frac{\partial a_i}{\partial \dot{r}_i} \bullet \frac{\partial \dot{r}_i}{\partial \rho_j} \tag{5}$$

Similarly, its gyroscopic tensor can be computed in matrix form as:

$$\Upsilon_{ij} = \frac{\partial \ddot{\rho}_i}{\partial \dot{\rho}_j} = -2\Omega^{\times} + \frac{\partial}{\partial \dot{\rho}_j}\left[a_{\mathbf{i}}(r_i, \dot{r}_i, t)\right] = -2\Omega^{\times} + \frac{\partial a_i}{\partial \dot{r}_i} \bullet \frac{\partial \dot{r}_i}{\partial \dot{\rho}_j} \tag{6}$$

Taking the instantaneous orbit of 0 as reference, we can now look at the motion with respect to the moving origin, still nonlinear in the kinematics, by expanding the perturbation force in Taylor series about the reference configuration. Consequently, the TANGENT equations of motion can be written as:

$$m_i 1_3 \ddot{\rho}_i + [\Upsilon]_i \dot{\rho}_i + [\Gamma]_i \rho_i = -\dot{\mathrm{V}}_0 + C_{oi}\left[\frac{f_{\mathbf{i}}(\rho_i, \dot{\rho}_i, \rho_j, \dot{\rho}_j, ...)}{m_i}\right]_0 + H.O.T. \tag{7}$$

As an example, consider a one-dimensional cloud. Consider the simple case of circular orbit with $R_0 = \begin{pmatrix} 0 & 0 & R_0 \end{pmatrix} F_o$ and $\Omega = \begin{pmatrix} \omega_0 & 0 & 0 \end{pmatrix} F_o$, for which the gravitational gradient tensor becomes:

$$\Gamma_{ij} = \frac{\partial \ddot{\rho}_i}{\partial \rho_j} = -\left(\dot{\Omega}^{\times} + \Omega^{\times}\Omega^{\times}\right) - \frac{\mu}{|R_0|^3}\frac{\partial}{\partial \rho_j}\left[R_0 + \rho_i - 3\frac{(R_0 \bullet \rho_i)}{|R_0|^2}R_0\right] \tag{8}$$

Then, the components of the gravitational gradient tensor are $\Gamma_{11} = -\omega_0^2$, $\Gamma_{33} = 3\omega_0^2$, which imply that the motion along x (along normal to orbital plane) is compressive, the motion along y (along velocity vector) experience no force, and the motion along z (along local vertical) is tensile.

3.2 Opto-mechanical Interactions

A spherical particle in the presence of light will experience both a scattering force in the direction of the beam axis, which is proportional to the irradiance, and a gradient force that may be expressed as F_{grad}=-(1/2)α(gradE)^2, where α is the polarizability of the particle [1], [3], . The gradient force is the direction of the beam axis is negligible unless the beam is tightly focus. Beam shaping of a cloud of particles is possible by molding the cloud in with the gradient force, say in the x-y plane, and by further molding the cloud in the z-direction by the combined optical scattering force and gravitational forces arising from the orbital dynamics (tidal forces). At the moment of release the velocity distribution of the cloud may be represented by a probability distribution such as the Maxwell-Boltzmann distribution. Without intervention, the cloud will diffuse to a rarified state where the particles move ballistically. The gradient force required to "freeze" the distribution in the x-y plane must then be of the order of F_{grad}=m√(2k_BT/m)/Δt, where Δt is the beam exposure time, T is the temperature, m is the particle mass, and k_B is Boltzmann's constant. The expansion of a rarefied gas cloud in vacuum expands as exp(-τ^2/t^2) where τ^2 = mR^2/2k_BT, and R is a diffusion length [18]. The required irradiance, I, may therefore be estimated as I = 4k_BT/αη, where η=377 [Ω] is the impedance of free space, and α =4πε$_0$$a^3$, where a is the radius of a grain, and ε$_0$=8.9E-12 [F/m]. For a radius of 1 micron, the irradiance becomes of the order of 13 kW/m^2, a CW laser power level which is within the range of commercial lasers in the visible band, including Nd:YAG laser at 532 nm. Although the radiation pressure force on a macroscopic body is weak, a few milliwatts of focused laser power are sufficient to achieve a force in the piconewton range. For a micron-sized body, the laser power is in the nanowatt range. Figure 4 depicts the estimates of orbital forces and optical power involved in cloud trapping as a function of grain diameter.

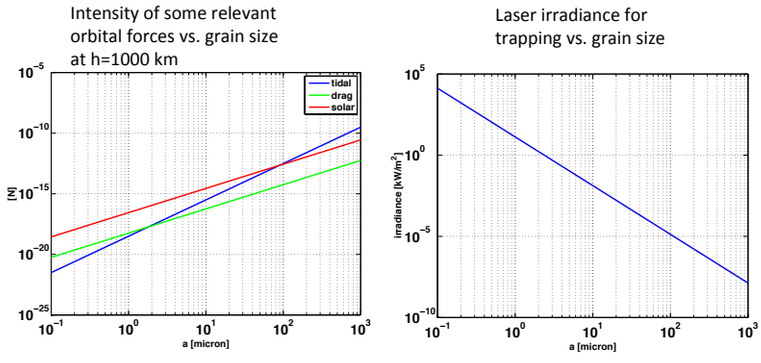

Figure 4. Estimates of orbital forces and optical power involved in cloud trapping.

4 Granular spacecraft modeling and simulation

Two simulations are currently being developed for systems engineering evaluations of proof-of-concept: one simulation of dynamics and control of "virtual truss" model of imaging system in formation, and one simulation of gravito-electrodynamics and control of cloud of grains subject to environmental disturbances and field control (electromagnetic, optical, gravitational). The focus of this paper is the second one.

The cloud simulation software is based on building a model of a large number of identical grains. This simulation environment allows trade studies for autonomy selection, trade studies for orbit selection for different applications, testing of autonomy algorithms at grain level and cloud level, development and testing of modeling and propagation algorithms. The grain model involves fully nonlinear dynamics with sensors/actuator models. One level of control for cloud shape maintenance, drift control, and another level of control is for cloud attitude stabilization. The cloud model involves an equivalent rigid body with coupled micro/macro motion. The disturbances modeled are Gravity, Third-Body, Drag, solar, EM field, thermal balance.

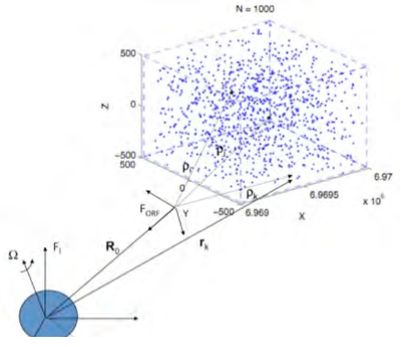

Figure 5. Orbital parameters of cloud in orbit.

The assumptions we used to model the dynamics are as follows: 1) The inertial frame is fixed at Earth's center. 2) The orbiting Frame ORF follows Keplerian orbit. 3) the cloud system dynamics is referred to ORF. 4) the attitude of each grain uses the principal body frame as body fixed frame. 5) the atmosphere is assumed to be rigidly rotating with the Earth. Regarding the grains forming the cloud: 1) each grain is modeled as a rigid body; 2) a simple attitude estimator provides attitude estimates, 3) a simple guidance logic commands the position and attitude of each grain, 4) a simple local feedback controller based on PD control of local states is used to stabilize the attitude of the vehicle. Regarding the cloud: 1) the cloud as a whole is modeled as an equivalent rigid body in orbit, and 2) an associated graph establishes grain connectivity and enables coupling between modes of motion at the micro and macro scales; 3) a simple guidance and estimation logic is modeled to estimate and command the attitude of this equivalent rigid body; 4) a cloud shape maintenance controller is based on the dynamics of a stable virtual truss in the orbiting frame. Regarding the environmental perturbations acting on the cloud: 1) a non-spherical gravity field including J0 (Earth's spherical field) zonal component, J2 (Earth's oblateness) and J3 zonal components is implemented; 2) atmospheric drag is modeled with an exponential model; 3) solar pressure is modeled assuming the Sun is inertially fixed; and 4) the Earth's magnetic field is model using an equivalent dipole model. The equations of motion are written in a referential system with respect to the origin of the orbiting frame and the state is propagated forward in time using an incremental predictor-corrector scheme.

Figure 5, shows the kinematic parameters of a 1000 element cloud in orbit. The motion of the system is described with respect to a local vertical-local horizontal (LV-LH) orbiting reference frame (x,y,z)=F_{ORF} of origin O_{ORF} which rotates with mean motion Ω and orbital semi-major axis R_0. The orbital geometry at the initial time is defined in terms of its six orbital elements, and the orbital dynamics equation for point O_{ORF} is propagated forward in time under the influence of the gravitational field of the primary and other external perturbations, described below. The origin of this frame coincides with the initial position of the center of mass of the system, and the coordinate axes are z along the local vertical, x toward the flight direction, and y in the orbit normal direction. The inertial reference frame (X,Y,Z)=F_I is geocentric inertial for LEO (X points toward the vernal equinox, Z toward the North Pole, and Y completes the right handed reference frame), and heliocentric inertial for other applications. The orbit of the origin of F_{ORF} is defined by the six orbital elements a (semimajor axis), e (eccentricity), i (inclination), Ω_L (longitude of ascending node), w (argument of perigee), ν (true anomaly), and time of passage through periapsis. From Figure 1, the position vector of a generic grain with respect to O_{ORF} is denoted by $\boldsymbol{\rho}_i$, and we have $\mathbf{r}_i=\mathbf{R}_0+\boldsymbol{\rho}_i$. We define the state vector as

$$\mathbf{X}=\left(\mathbf{r}_E,\dot{\mathbf{r}}_E,\mathbf{R}_0,\dot{\mathbf{R}}_0,\ldots\rho_i,\mathbf{q}_i,\dot{\rho}_i,\omega_i,\mathbf{R}_s,\dot{\mathbf{R}}_s,\rho_s,\dot{\rho}_s,\mathbf{q}_s,\omega_s\right) \tag{9}$$

where $\mathbf{q}_i$ and $\boldsymbol{\omega}_i$ represent the quaternion and angular velocity vector of the i-th grain with respect to F_I. The translation and rotation kinematics at the grain level are:

$$\text{grain}\begin{cases}\mathbf{V}_0=\dot{\mathbf{R}}_0\\ \mathbf{v}_i=\dot{\rho}_i\\ \dot{\mathbf{R}}_{bi}=-\omega^{\times}\mathbf{R}_{bi}\end{cases}\qquad\text{cloud}\begin{cases}\mathbf{V}_s=\dot{\mathbf{R}}_s\\ \mathbf{v}_s=\dot{\rho}_s\\ \dot{\mathbf{C}}_{si}=-\omega_s^{\times}\mathbf{C}_{si}\end{cases} \tag{10}$$

The angular momentum balance is:

$$\begin{aligned}&\text{grain}\quad \mathbf{J}_i\dot{\omega}_i+\omega_i^{\times}\mathbf{J}_i\omega_i=\sum_{j=1}^{Npert}\tau_j\\ &\text{cloud}\quad \mathbf{J}_s\dot{\omega}_s+\omega_s^{\times}\mathbf{J}_s\omega_s=\tau_s\end{aligned} \tag{11}$$

and the linear momentum balance is:

$$\text{grain}\begin{cases}\dot{\mathbf{V}}_0=-\mu_E\dfrac{\mathbf{R}_0}{\left|R_0\right|^3}+\dfrac{\sum_{j=1}^{Npert}\mathbf{f}_j}{m_{total}}\\ \ddot{\rho}_i=-\dot{\mathbf{V}}_0-\dot{\boldsymbol{\Omega}}^{\times}\rho_i+\boldsymbol{\Omega}^{\times}\boldsymbol{\Omega}^{\times}\rho_i-2\boldsymbol{\Omega}^{\times}\dot{\rho}_i+\mathrm{A}_i\ddot{\mathbf{r}}_i\\ \ddot{\mathbf{r}}_i=-\mu_E\dfrac{\mathbf{r}_i}{\left|\mathbf{r}_i\right|^3}+\dfrac{\left(\mathbf{f}_a+\mathbf{f}_e\right)_i}{m_i}\end{cases}\qquad\text{cloud}\begin{cases}\dot{\mathbf{V}}_s=-\mu_E\dfrac{\mathbf{R}_s}{\left|R_s\right|^3}+\dfrac{(\mathbf{f}_{J2}+\mathbf{f}_{J3})_s}{m_s}\\ \ddot{\rho}_s=-\dot{\mathbf{V}}_s-\dot{\boldsymbol{\Omega}}^{\times}\rho_s+\boldsymbol{\Omega}^{\times}\boldsymbol{\Omega}^{\times}\rho_s-2\boldsymbol{\Omega}^{\times}\dot{\rho}_s+C_{si}\dfrac{\mathbf{f}_s}{m_s}\end{cases} \tag{12}$$

where: A_i= rotation matrix of i-th body frame wrt. Inertial; R_0= orbital radius vector to origin of ORF; Ω = orbital rate; C_{si}= rotation matrix of cloud body frame wrt. Inertial; $f_{a,e}$ = actuation + external forces (gravity, aerodynamics, magnetic, solar); $m_{i,s}$ = grain/cloud mass; $w_{i,s}$ = body, cloud angular rate; $\tau_{a,e}$ = actuation + external torques; $J_{i,s}$ = grain/cloud moment of inertia.

5 Application to Control of a Representative Optical Imaging System

Resolution and aperture sizes for astrophysical optical systems are ever increasing in demand [14], [16]. With near-term plans to build 30 meter ground-based telescopes for astronomy, the demand for higher resolution optics in space continues to grow not only for exo-planet detection, but also for earth-based science, including hyper-spectral imaging and for monitoring of the oceans and land masses (e.g. seismic monitoring). ATLAST, still several decades away, is the largest practical space telescope designed using state-of-the-art light-weight segmented mirror technology: it may have an aperture up to 18 m. The aperture formed by the granular spacecraft cloud does not need to be continuous. Used interferometrically, for example, as in a Golay array [4], imagery can be synthesized over an enormous scale. As part of our investigation, we have considered refractive, reflective and holographic systems and outlined optical correction and collection systems. In addition to forming a single monolithic optical element with the cloud, we also considered forming smaller self-coherent patches, similar to segments in a segmented aperture, but not required to be phased with respect to each other. The "segments" can be continuous or separated by large amounts to form a sparse array. A corrector is then used to compensate for phase differences between each "segment". A Fizeau interferometer is a straightforward corrector for a reflective system. A more advance corrector would be a multiple aperture system utilizing multi-scale lens design, as described by [4]. The multi-scale lens design has the additional benefit of an increased field of view of the optical system and will allow for less movement of the entire collection of sub-apertures when changing the line of sight of the system.

An optical imaging system design has been selected as the best candidate architecture for a space system involving a cloud. The concept design is shown in Figure 6. The sequence of optics is as follows: the starlight is focused by granular spacecraft optic "patch", creating a spherical wavefront. Light from all patches converges at an intermediate focus, which has an image-plane coded aperture. The light then reflects off secondary mirror (Gregorian) and the light from each patch is collimated. Each beam goes to a separate adaptive optics system. A fast steering

mirror and a deformable mirror correct pointing and low to mid-spatial frequency aberrations. An optical delay line is used to correct phasing difference between the patches and allow for Fourier transform spectroscopy. A beam-splitter is included to allow some of the light to go to a Shack-Hartmann sensor to measure aberrations in the system. For this system, the selected approach for cloud management/sensing/control is multistage, with an outer stage for formation stabilization, and an inner stage for telescope wavefront sensing and correction, relegating fine adaptive optics to a deformable/fast steering mirror stage in the optical bench. The system's relative range/bearing sensing and metrology is based on virtual telescope formation flying, in which distributed relative sensing is accomplished using Ka-Band transceivers/patch antennas, and a centralized laser metrology system, relying on a single laser source on the main light-collecting spacecraft, while single reflecting target are on other free-flying elements except granular spacecraft.

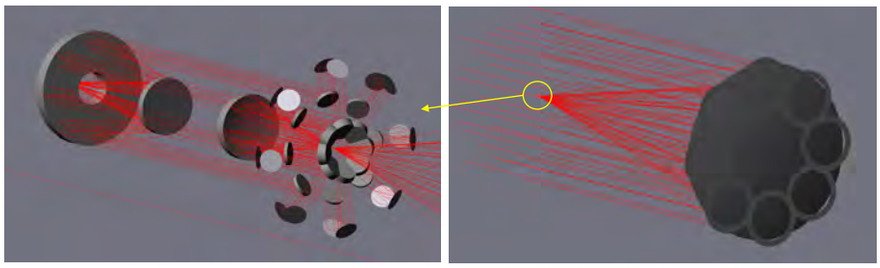

Figure 6. Reflective imaging system concept design with 8 cloud patches forming the aperture.

The cloud sensing approach is based on imaging/laser scanning, relying on custom or commercial stereo vision or laser scanning systems which can create precise 3-D model of complex objects. The approach for cloud control is multistage, based on laser cooling, and involves three levels: a) Trapping ("corralling") through gradient forces to provide containment against cloud diffusion due to thermal, radiation, and gravity and cloud cooling; b) shaping/alignment through laser pressure, to change amorphous cloud into disk or rectangular carpet; and c) alignment of grains to wavefront direction, which implements wavefront/boresight control through adaptive optics in order to maintain optical figure. Related work is presented in [2], [10], [11], [14]. For any size/shape particle, the electromagnetic energy is minimized when the particle is in the brightest region of the laser beam, and this is the basis for light-induced control. Corralling assumes mechanically releasing the cloud with low ejection velocities, then applying 3-axis laser illumination to corral the cloud via optical gradient forces. The cooling approach can be achieved by means of gradient forces, which involves rotating the linear polarization direction of the control laser at the rocking frequency. This effectively freezes the oscillations in a rotating reference frame. By adiabatically slowing the rotation of the polarization axis, some population of particles can be made to assume the same orientation, e.g., with the flat mirrored side of the rod facing the center of curvature. Cloud shaping is carried out via raster scanning of the beam across granular patch. An optimization is needed of the time dependent beam power and beam velocity to capture the most particles, and will be subject of future work. Grain alignment for phase coherence is achieved by applying linearly polarized control laser to orient particles along dominant polarization axis (long axis of rod), so that the particles will rock under the influence of polarization torque and radiation pressure torque.

A representative cloud with varying number of grains is simulated to identify the limitations in computation time as the number of grains grows. We can derive a control law to track a desired surface in the ORF (equivalently to maintain a reference cloud shape) as follows [15], [21], [22]. Define the tracking error $e_Z = q(x,y) - q_d(x,y)$, where $q_d(x,y)$ are the desired surface, and q(x,y) the current position of the grain belonging to that surface with respect to the origin of ORF. By imposing an exponentially stable error dynamics in the form $\ddot{e}_Z + 2\zeta_Z \omega_Z \dot{e}_Z + \omega_Z^2 e_Z = 0$, we can make sure the error *e* is driven to zero. Therefore, using the equations of motion expressed in ORF coordinates, the feedback-feedforward control law with components in ORF becomes:

$$u = -f_{pert} + f_{gyro} + m\ddot{q}_{des} - K_d \dot{e} - K_p e \,. \tag{13}$$

where f_{pert} is the resultant of the gravitational forces on the grain, f_{gyro} are the Coriolis and centrifugal forces acting on the grain, Kd is a derivative gain, and Kp is a proportional gain. Both f_{pert} and f_{gyro} can be modeled, act on a time scale which is very long, and can be canceled out by the feed-forward control scheme. These control forces are applied by the laser scanning system, coupling mechanically with the grains via opto-mechanical interaction.

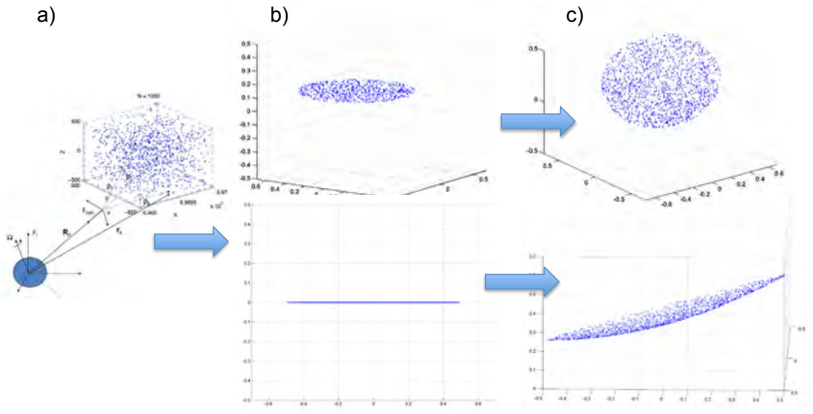

Figure 7. Re-shaping of a) amorphous cloud to b) disk and c) paraboloid.

6 Numerical results and discussion

The simulation results shown in Figure 7 were obtained by commanding the grains to conform to a prescribed optical surface. The cloud is first shaped into a disk, then into a paraboloid of specified focal length and diameter. The numerical results indicate that the force required to shape 1 meter diameter disk into parabola is of the order of 10^{-8} N. Assuming a grain shape which is asymmetric to incoming light, the torque required to align 1 micron grain is of the order of 10^{-15} Nm. For the computation time as a function of the number of grains N, preliminary results indicate an order $N^{1.43}$ scaling on a 8Gb, 1067 MHz RAM MacOSX computer with a 3.06 GHz Intel Core 2 Duo processor. With this metric, the same simulation for a system of N=1000 grains takes 5.4 hours, and 146 hours (i.e., 6 days) for a system with N=10,000 grains. Therefore, efficient ways to simulate this complex system, where not only the time scales of natural system dynamics, but also the sampling times of the Guidance, Navigation, and Control are included, remain to be fully explored. These methodologies would include GPU acceleration and multigrid solvers for the cloud dynamics, and will be the subject of future investigations [9], [20]. Figure 8 shows snapshots of the simulations of the entire imaging system with the cloud as an aperture.

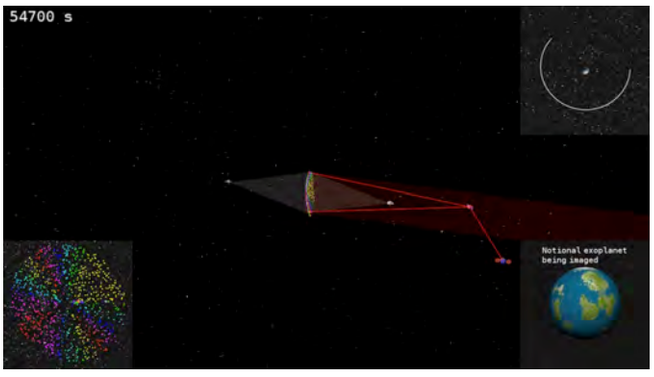

Figure 8. Snapshot of simulation.

Conclusions

In this paper, we have presented some ideas regarding the modeling, dynamics and control aspects of *granular spacecraft*. We have addressed the modeling and autonomous operation of a distributed assembly (the cloud) of large numbers of grains, controlled by opto-mechanical interactions. The modeling and simulation of a representative concept was also discussed. The application considered so far was a reflective imaging system for astrophysics, but many unexplored applications of granular spacecraft are yet to be discovered.

Acknowledgments

This research was carried out at the Jet Propulsion Laboratory, California Institute of Technology, under a contract with the National Aeronautic and Space Administration under the NASA Innovative Advanced Concepts Program.

References

[1] Ashkin, A.: Acceleration and trapping of particles by radiation pressure, Phys. Rev. Lett. **24**. 156-159, 1970.

[2] Axelrad, D.R.: Micromechanics of Solids, Elsevier Scientific Publishing Company, Amsterdam, 1978.

[3] Born, M., and Wolf, E.: *Principles of Optics*, 2nd edition, Pergamon Press, 1964, pp. 400.

[4] Brady, D.J., Hagen, N.: *Multiscale lens design*, Opt. Express 17, 10659-10674, 2009.

[5] Eringen ,C.: Microcontinuum Field Theories, Springer Verlag, 1999.

[6] Fuchs, N.A.: *The Mechanics of Aerosols*, Dover Publications, 1989.

[7] Gazi, V., and Passino, K.: Stability Analysis of Clouds, Proc. Of the American Control Conference, Anchorage, AK, May 8-10, 2002, pp. 1813-1818.

[8] Ghanem, R., and Spanos, P.: Stochastic Finite Elements, a Spectral Approach, Dover Publications, New York, 2003.

[9] Greengard, L.: The numerical solution of the N-body Problem, Computers in Physics, March-April 1990, pp. 142-152.

[10] Grzegorczyk, T., Kemp, B. A., Kong, J.A.: Trapping and binding of an arbitrary number of cylindrical particles in an in-plane electromagnetic field, J. Opt. Soc. Am. A, 23(9) Sept. 2006.

[11] Grzegorczyk, T., Kemp, B. A., Kong, J.A.: *Passive guiding and sorting of small particles with optical binding forces*, Opt. Lett., 31(22), Nov. 2006.

[12] Kadowaki, H., and Liu, W.K.: A Multiscale Approach for the Micropolar Continuum Model, Computer Modeling in Engineering and Science, 2005, vol.7, no. 3, pp. 269-282.

[13] Kokhanovsky. A. A.: *Cloud Optics*, Springer, 2006.

[14] Labeyrie, A.: Standing Wave and Pellicle: A Possible Approach to Very Large Space Telescopes, Astronomy and Atrophysics, 77, L1-L2, 1979.

[15] Lerman, K., Martinoli, A., Galstyan, A.: *A Review of Probabilistic Macroscopic Models for Swarm Robotic Systems*, in Swarm Robotics Workshop: State-of-the-art survey, edited by E. Sahin and W. Spears, LCNS 3342, Springer-Verlag, Berlin, 2005, pp.143-152.

[16] Mettler E., Breckenridge W.G., and Quadrelli M.B.: *Large Aperture Telescopes in Formation: Modeling, Metrology, and Control,* The Journal of the Astronautical Sciences, vol. 53, no.5 October-December 2005, pp.391-412.

[17] Mogilner, A., Edelstein-Keshet, L.: A Non-local Model for a Cloud, Journal of Math. Bio., 1999, no. 38, pp. 534-570.

[18]Molmud, P., “Expansion of a Rarefield Gas Cloud into a Vacuum,” The Physics of fluids 3, 362-366 (1960).

[19] Palmer, A.J.: *Radiation-induced Orientation of Atmospheric Aerosols*, J. OP. Soc. America A, vol. 8, no. 2, Feb. 1991.

[20]Pfalzner, S, and Gibbon, P.: Many-Body Tree Methods in Physics, Cambridge University Press, 1996.

[21]Reif, J.H., and Wang, H., Social Potential Fields: A Distributed Behavioral Control for Autonomous Robots, Robotics and Autonomous Systems 27 (1999) 171-194.

[22]Siljak, D.D.: Decentralized Control of Complex Systems, Academic Press, 1990.

[23] Van de Hulst, H. C.: *Light Scattering by Small Particles*, Dover Publications, 1981.